Supplementary Information

Table of Contents

1. Material and Methods

All starting materials were used as received from commercial sources unless otherwise stated, while solvents were freshly distilled by standard procedures prior to use. The experiments were carried out under the nitrogen atmosphere with standard Schlenk techniques. 2,6-di(1*H*-imidazol-1-yl)anthracene (**L1**)[1], 2,6-bis(1*H*-benzo[*d*]imidazol-1-yl)anthracene (**L2**)[1] and dinuclear gold carbene complexes[2] were synthesized according to published procedures. The ^{1}H, ^{13}C{^{1}H} and 2D NMR spectra were recorded on Bruker AVANCE III 400, AVANCE III 600 and JEOL ECZ400R spectrometers. Chemical shifts (δ) are expressed in ppm downfield from tetramethylsilane using the residual protonated solvent as an internal standard. All coupling constants are expressed in Hertz. Mass spectra were obtained with a Bruker microTOF-Q II mass spectrometer (Bruker Daltonics USA) in the electrospray ionisation (ESI) mode. The UV-Vis experiments were conducted on an Agilent Cary-100 spectrophotometer. The fluorescence experiments were performed on a Horiba QM8000 spectrometer.

2. Synthesis of Bisimidazolium Salts H_2-L$(PF_6)_2$.

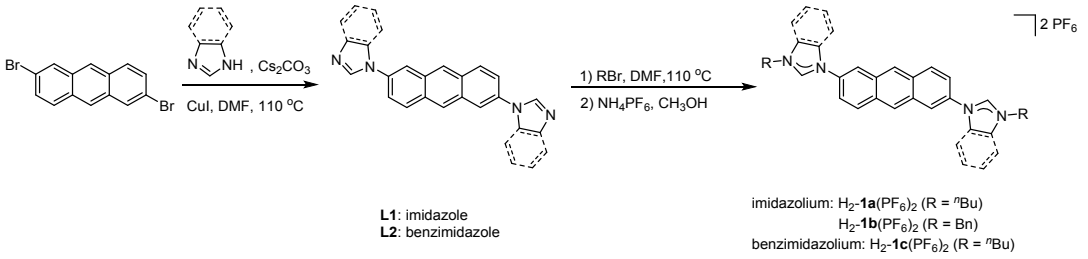

Scheme S1. General synthesis of azole ligands (**L1**, **L2**) and bis(imidazolium) salt H_2-**L**$(PF_6)_2$ (**L** = **1a-c**).

2.1 Synthesis of Ligand L1 and L2.

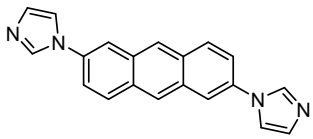

trans-4,4′-Dibromostilbene (200 mg, 0.60 mmol), imidazole (408.5 mg, 6.0 mmol), K_2CO_3 (829.2 mg, 6.0 mmol) and $CuSO_4$ (14.4 mg, 0.09 mmol) were mixed in a reaction still and heated to 180 °C for 24 h in an oven. The reaction mixture was cooled to ambient temperature and washed three times with water. The solid residue was extracted with dichloromethane (30 mL), and the extract was concentrated *in vacuo* to yield **L1** as a yellow solid. Yield:167.6 mg (0.54 mmol, 90%). ^{1}H NMR (400 MHz, $CDCl_3$): δ = 8.53 (s, 2H), 8.16 (d, J = 9.0 Hz, 2H), 8.09-8.03 (m, 2H), 8.00 (d, J = 2.1 Hz, 2H), 7.60 (dd, J = 9.0, 2.2 Hz, 2H), 7.47 (t, J = 1.3 Hz, 2H), 7.32-7.28 (m, 2H) ppm. HRMS (ESI, positive ions): m/z = 311.1297 (calcd for $[C_{20}H_{14}N_4+H]^+$ 311.1291).

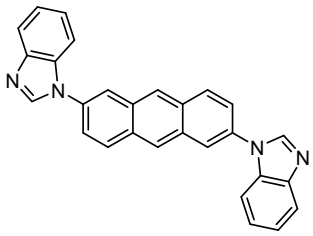

trans-4,4′-Dibromostilbene (200 mg, 0.60 mmol), benzimidazole (708.8 mg, 6.0 mmol), K_2CO_3 (829.2 mg, 6.0 mmol) and $CuSO_4$ (14.4 mg, 0.09 mmol) were mixed in a reaction still and heated to 180 °C for 36 h in an oven. The reaction mixture was cooled to ambient temperature and washed three times with water. The solid residue was extracted with dichloromethane (30 mL), and the extract was concentrated *in vacuo* to yield **L2** as a yellow solid. Yield: 206.9 mg (0.50 mmol, 84%). ^{1}H NMR (400 MHz, DMSO-d_6): δ = 8.89 (s,

2H), 8.78 (s, 2H), 8.49 (s, 2H), 8.42 (d, J = 9 Hz, 2H), 7.93 (dd, J = 9.0, 2.2 Hz, 2H), 7.84 (dt, J = 7.4, 1.6 Hz, 4H), 7.46–7.34 (m, 4H) ppm. HRMS (ESI, positive ions): m/z = 411.1588 (calcd for $[C_{28}H_{18}N_4+H]^+$ 411.1604).

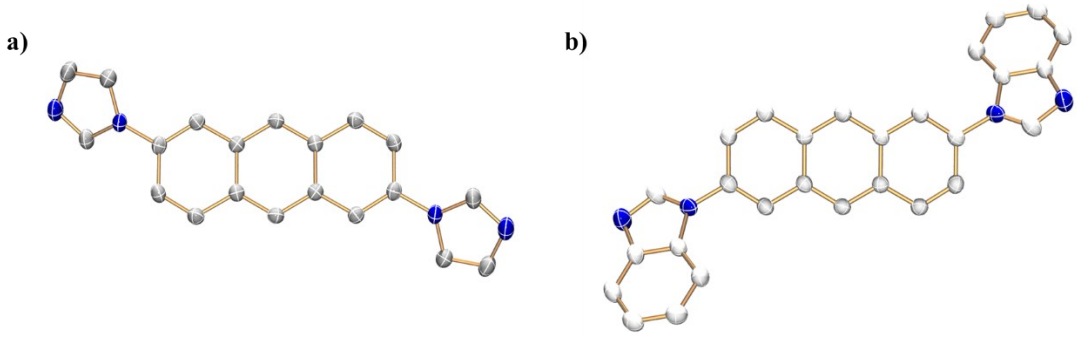

Figure S1. a) Molecular structure of **L1**; b) Molecular structure of **L2**. (N, blue; C, grey; hydrogen atoms have been omitted for clarity.)

2.2 Synthesis of Compound H_2-1a$(PF_6)_2$.

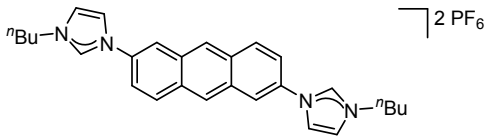

A mixture of **L1** (100.0 mg, 0.322 mmol) and 1-bromobutane (176.5 mg, 1.288 mmol) was suspended in DMF (2 mL) and heated to 110 °C for 12 h. The reaction mixture was cooled to ambient temperature, then ethyl acetate (30 mL) was added to the mixture and led to an off-white precipitation. The solid was isolated by filtration and washed with ethyl acetate (3 × 5 mL) and dried *in vacuo*. The off-white solid obtained was then transferred to a round-bottom flask containing methanol (20 mL). Upon addition of a solution of NH_4PF_6 (157.4 mg, 0.966 mmol) in methanol (10 mL) to this solution, the brown bis(imidazolium) salt H_2-**1a**$(PF_6)_2$ precipitated immediately. The precipitated solid was collected by filtration, washed with small portions of cold methanol and dried *in vacuo*. Yield: 202.2 mg (0.283 mmol, 88%, over two steps). ^{1}H NMR (400 MHz, DMSO-d_6): δ = 10.02 (s, 2H), 8.88 (s, 2H), 8.64 (s, 2H), 8.57-8.48 (m, 4H), 8.16-8.09 (m, 2H), 8.02-7.93(m, 2H), 4.31 (t, J = 7.2, 4H), 1.99-1.83 (m, 4H), 1.38 (dt, J = 14.5 Hz, 7.3 Hz, 4H), 0.97 (t, J = 7.3 Hz, 6H) ppm. ^{13}C{^{1}H} NMR (100 MHz, DMSO-d_6): δ = 135.7, 132.5, 131.1, 131.0, 130.9, 127.8, 123.5, 121.3, 120.5, 120.4, 49.3, 31.2, 18.9, 13.3 ppm. HRMS (ESI,

positive ions): *m/z* = 569.2125 (calcd for $[H_2\text{-}\mathbf{1a}+PF_6]^+$ 569.2263), *m/z* = 212.1304 (calcd for $[H_2\text{-}\mathbf{1a}]^{2+}$ 212.1308).

2.3 Synthesis of Compound H_2-1b$(PF_6)_2$.

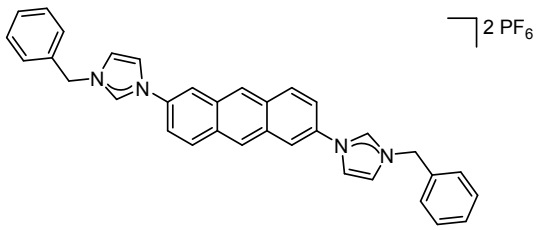

A mixture of **L1** (100.0 mg, 0.322 mmol) and (bromomethyl)benzene (165.2 mg, 0.966 mmol) was suspended in DMF (2 mL) and heated to 110 °C for 12 h. The reaction mixture was cooled to ambient temperature, then ethyl acetate (30 mL) was added to the mixture and led to an off-white precipitation. The solid was isolated by filtration and washed with ethyl acetate (3 × 5 mL) and dried *in vacuo*. The off-white solid obtained was then transferred to a round-bottom flask containing methanol (20 mL). Upon addition of a solution of NH_4PF_6 (157.4 mg, 0.966 mmol) in methanol (10 mL) to this solution, the brown bis(imidazolium) salt H_2-**1b**$(PF_6)_2$ precipitated immediately. The precipitated solid was collected by filtration, washed with small portions of cold methanol and dried *in vacuo*. Yield: 208.9 mg (0.267 mmol, 83%, over two steps). ^{1}H NMR (400 MHz, DMSO-d_6): δ = 10.18 (s, 2H), 8.88 (s, 2H), 8.66 (s, 2H), 8.55 (s, 4H), 8.13 (s, 2H), 8.00 (d, J = 8.0 Hz, 2H), 7.60-7.54 (m, 4H), 7.50-7.42 (m, 6H), 5.58 (s, 4H) ppm. ^{13}C{^{1}H} NMR (100 MHz, DMSO-d_6): δ = 135.9, 134.4, 132.4, 131.0, 130.9, 129.0, 128.9, 128.5, 127.8, 123.5, 121.9, 120.6, 99.4, 52.6 ppm. HRMS (ESI, positive ions): *m/z* = 246.1143 (calcd for $[H_2\text{-}\mathbf{1b}]^{2+}$ 246.1151).

2.4 Synthesis of Compound H_2-1c$(PF_6)_2$.

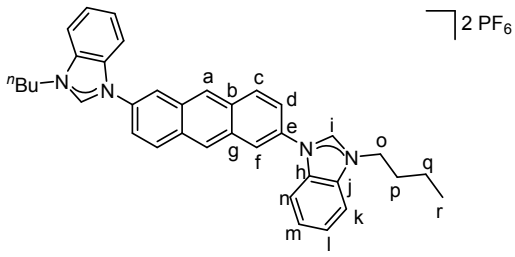

A mixture of **L2** (150.0 mg, 0.365 mmol) and 1-bromobutane (200.0 mg, 1.460 mmol) was suspended in DMF (3 mL) and heated to 110 °C for 12 h. The reaction mixture was cooled to ambient temperature, then ethyl acetate (35 mL) was added

to the mixture and led to an off-white precipitation. The solid was isolated by filtration and washed with ethyl acetate (3 × 7 mL) and dried *in vacuo*. The off-white solid obtained was then transferred to a round-bottom flask containing methanol (25 mL). Upon addition of a solution of NH_4PF_6 (178.5 mg, 1.095 mmol) in methanol (10 mL) to this solution, the brown bis(imidazolium) salt H_2-**1c**$(PF_6)_2$ precipitated immediately. The precipitated solid was collected by filtration, washed with small portions of cold methanol and dried *in vacuo*. Yield: 252.5 mg (0.310 mmol, 85%, over two steps). ^{1}H NMR (400 MHz, DMSO-d_6): δ = 10.38 (s, 2H, H_i), 9.07 (s, 2H, H_a), 8.75 (s, 2H, H_f), 8.61 (d, J = 9.1 Hz, 2H, H_c), 8.30 (d, J = 8.1 Hz, 2H, H_n), 8.07 (d, J = 8.1 Hz, 2H, H_k), 8.02 (d, J = 9.1 Hz, 2H, H_d), 7.86-7.78 (m, 4H, H_m, H_l), 4.65 (t, J = 7.2 Hz, 4H, H_o), 2.09-2.01 (m, 4H, H_p), 1.54-1.45 (m, 4H ,H_q), 1.00 (t, J = 7.3 Hz, 6H, H_r) ppm. $^{13}C\{^1H\}$ NMR (100 MHz, DMSO-d_6): δ = 142.8 (C_i), 131.4 (C_j), 131.1 (C_h), 131.2 ($C_b/_g$), 131.3 (C_c), 128.2 (C_a), 127.6 (C_m), 127.1 (C_l), 124.6 (C_f), 123.1 (C_d), 114.2 (C_n), 113.8 (C_k), 47.0 (C_o), 30.5 (C_p), 19.2 (C_q), 13.5 (C_r) ppm. HRMS (ESI, positive ions): m/z = 669.2435 (calcd for $[H_2$-**1c**$+PF_6]^+$ 669.2576).

3. Synthesis of Complex *anti*-$[Ag_2(L)_2](PF_6)_2$ and *syn*-4$(OTf)_4$.

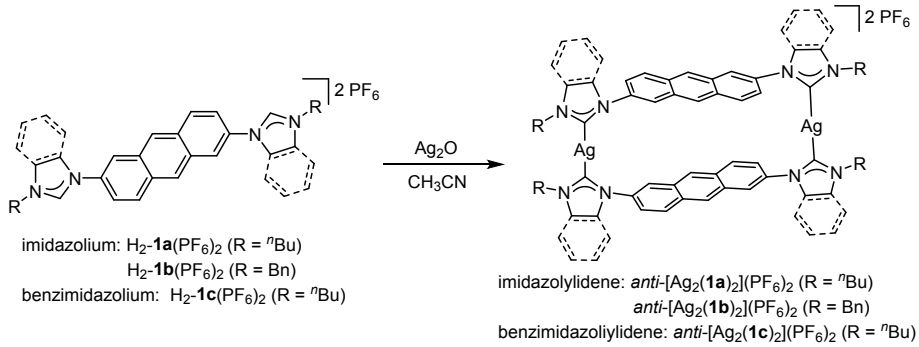

Scheme S2. General synthesis of complexes *anti*-$Ag_2(\mathbf{L})_2(PF_6)_2$ (**L** = **1a-c**).

3.1 Synthesis of Complex *anti*-$[Ag_2(1a)_2](PF_6)_2$.

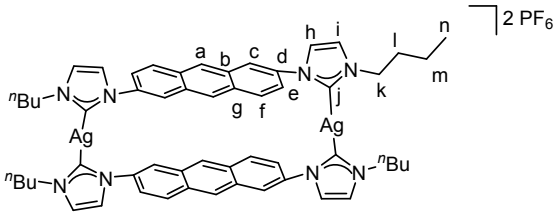

A sample of H_2-**1a**$(PF_6)_2$ (50.0 mg, 0.070 mmol) was dissolved in CH_3CN (10 mL) and to this solution was added Ag_2O (48.7 mg, 0.210 mmol). The resulting suspension was heated to

65 °C for 24 h under exclusion of light. After cooling to ambient temperature, the obtained suspension was filtered slowly through a short pad of Celite to obtain a clear solution. The filtrate was concentrated to 2 mL and diethyl ether (20 mL) was added. This led to the precipitation of a brown solid. The solid was collected by filtration, washed with diethyl ether, and dried *in vacuo* to give *anti*-[Ag_2(**1a**)$_2$](PF_6)$_2$ as a light brown solid. Yield: 40.5 mg (0.030 mmol, 85%). ^{1}H NMR (600 MHz, DMSO-d_6): δ = 8.26 (s, 4H, H_a), 8.08 (s, 4H, H_h), 7.90 (s, 4H, H_i), 7.81 (d, J = 8.9 Hz, 4H, H_f), 7.74 (d, J = 8.7 Hz, 4H, H_e), 7.43 (s, 4H, H_c), 4.41 (t, J = 7.4 Hz, 8H, H_k), 2.00 (p, J = 7.4 Hz, 8H, H_l), 1.47 (h, J = 7.4 Hz, 8H, H_m), 1.02 (t, J = 7.3 Hz, 12H, H_n) ppm. ^{13}C{^{1}H} NMR (150 MHz, DMSO-d_6): δ = 178.4 (C_j), 136.3 (C_d), 130.1 (C_b), 130.0 (C_g), 129.8 (C_e), 125.6 (C_c), 123.5 (C_i), 121.9 (C_h), 121.5 (C_f), 119.6 (C_a), 51.9 (C_k), 33.3 (C_l), 19.5 (C_m), 13.6 (C_n) ppm. HRMS (ESI, positive ions): *m/z* = 530.1664 (calcd for *anti*-[Ag_2(**1a**)$_2$]$^{2+}$ 530.1517).

3.2 Synthesis of Complex *anti*-[Ag_2(**1b**)$_2$](PF_6)$_2$.

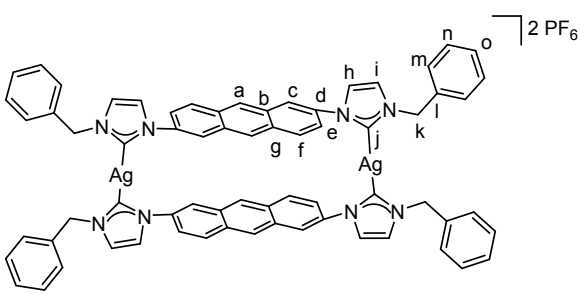

A sample of H_2-**1b**(PF_6)$_2$ (49.3 mg, 0.063 mmol) was dissolved in CH_3CN (10 mL) and to this solution was added Ag_2O (43.8 mg, 0.189 mmol). The resulting suspension was heated to 60 °C for 24 h under exclusion of light. After cooling to ambient temperature, the obtained suspension was filtered slowly through a short pad of Celite to obtain a clear solution. The filtrate was concentrated to 2 mL and diethyl ether (20 mL) was added. This led to the precipitation of a brown solid. The solid was collected by filtration, washed with diethyl ether, and dried *in vacuo* to give *anti*-[Ag_2(**1b**)$_2$](PF_6)$_2$ as a light brown solid. Yield: 40.3 mg (0.027 mmol, 86%). ^{1}H NMR (400 MHz, DMSO-d_6): δ = 8.31 (s, 4H, H_a), 8.11 (s, 4H, H_h), 7.89 (s, 4H, H_i), 7.81 (d, J = 8.4 Hz, 4H, H_f), 7.73 (d, J = 8.4 Hz, 4H, H_e), 7.57 (s, 4H, H_c), 7.40 (s, 8H, H_m), 7.30-7.36(m, br, 12H, H_n, H_o), 5.58 (s, 8H, H_k) ppm. ^{13}C{^{1}H} NMR (100 MHz, DMSO-d_6): δ = 179.2 (C_j), 136.6 (C_l), 136.3 (C_d), 130.2 (C_g), 130.1 (C_n), 129.9 (C_b), 128.9 (C_f), 128.2 (C_o), 127.5 (C_m), 125.9 (C_c), 123.7 (C_i), 122.7 (C_h), 121.7 (C_e), 120.0 (C_a), 55.1 (C_k) ppm. HRMS (ESI, positive ions): *m/z* =

598.1185 (calcd for *anti*-$[Ag_2(\mathbf{1b})_2]^{2+}$ 598.1206).

3.3 Synthesis of Complex *anti*-$[Ag_2(1c)_2](PF_6)_2$.

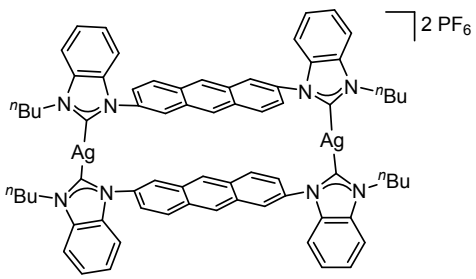

A sample of H_2-**1c**$(PF_6)_2$ (50.0 mg, 0.061 mmol) was dissolved in CH_3CN (10 mL) and to this solution was added Ag_2O (42.4 mg, 0.183 mmol). The resulting suspension was heated to 70 °C for 24 h under exclusion of light. After cooling to ambient temperature, the obtained suspension was filtered slowly through a short pad of Celite to obtain a clear solution. The filtrate was concentrated to 2 mL and diethyl ether (20 mL) was added. This led to the precipitation of a brown solid. The solid was collected by filtration, washed with diethyl ether, and dried *in vacuo* to give *anti*-$[Ag_2(\mathbf{1c})_2](PF_6)_2$ as a light brown solid. Yield: 35.5 mg (0.024 mmol, 75%).^{1}H NMR (400 MHz, DMSO-d_6): δ = 8.42 (s, 4H), 8.16 (s, 4H), 8.07 (d, J = 8.1 Hz, 4H), 7.94 (s, 8H), 7.72 (s, 4H), 7.61 (t, J = 7.6 Hz, 4H), 7.53 (d, J = 7.7 Hz, 4H), 4.80 (s, 8H, NCH_2), 2.07 (s, 8H, NCH_3CH_2), 1.54 (s, 8H, $NCH_3CH_2CH_2$), 1.03 (s, 12H, CH_3) ppm. ^{13}C{^{1}H} NMR (100 MHz, DMSO-d_6): δ = 187.9 (N-C-N), 135.1, 133.6, 133.3, 131.0, 130.7, 130.4, 127.3, 124.9, 124.8, 124.6, 124.1, 112.6, 112.3, 48.9 (NCH_2), 32.1 (NCH_3CH_2), 19.6 ($NCH_3CH_2CH_2$), 13.6 (CH_3) ppm. HRMS (ESI, positive ions): m/z = 630.1703 (calcd for *anti*-$[Ag_2(\mathbf{1c})]^{2+}$ 630.1832).

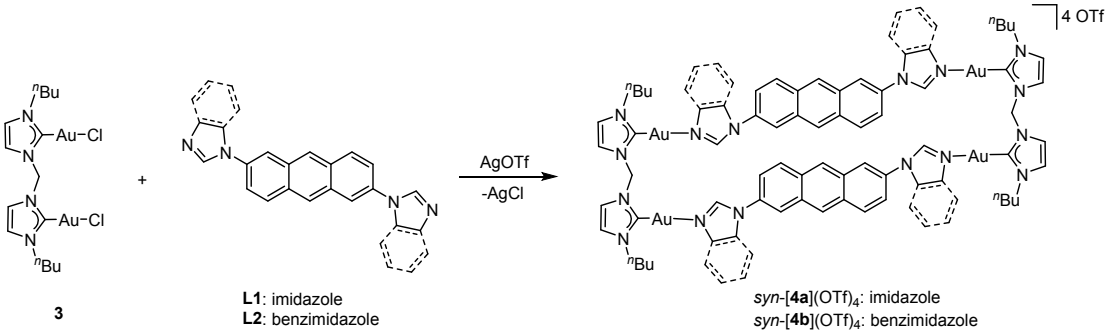

Scheme S3. Coordination-driven self-assembly of organometallic rectangles syn-[**4**]$(OTf)_4$.

3.4 Synthesis of Complex syn-[**4a**]$(OTf)_4$.

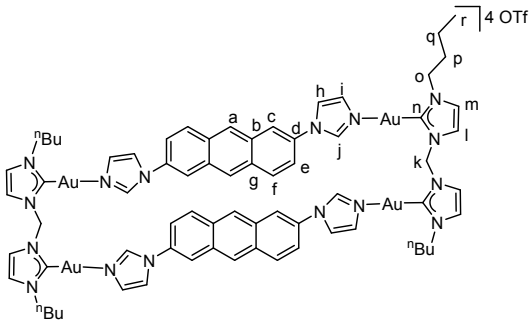

To a solution of dinuclear gold carbene complexe **3** (203.1 mg, 0.280 mmol) in 20 mL CH_2Cl_2, **L1** (86.9 mg, 0.280 mmol) and AgOTf (156.7 mg, 0.610 mmol) were added sequentially. The resulting mixture was stirred at room temperature for 24 h under exclusion of light. After the reaction completed, the light gray precipitate was separated and then washed with CH_2Cl_2. The solid residue was extracted with acetonitrile (60 mL). Then the extract was concentrated *in vacuo* to yield *syn*-[**4a**](OTf)$_4$. Yield: 247.5 mg (0.098 mmol, 70%). ^{1}H NMR (400 MHz, DMSO-d_6): δ = 8.98 (s, 4H, H_j), 8.23 (s, 4H, H_h), 8.05 (s, 4H, H_l), 7.95 (d, J = 9.2 Hz, 4H, H_f), 7.90 (s, 4H, H_c), 7.81 (d, J = 5.3 Hz, 8H, H_m, H_a), 7.65 (d, J = 9.1 Hz, 4H, H_e), 7.48 (s, 4H, H_i), 6.80 (s, 4H, H_k), 4.34 (t, J = 7.1 Hz, 8H, H_o), 1.87 (p, J = 7.1 Hz, 8H, H_p), 1.37-1.28 (m, 8H, H_q), 0.94 (t, J = 7.3 Hz, 12H, H_r) ppm. ^{13}C{^{1}H} NMR (100 MHz, DMSO-d_6): δ = 166.0 (C_n), 138.0 (C_j), 131.6 (C_g), 130.3 (C_f), 129.7 (C_d), 129.4 (C_i), 126.1 (C_c), 123.6 (C_m), 122.3 (C_l), 119.1 (C_b), 118.9 (C_h), 118.4 (C_e), 117.0 (C_a), 62.5 (C_k), 51.0 (C_o), 32.4 (C_p), 19.0 (C_q), 13.5 (C_r) ppm. HRMS (ESI, positive ions): *m/z* = 1113.1998 (calcd for [*syn*-[**4a**](OTf)$_2$]$^{2+}$ 1113.2065), 692.4965 (calcd for [*syn*-[**4a**](OTf)]$^{3+}$ 692.4868), 482.1455 (calcd for [*syn*-[**4a**]]$^{4+}$ 482.1270).

3.5 Synthesis of Complex *syn*-[4b](OTf)$_4$.

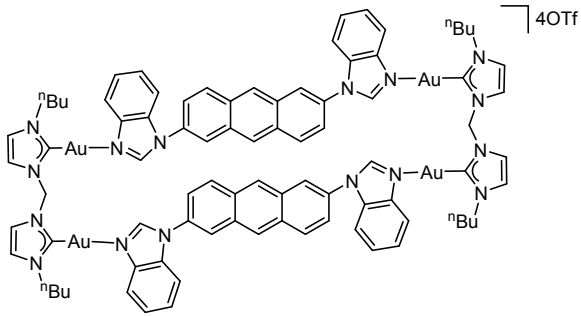

To a solution of complex **3** (203.1 mg, 0.28 mmol) in 25 mL CH_2Cl_2, compound **L2** (114.9 mg, 0.28 mmol) and AgOTf (156.7 mg, 0.61 mmol) were added sequentially. The resulting mixture was stirred at room temperature for 24 h under exclusion of light. After the reaction completed, the light gray precipitate was separated and then washed with CH_2Cl_2. The solid residue was extracted with acetonitrile (55 mL). Then the extract was concentrated *in vacuo* to yield *syn*-[**4b**](OTf)$_4$. Yield: 248.0 g (0.091 mmol, 65%). ^{1}H NMR (400 MHz, DMSO-d_6):

δ = 9.39 (s, 4H), 8.19 (s, 4H), 8.16 (d, J = 2.1 Hz, 4H), 7.94 (d, J = 9.1 Hz, 4H), 7.89-7.82 (m, 16H), 7.54 (d, J = 9.1 Hz, 4H), 7.24 (m, 8H), 6.96 (br, s, 4H), 4.38 (t, 8H), 1.90 (m, 8H), 1.32 (m, 8H), 0.90 (t, 12H) ppm. $^{13}C\{^1H\}$ NMR (100 MHz, DMSO-d_6): δ = 166.4, 145.2, 138.8, 130.9, 130.4, 130.0, 129.8, 129.7, 126.6, 125.7, 123.8, 122.3, 121.1, 120.7, 119.1 118.2, 111.9, 62.8, 51.1, 32.5, 19.1, 13.4 ppm. HRMS (ESI, positive ions): m/z = 1213.7278 (calcd for [*syn*-[**4b**](OTf)$_2$]$^{2+}$ 1213.7394), 759.1788 (calcd for [*syn*-[**4b**](OTf)]$^{3+}$ 759.1744), 532.1548 (calcd for [*syn*-[**4b**]]$^{4+}$ 532.1426).

4. Photodimerization.

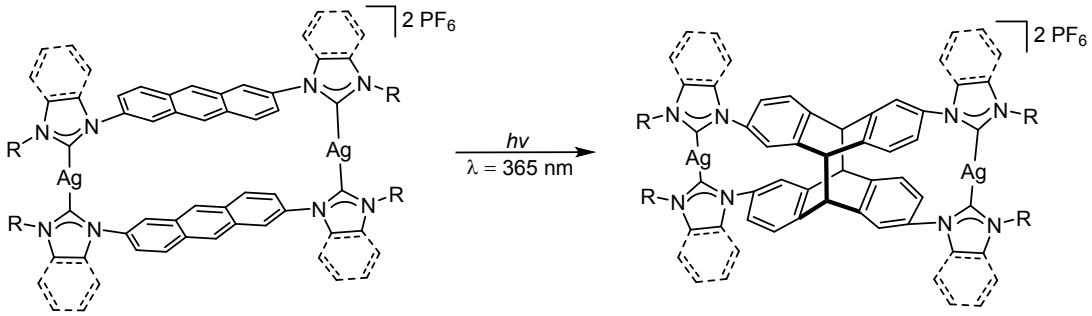

imidazolylidene: *anti*-[Ag$_2$(**1a**)$_2$](PF$_6$)$_2$ (R = ^{n}Bu)
anti-[Ag$_2$(**1b**)$_2$](PF$_6$)$_2$ (R = Bn)
benzimidazoliylidene: *anti*-[Ag$_2$(**1c**)$_2$](PF$_6$)$_2$ (R = ^{n}Bu)

imidazolylidene: *anti*-[Ag$_2$(**2a**)](PF$_6$)$_2$ (R = ^{n}Bu)
anti-[Ag$_2$(**2b**)](PF$_6$)$_2$ (R = Bn)
benzimidazoliylidene: *anti*-[Ag$_2$(**2c**)](PF$_6$)$_2$ (R = ^{n}Bu)

Scheme S4. Photolytic transformation to synthesize complex *anti*-[Ag$_2$(**2**)](PF$_6$)$_2$.

4.1 Synthesis of Complex *anti*-[Ag$_2$(2a)](PF$_6$)$_2$ by Photochemical [4+4] Cycloaddition.

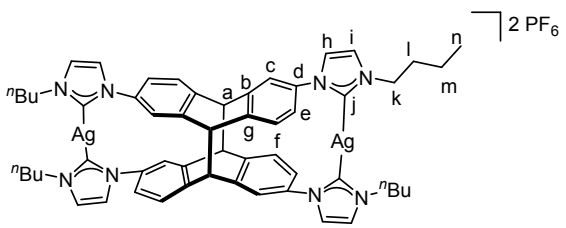

A solution of *anti*-[Ag$_2$(**1a**)$_2$](PF$_6$)$_2$ (30.0 mg, 0.022 mmol) in DMSO-d_6 (0.5 mL, c = 0.044 M) in an NMR tube was irradiated with a Philips mercury high-pressure lamp (λ = 365 nm) at ambient temperature for 30 min. Over this time the initially light brown solution turned maroon. The conversion to *anti*-[Ag$_2$(**2a**)](PF$_6$)$_2$ was quantitative as judged by ^{1}H NMR spectroscopy. ^{1}H NMR (400 MHz, DMSO-d_6): δ = 7.68 (d, J = 1.7 Hz, 4H, H$_i$), 7.67 (d, J = 1.7 Hz, 4H, H$_h$), 7.13 (s, 2H, H$_f$), 7.10-7.11(m, 6H, H$_c$, H$_f$), 7.05 (d, J = 2.1 Hz, 2H, H$_e$), 7.03 (d, J = 2.2 Hz, 2H, H$_e$), 4.86 (s, 4H, H$_a$), 4.24 (t, J = 6.9Hz, 8H, H$_k$),

1.89 (dt, J = 7.3 Hz, 8H, H_l), 1.34-1.45 (m, 8H, H_m), 1.00 (t, J = 7.4 Hz, 12H, H_n) ppm. $^{13}C\{^1H\}$ NMR (100 MHz, DMSO-d_6): δ = 180.1 (C_j), 143.7 (C_b), 143.4 (C_g), 138.0 (C_d), 128.2 (C_c), 125.6 (C_f), 123.7 (C_e), 122.4 ($C_{i/h}$), 51.7 (C_a), 50.6 (C_k), 33.0 (C_l), 19.2 (C_m), 13.5 (C_n) ppm. HRMS (ESI, positive ions): m/z = 530.1545 (calcd for *anti*-$[Ag_2(\mathbf{2a})]^+$ 530.1517).

4.2 Synthesis of Complex *anti*-$[Ag_2(2b)](PF_6)_2$ by Photochemical [4+4] Cycloaddition.

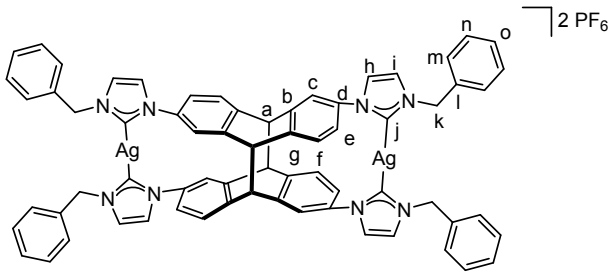

A solution of *anti*-$[Ag_2(\mathbf{1b})_2](PF_6)_2$ (30.0 mg, 0.020 mmol) in DMSO-d_6 (0.5 mL, c = 0.040 M) in an NMR tube was irradiated with a Philips mercury high-pressure lamp (λ = 365 nm) at ambient temperature for 25 min. Over this time the initially light brown solution turned maroon. The conversion to *anti*-$[Ag_2(\mathbf{2b})](PF_6)_2$ was quantitative as judged by ^1H NMR spectroscopy. ^1H NMR (400 MHz, DMSO-d_6): δ = 7.75 (d, J = 1.7 Hz, 4H, H_i), 7.70 (d, J = 1.7 Hz, 4H, H_h), 7.46 (d, J = 1.9 Hz, 2H, H_m), 7.44 (d, J = 1.4 Hz, 6H, H_m), 7.41 (d, J = 2.2 Hz, 2H, H_n), 7.40 (s, 4H, H_o), 7.38-7.36(m, br, 6H, H_n), 7.12 (m, 6H, H_c, H_e), 7.10 (s, 2H, H_e), 7.02 (d, J = 2.1 Hz, 2H, H_f), 7.00 (d, J = 2.1 Hz, 2H, H_f), 5.46 (s, 8H, H_k), 4.83 (s, 4H, H_a) ppm. $^{13}C\{^1H\}$ NMR (100 MHz, DMSO-d_6): δ = 180.5 (C_j), 143.6 (C_d), 143.2 (C_b), 137.9 (C_g), 137.0 (C_l), 128.9 (C_n), 128.2 (C_o), 128.1 (C_m), 128.0 (C_e), 127.9 (C_f), 125.5 (C_c), 123.5 (C_i), 122.8 (C_h), 54.1 (C_k), 51.6 (C_a) ppm. HRMS (ESI, positive ions): m/z = 598.1328 (calcd for *anti*-$[Ag_2(\mathbf{2b})]^{2+}$ 598.1206).

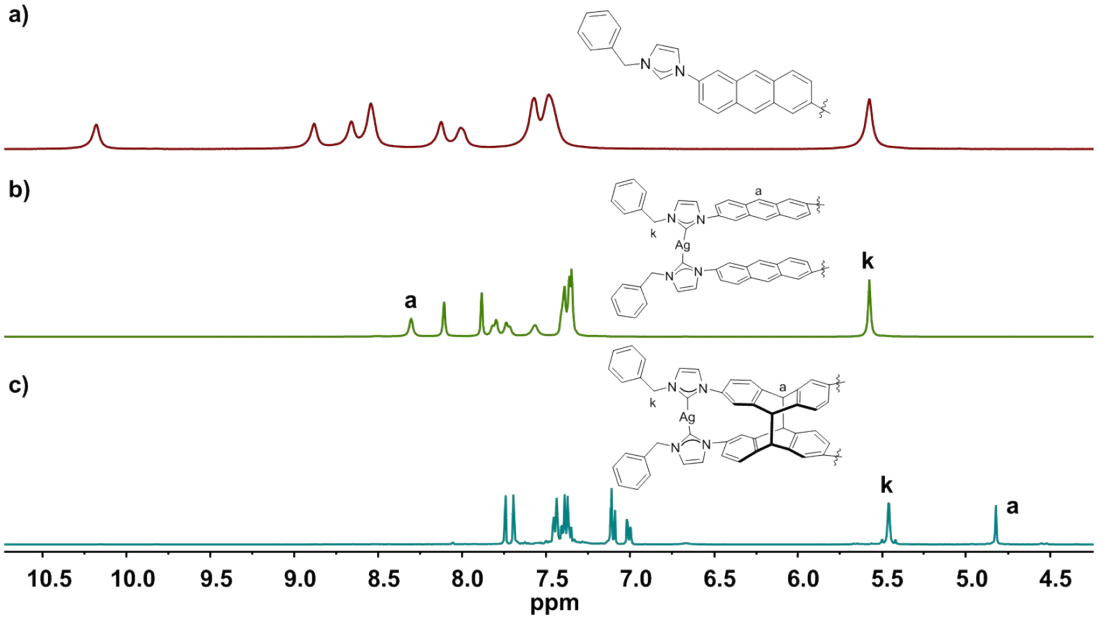

Figure S2. Sections of the ^{1}H NMR spectra in [D$_6$]DMSO of a) bisimidazolium salt H$_2$-**1b**(PF$_6$)$_2$; b) complex *anti*-[Ag$_2$(**1b**)$_2$](PF$_6$)$_2$ before irradiation; c) complex *anti*-[Ag$_2$(**2b**)](PF$_6$)$_2$ obtained after irradiation.

4.3 Synthesis of Complex *anti*-[Ag$_2$(2c)](PF$_6$)$_2$ by Photochemical [4+4] Cycloaddition.

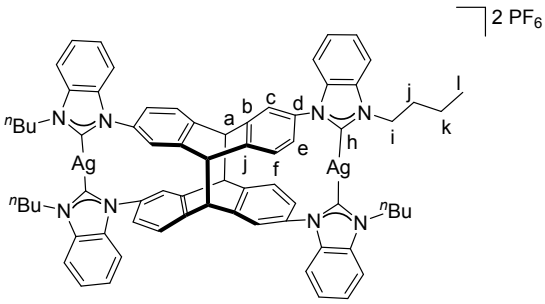

A solution of *anti*-[Ag$_2$(**1c**)$_2$](PF$_6$)$_2$ (30.0 mg, 0.019 mmol) in DMSO-d_6 (0.5 mL, c = 0.038 M) in an NMR tube was irradiated with a Philips mercury high-pressure lamp (λ = 365 nm) at ambient temperature for 45 min. Over this time the initially light brown solution turned maroon. The conversion to *anti*-[Ag$_2$(**2c**)](PF$_6$)$_2$ was quantitative as judged by ^{1}H NMR spectroscopy. ^{1}H NMR (400 MHz, DMSO-d_6): δ = 8.00 (d, J = 8.3 Hz, 4H, H$_f$), 7.55 (ddd, J = 8.2 , 5.5 , 2.7 Hz, 4H, H$_e$), 7.46-7.40 (m, 12H, benzimidazole-H), 7.27 (s, 4H, H$_c$), 7.26 (d, J = 2.4 Hz, 4H, benzimidazole-H), 5.00 (s, 4H, H$_a$), 4.68 (td, J = 14.1, 6.8 Hz, 8H, H$_i$), 2.02 (p, J = 7.4 Hz, 8H, H$_j$), 1.62-1.41 (m, 8H, H$_k$), 1.05 (t, J = 7.4Hz, 12H, H$_l$) ppm. ^{13}C{^{1}H} NMR (100 MHz, DMSO-d_6): δ = 188.4 (C$_h$), 144.1(C$_d$), 143.9(C$_b$), 135.6, 133.6(C$_j$), 133.1,

129.2(C_c), 126.2, 124.9, 124.8, 124.6 (C_e), 112.5 (C_f), 112.0, 51.7 (C_a), 48.4 (C_i), 32.1 (C_j), 19.7 (C_k), 13.7 (C_l) ppm.

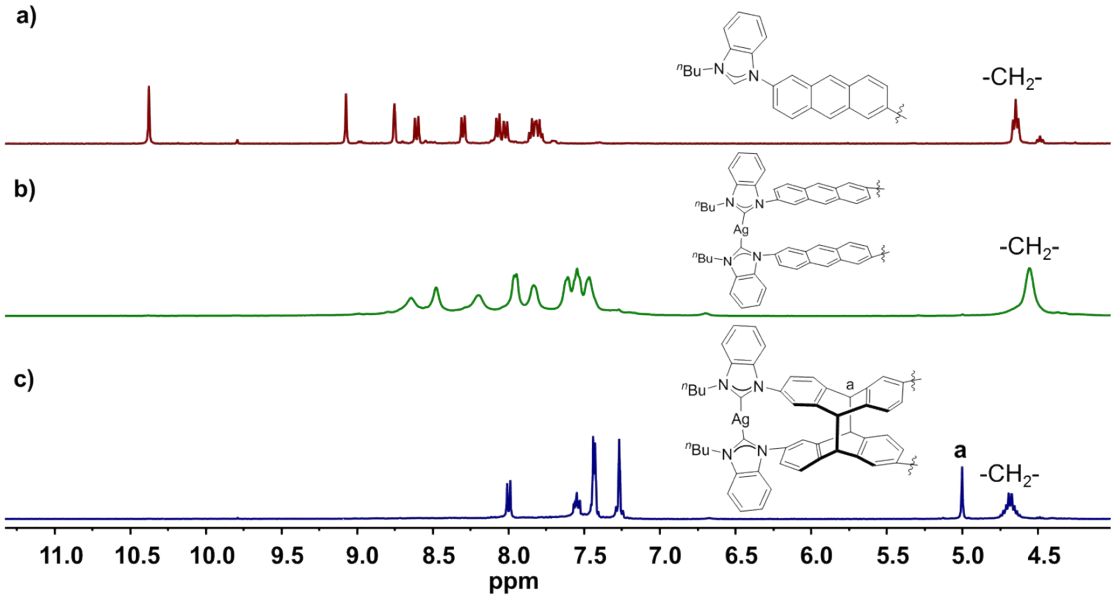

Figure S3. Sections of the ^{1}H NMR spectra in [D_6]DMSO of a) bisimidazolium salt H_2-**1c**$(PF_6)_2$; b) complex *anti*-[Ag_2(**1c**)$_2$]$(PF_6)_2$ before irradiation; c) complex *anti*-[Ag_2(**2c**)]$(PF_6)_2$ obtained after irradiation.

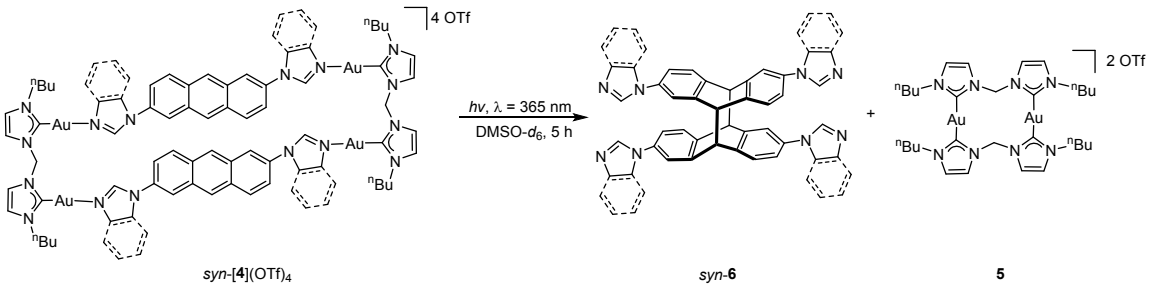

Scheme S5. Photolytic transformation to synthesize compound *syn*-**6**.

4.4 Synthesis of Compound *syn*-6a by Photochemical [4+4] Cycloaddition.

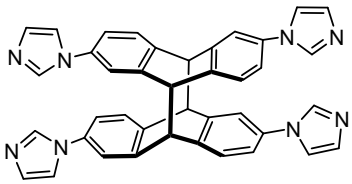

A solution of *syn*-[**4a**](OTf)$_4$ (7.0 mg, 2.8 × 10^{-3} mmol) in DMSO-d_6 (0.5 mL, c = 5.6 × 10^{-3} M) in an NMR tube was irradiated with a Philips mercury high-pressure lamp (λ = 365 nm) at ambient temperature for 3 h. Over this time the initially colorless solution turned yellow and a black solid precipitated. The conversion to *syn*-**6a** was quantitative as judged by ^{1}H NMR spectroscopy. The solid was filtered off and diethyl ether (20 mL) was added to the filtrate and led to a yellow precipitation. The precipitation was purified by column chromatography (NEt_3/CH_2Cl_2/MeOH) to give *syn*-**6a**. Yield: 85% (1.5 mg, 2.4 × 10^{-3} mmol). ^{1}H NMR (400 MHz, DMSO-d_6): δ = 8.04 (s, 4H), 7.54 (s, 4H), 7.35 (d, J = 1.9 Hz, 4H), 7.17 (d, J = 7.9 Hz, 4H), 7.11-7.09 (m, 4H), 7.02 (s, 4H), 4.83 (s, 4H) ppm. HRMS (ESI, positive ions): m/z = 621.2364 (calcd for [*syn*-**6a**+H]$^+$ 621.2510).

4.5 Synthesis of Compound *syn*-6b by Photochemical [4+4] Cycloaddition.

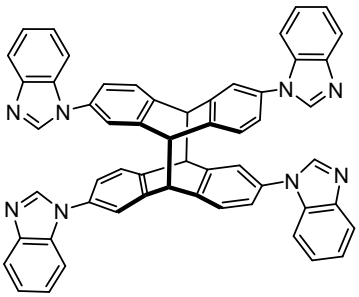

A solution of *syn*-[**4b**](OTf)$_4$ (7.0 mg, 2.6 × 10^{-3} mmol) in DMSO-d_6 (0.5 mL, c = 5.2 × 10^{-3} M) in an NMR tube was irradiated with a Philips mercury high-pressure lamp (λ = 365 nm) at ambient temperature for 3.5 h. Over this time the initially colorless solution turned yellow and a black solid precipitated. The conversion to *syn*-**6b** was quantitative as judged by ^{1}H NMR spectroscopy. The solid was filtered off and diethyl ether (35 mL) was added to the filtrate and led to a yellow precipitation. The precipitation was purified by column chromatography (NEt_3/CH_2Cl_2/MeOH) to give *syn*-**6b**. Yield: 75% (1.6 mg, 2.0 × 10^{-3} mmol). ^{1}H NMR (400 MHz, $CDCl_3$): δ = 7.94 (s, 4H), 7.85 (d, J = 8.1 Hz, 4H), 7.35-7.32 (m, 8H), 7.19-7.17 (m, 8H), 7.05-7.01 (m, 8H), 4.94 (s, 4H). HRMS (ESI, positive ions): m/z = 821.3131 (calcd for [*syn*-**6b**+H]$^+$ 821.3136).

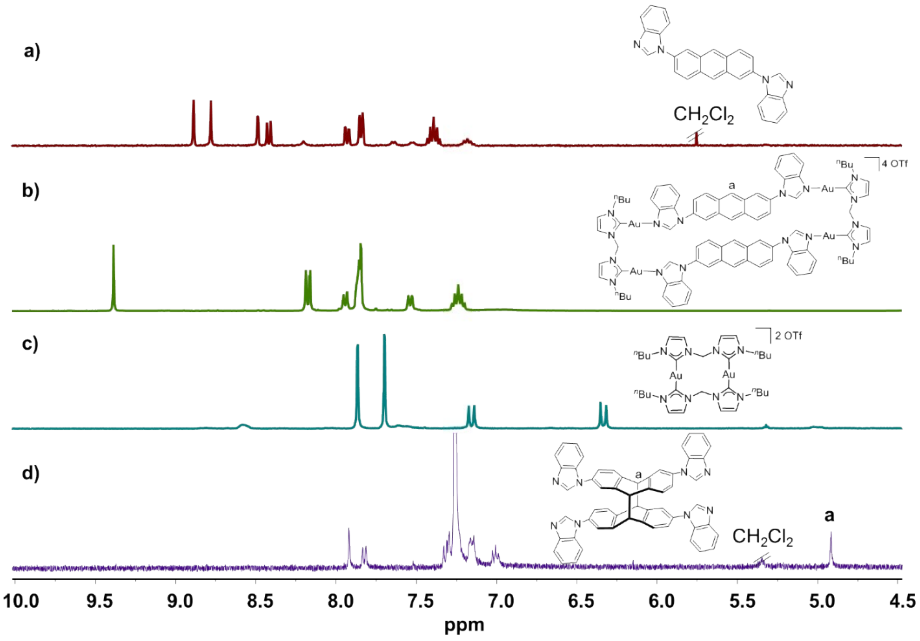

Figure S4. Sections of ^{1}H NMR spectra (400 MHz, 298 K) of a) **L2** in DMSO-d_6, b) *syn*-[**4b**](OTf)$_4$ in DMSO-d_6, c) **5** in DMSO-d_6, d) *syn*-**6b** in $CDCl_3$.

4.6 Synthesis of Complex *syn*-[Ag$_2$**7a**](PF$_6$)$_2$.

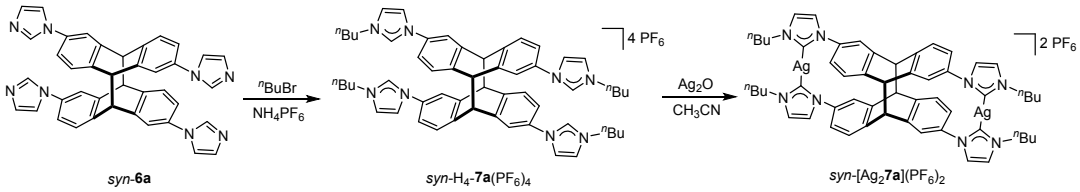

Scheme S6. Synthesis of *syn*-[Ag$_2$**7a**](PF$_6$)$_2$.

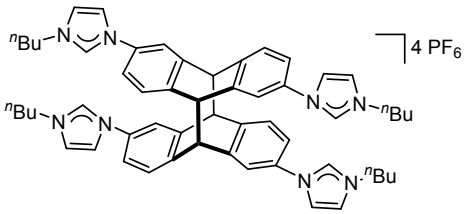

A mixture of *syn*-**6a** (15 mg, 0.024 mmol) and 1-bromobutane (26.3 mg, 0.192 mmol) was suspended in DMF (0.5 mL) and heated to 110 °C for 12 h. The reaction mixture was cooled to ambient temperature, then ethyl acetate (10 mL) was added to the mixture and led to an off-white precipitation. The solid was isolated by filtration and washed with ethyl acetate (3 × 2 mL) and dried *in vacuo*. The light yellow solid obtained was then transferred to a round-bottom flask containing methanol (5 mL). Upon addition of a solution of NH_4PF_6 (19.6 mg, 0.12 mmol) in methanol (2 mL) to this solution,

the light yellow tetrakisimidazolium salt *syn*-H_4-**7a**$(PF_6)_4$ precipitated immediately. The precipitated solid was collected by filtration, washed with small portions of cold methanol and dried *in vacuo*. Yield: 27.4 mg (0.019 mmol, 80%, over two steps). ^{1}H NMR (400 MHz, DMSO-d_6): δ = 9.63 (s, 4H, $H_{imidazole}$), 8.14 (s, 4H), 7.98 (s, 4H), 7.47 (d, J = 2.2 Hz, 4H), 7.40 (s, 2H), 7.38 (s, 2H), 7.32 (d, J = 2.2 Hz, 2H), 7.30 (d, J = 2.3 Hz, 2H), 5.02 (s, 4H,), 4.19 (t, J = 7.3 Hz, 8H, -CH_2CH$_2$CH$_2$CH$_3$), 1.83 (p, J = 7.5 Hz, 8H, -CH$_2$$CH_2CH_2CH_3$), 1.26-1.36 (m, 8H, -CH$_2CH_2$$CH_2CH_3$), 0.93 (t, J = 7.3 Hz, 12H, -CH$_2$CH$_2$CH$_2$$CH_3$) ppm. HRMS (ESI, positive ions): *m/z* = 569.2262 (calcd for [*syn*-H_4-(**7a**)+2PF_6]$^{2+}$ 569.2263), 331.1621 (calcd for [*syn*-H_4-(**7a**)+PF_6]$^{3+}$ 331.1626), 212.1295 (calcd for [*syn*-H_4-(**7a**)]$^{4+}$ 212.1308).

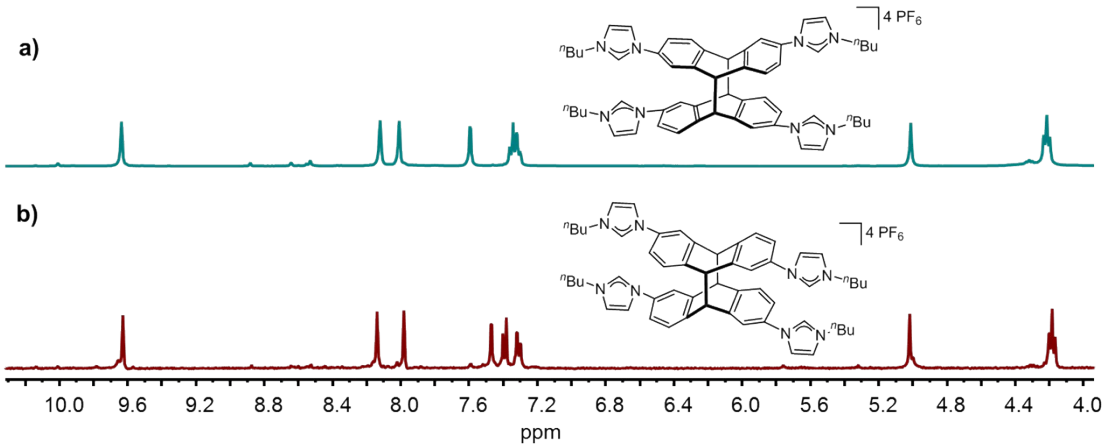

Figure S5. Sections of ^{1}H NMR spectra (400 MHz, 298 K) of a) *anti*-H_4-**1a**$(PF_6)_4$, b) *syn*-H_4-**7a**$(PF_6)_4$ in DMSO-d_6.

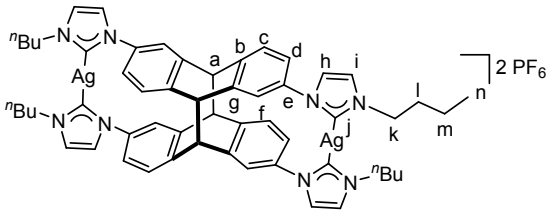

A sample of *syn*-H_4-**7a**$(PF_6)_4$ (27.4 mg, 0.019 mmol, 0.070 mmol) was dissolved in CH_3CN (4 mL) and to this solution was added Ag_2O (13.2 mg, 0.057 mmol). The resulting suspension was heated to 65 °C for 24 h under exclusion of light. After cooling to ambient temperature, the obtained suspension was filtered slowly through a short pad of Celite to obtain a clear solution. The filtrate was concentrated to 1 mL and diethyl ether (10 mL) was added. This led to the precipitation of a brown solid. The solid was collected by filtration, washed with diethyl ether, and dried *in vacuo* to give *syn*-[Ag_2**7a**]$(PF_6)_2$ as a light yellow solid. Yield: 21.6 mg (0.016 mmol, 87%). ^{1}H NMR (600

MHz, DMSO-d_6): δ = 7.67 (s, 4H, H_i), 7.50 (s, 4H, H_h), 7.28 (s, 4H, H_f), 7.19 (d, J = 7.8 Hz, 4H, H_c), 6.99 (d, J = 7.4 Hz, 4H, H_d), 4.97 (s, 4H, H_a), 4.30-4.18 (m, 8H, H_k), 1.94-1.79 (m, 8H, H_l), 1.40-1.34 (m, 8H, H_m), 0.97 (t, J = 7.3 Hz, 12H, H_n) ppm. $^{13}C\{^1H\}$ NMR (150 MHz, DMSO-d_6): δ = 174.3 (C_j), 144.4 (C_b), 143.5 (C_g), 137.8 (C_e), 128.0 (C_c), 125.8 (C_f), 123.3 (C_d), 123.2 (C_h), 122.2 (C_i), 51.2 (C_a), 50.9 (C_k), 33.2 (C_l), 19.4 (C_m), 13.4 (C_n) ppm. HRMS (ESI, positive ions): m/z = 1205.2376 (calcd for *syn*-[Ag_2(**7a**)]$(PF_6)^+$ 1205.2682), 530.1418 (calcd for *syn*-[Ag_2(**7a**)]$^{2+}$ 530.1517).

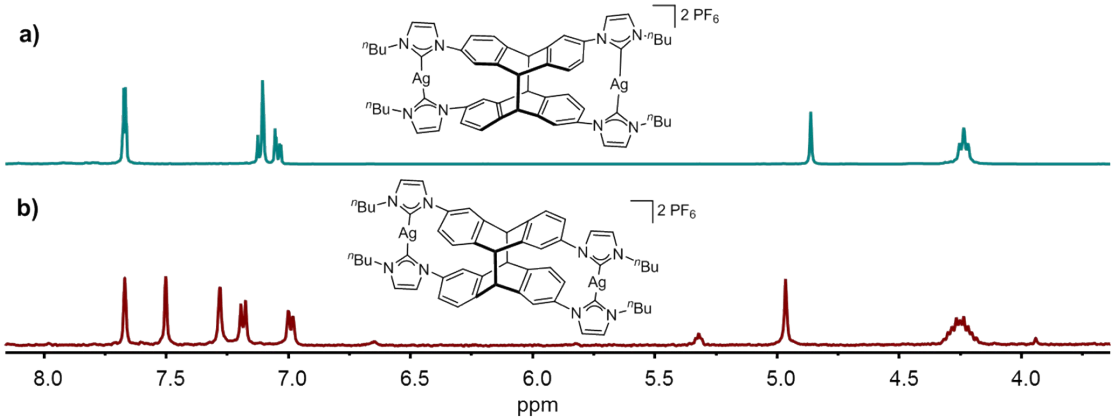

Figure S6. Sections of ^1H NMR spectra (400 MHz, 298 K) of a) *anti*-[Ag_2**1a**]$(PF_6)_2$, b) *syn*-[Ag_2**7a**]$(PF_6)_2$ in DMSO-d_6.

5. De-Metalation Reaction of *anti*-[Ag_2(2)]$(PF_6)_2$.

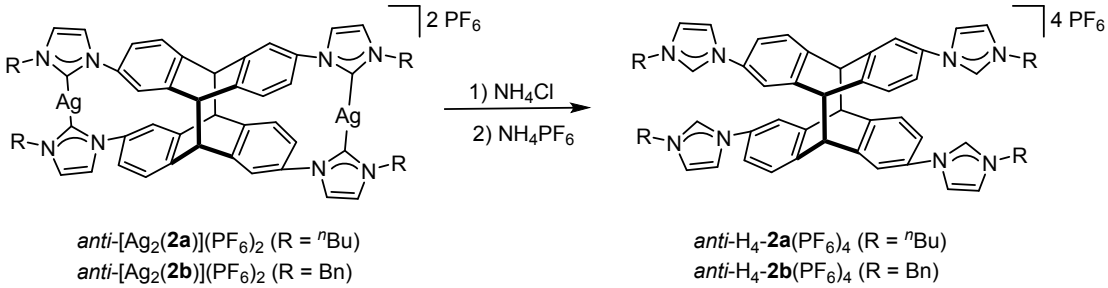

Scheme S7. Synthesis of tetrakisimidazolium salts *anti*-H_4-**L**$(PF_6)_4$.

5.1 Synthesis of Complex *anti*-H_4-2a$(PF_6)_4$.

A sample of *anti*-[Ag_2(**2a**)]$(PF_6)_2$ (27.0 mg, 0.020 mmol) was suspended in a solution of MeOH (20

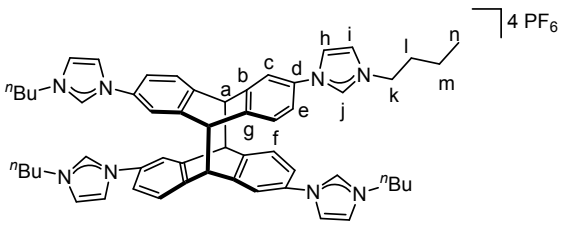

mL) and to this solution was added NH_4Cl (3.2 mg, 0.060 mmol). A white solid (AgCl) precipitated immediately and the reaction mixture was stirred for another 4 h. The resulting suspension was filtered through Celite to obtain a clear solution. The solvent was removed under reduced pressure to give a light gray solid. The solid was dissolved in MeOH (15 mL) and a solution of NH_4PF_6 (16.3 mg, 0.10 mmol) in methanol (3 mL) was added. The mixture was stirred at ambient temperature overnight. After this period a white solid precipitated, which was isolated by filtration, washed with diethyl ether and dried *in vacuo*. Yield: 24.7 mg (0.017 mmol, 84%, two steps). ^{1}H NMR (400 MHz, DMSO-d_6): δ = 9.64 (s, 4H, H_j), 8.12 (s, 4H, H_i), 8.01 (s, 4H, H_h), 7.60 (s, 2H, H_c), 7.36 (s, 6H, H_c, H_f), 7.32 (d, J = 2.0 Hz, 2H, H_e), 7.30 (d, J = 2.0 Hz, 2H, H_e), 5.01 (s, 4H, H_a), 4.22 (t, J = 7.2 Hz, 8H, H_k), 1.86 (dt, J = 7.4 Hz, 8H, H_l), 1.28-1.37 (m, 8H, H_m), 0.93 (t, J = 7.3 Hz, 12H, H_n) ppm. ^{13}C{^{1}H} NMR (100 MHz, DMSO-d_6): δ = 144.7 (C_b), 143.8 (C_g), 134.8 (C_j), 132.5 (C_d), 128.9 (C_c), 123.5 (C_i), 120.9 (C_h), 120.4 (C_f), 119.1 (C_e), 51.4 (C_a), 49.2 (C_k), 31.1 (C_l), 18.9 (C_m), 13.3 (C_n) ppm. HRMS (ESI, positive ions): m/z = 569.2112 (calcd for [*anti*-H_4-(**2a**)+2PF_6]$^{2+}$ 569.2263).

5.2 Synthesis of Complex *anti*-H_4-2b(PF_6)$_4$.

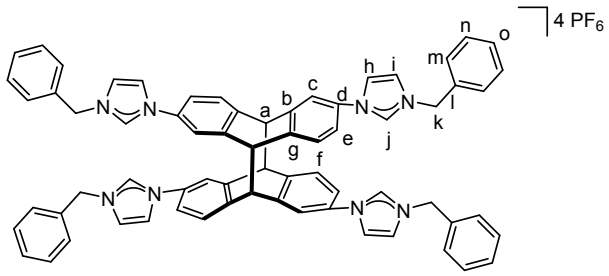

A sample of *anti*-[Ag_2(**2b**)](PF_6)$_2$ (29.8 mg, 0.020 mmol) was suspended in a solution of MeOH (20 mL) and to this solution was added NH_4Cl (3.2 mg, 0.060 mmol). A white solid (AgCl) precipitated immediately and the reaction mixture was stirred for another 4 h. The resulting suspension was filtered through Celite to obtain a clear solution. The solvent was removed under reduced pressure to give a light gray solid. The solid was dissolved in MeOH (15 mL) and a solution of NH_4PF_6 (16.3 mg, 0.10 mmol) in methanol (3 mL) was added. The mixture was stirred at ambient temperature overnight. After this period a white solid precipitated, which was isolated by filtration, washed with

diethyl ether and dried *in vacuo*. Yield: 25.0 mg (0.016 mmol, 80%, two steps). ^{1}H NMR (400 MHz, DMSO-d_6): δ = 9.82 (s, 4H, H_j), 8.14 (s, 4H, H_i), 8.03 (s, 4H, H_h), 7.61 (s, 4H, H_c), 7.52-7.49 (m, br, 8H, H_m), 7.46-7.43 (m, br, 12H, H_o, H_n), 7.36-7.31 (m, br, 8H, H_e, H_f), 5.46 (s, 8H, H_k), 5.01 (s, 4H, H_a) ppm. ^{13}C{^{1}H} NMR (100 MHz, DMSO-d_6): δ = 144.6 (C_g), 143.9 (C_b), 135.0 (C_j), 134.3 (C_l), 132.4 (C_d), 129.0(C_f), 128.9 (C_m), 128.5 ($C_{n,o}$), 123.4 (C_i), 121.4 (C_h), 120.4 (C_c), 119.2 (C_e), 52.5 (C_k), 51.3 (C_a) ppm. HRMS (ESI, positive ions): *m/z* = 637.1805 (calcd for [*anti*-H_4-(**2b**)+2PF_6]$^{2+}$ 637.1950).

6. Density Functional Theory Calculations.

All models were constructed using GaussView5.1 and were first optimized on the BP86D3(BJ)/def2-TZVPP-SMD level of theory (The optimizations of [Ag_2(**1a**)$_2$]$^{2+}$ and [**4a**]$^{4+}$ were carried out in CH_3CN and CH_2Cl_2 respectively; no counter ions were included). The resulting structures were then further refined by DFT calculations carried out with GAUSSAIN.[3]

6.1 DFT Calculations of [Ag_2(**1a**)$_2$]$^{2+}$.

Level of theory: BP86-D3(BJ)/def2-SVP-SMD

As illustrated in Figure S9, the *syn*-[Ag_2(**1a**)$_2$]$^{2+}$ is 2.4 kcal/mol higher than the *anti*-[Ag_2(**1a**)$_2$]$^{2+}$, which indicates that *anti*-[Ag_2(**1a**)$_2$]$^{2+}$ product is favored. Noteworthy, the calculated parameters of *anti*-[Ag_2(**1a**)$_2$]$^{2+}$ match well with the experimental parameters. ∡C-Ag C 176.5° (cal. 178.1°); N-C bond length: 1.428 Å/1.431 Å (cal. 1.431 Å /1.431 Å); C-Ag bond length: 2.089 Å /2.082 Å (cal. 2.081 Å /2.082 Å).

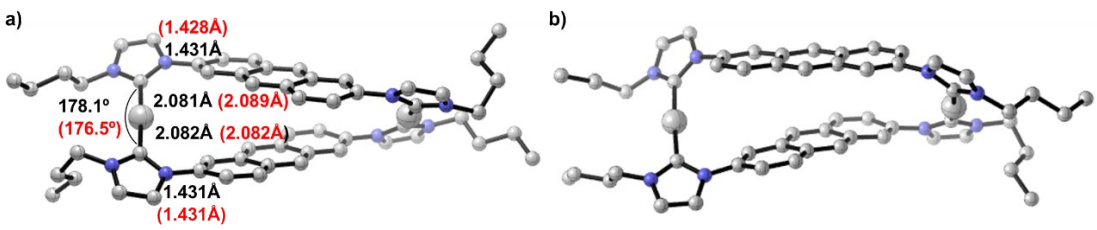

E_{RB-P86} = -1821308.1 Kcal/mol E_{RB-P86} = -1821305.7 Kcal/mol

Figure S7. DFT calculated structures and relative energies for a) *anti*-$[Ag_2(\mathbf{1a})_2]^{2+}$ and *syn*-$[Ag_2(\mathbf{1a})_2]^{2+}$ respectively.

6.2 DFT Calculations of $[\mathbf{4a}]^{4+}$.

Level of theory: BP86-D3(BJ)/def2-SVP-SMD

As illustrated in Figure S10, the *syn*-$[\mathbf{4a}]^{4+}$ was predicted to be 1.6 kcal/mol lower than the *anti*-$[\mathbf{4a}]^{4+}$, suggesting that *syn*-$[\mathbf{4a}]^{4+}$ product is preferred. It is worth noting that both *syn*-$[\mathbf{4a}]^{4+}$ isomer and *syn'*-$[\mathbf{4a}]^{4+}$ will lead to the *syn*-photodimer *syn*-**6a** after irradiation.

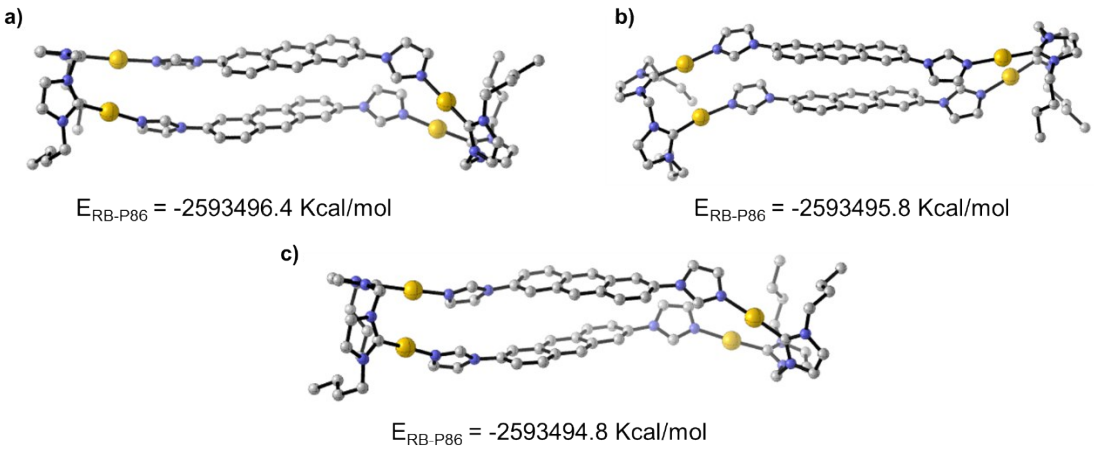

Figure S8. DFT calculated structures and relative energies for a) *syn*-$[\mathbf{4a}]^{4+}$, b) *syn'*-$[\mathbf{4a}]^{4+}$ and c) *anti*-$[\mathbf{4a}]^{4+}$ respectively.

These calculations suggested that the *syn*-$[\mathbf{4a}]^{4+}$ rectangle is the thermodynamically favored species by –1.6 kcal/mol. Although this energy difference is not so large, it is worthy to note that the anion part (OTf^-) has not been considered in the calculations. The coordination of anion part on $[\mathbf{4a}]^{4+}$, which has too many configurations and is hard to be calculated, could significantly improve the relative stability of *syn*-$[\mathbf{4a}]^{4+}$ to *anti*-$[\mathbf{4a}]^{4+}$.

7. Selected NMR, Luminescence and MS Spectra for New Compounds.

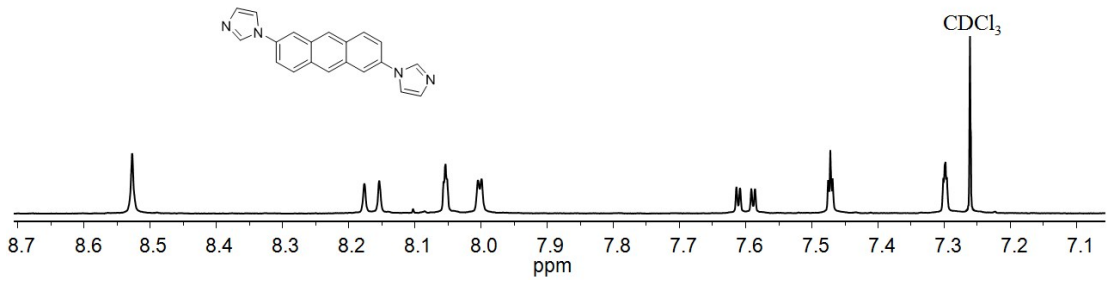

Figure S9. ^{1}H NMR spectrum (400 MHz in $CDCl_3$) of **L1**.

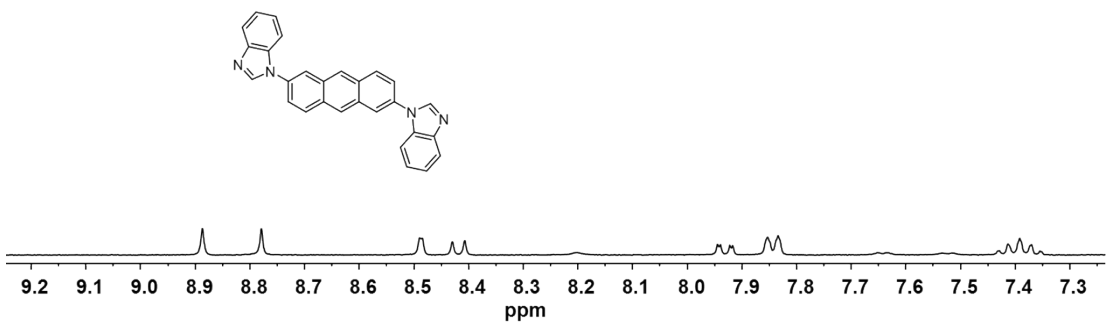

Figure S10. Section of ^{1}H NMR spectrum (400 MHz in DMSO-d_6) of **L2**.

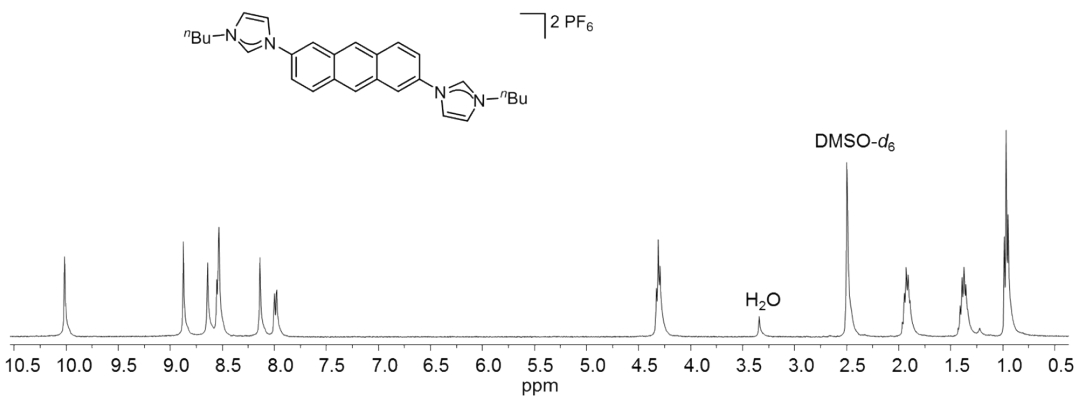

Figure S11. ^{1}H NMR spectrum (400 MHz in DMSO-d_6) of H_2-**1a**$(PF_6)_2$.

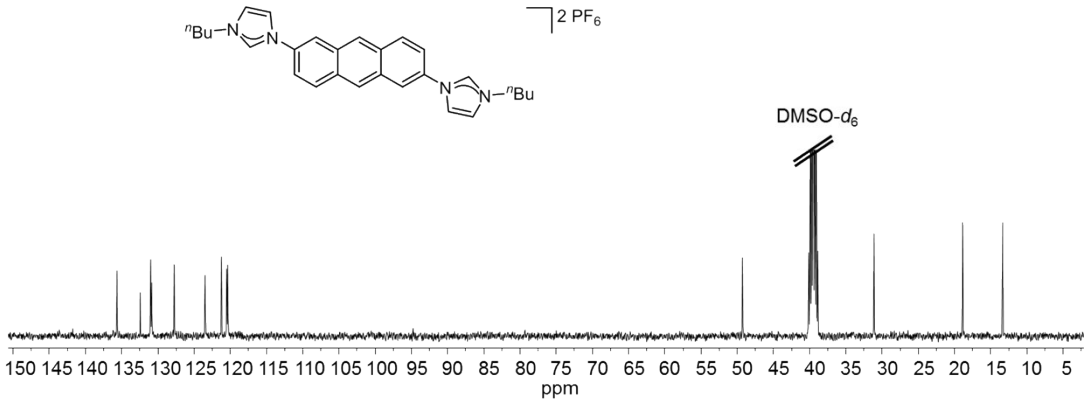

Figure S12. ^{13}C NMR spectrum (100 MHz in DMSO-d_6) of H_2-**1a**$(PF_6)_2$.

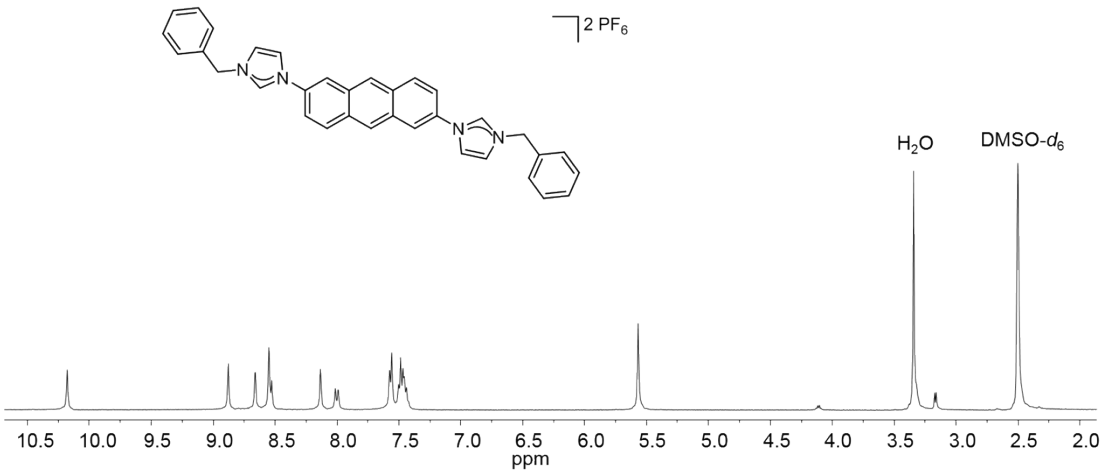

Figure S13. ^{1}H NMR spectrum (400 MHz in DMSO-d_6) of H_2-**1b**$(PF_6)_2$.

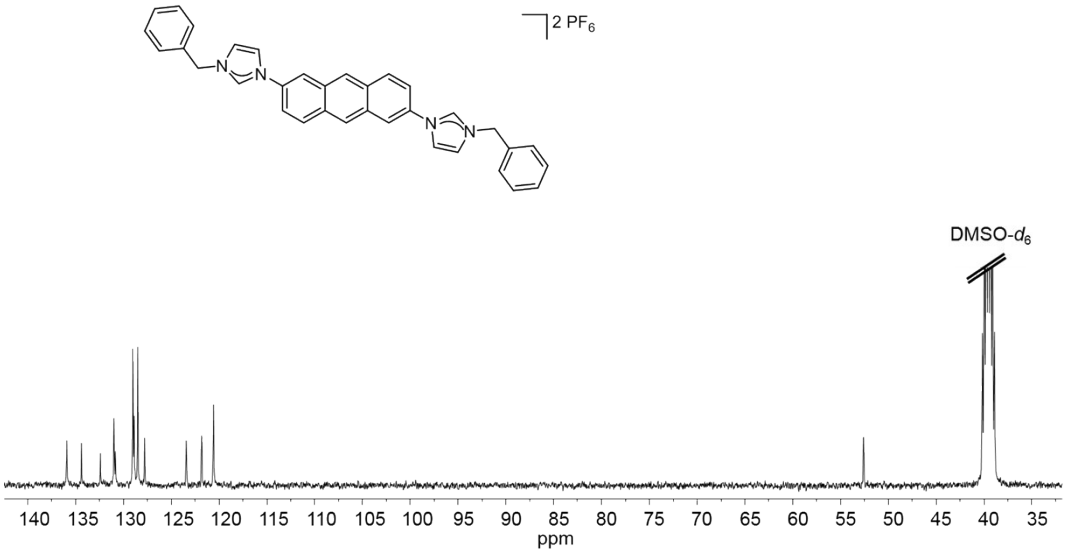

Figure S14. ^{13}C NMR spectrum (100 MHz in DMSO-d_6) of H_2-**1b**$(PF_6)_2$.

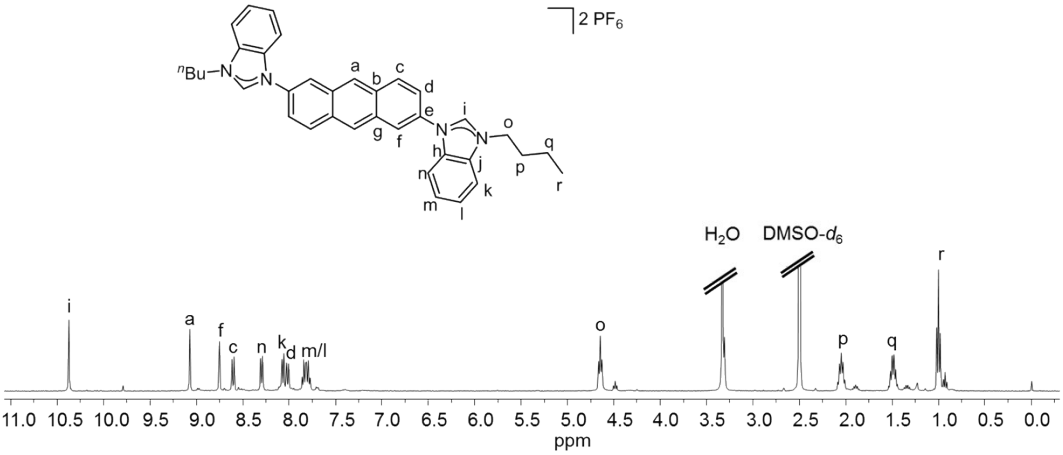

Figure S15. ^{1}H NMR spectrum (400 MHz in DMSO-d_6) of H_2-**1c**$(PF_6)_2$.

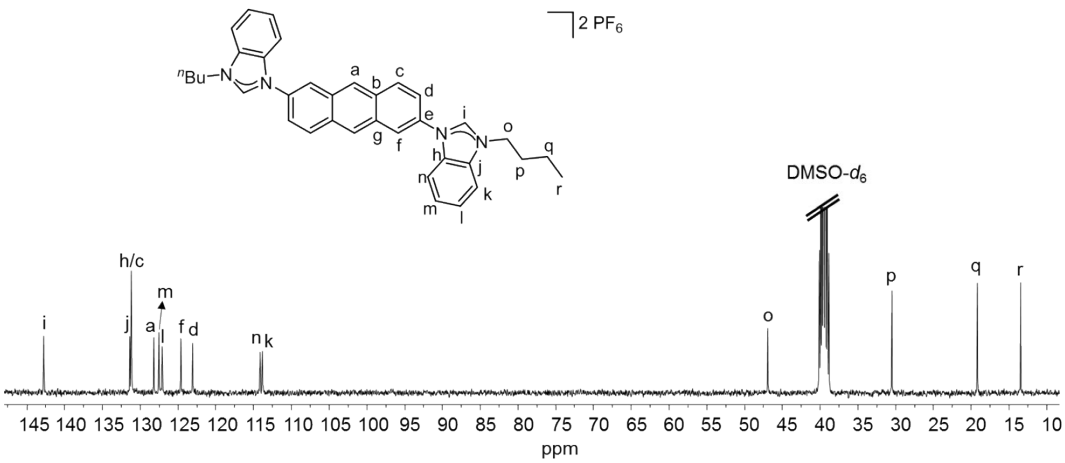

Figure S16. ^{13}C NMR spectrum (100 MHz in DMSO-d_6) of H_2-**1c**$(PF_6)_2$.

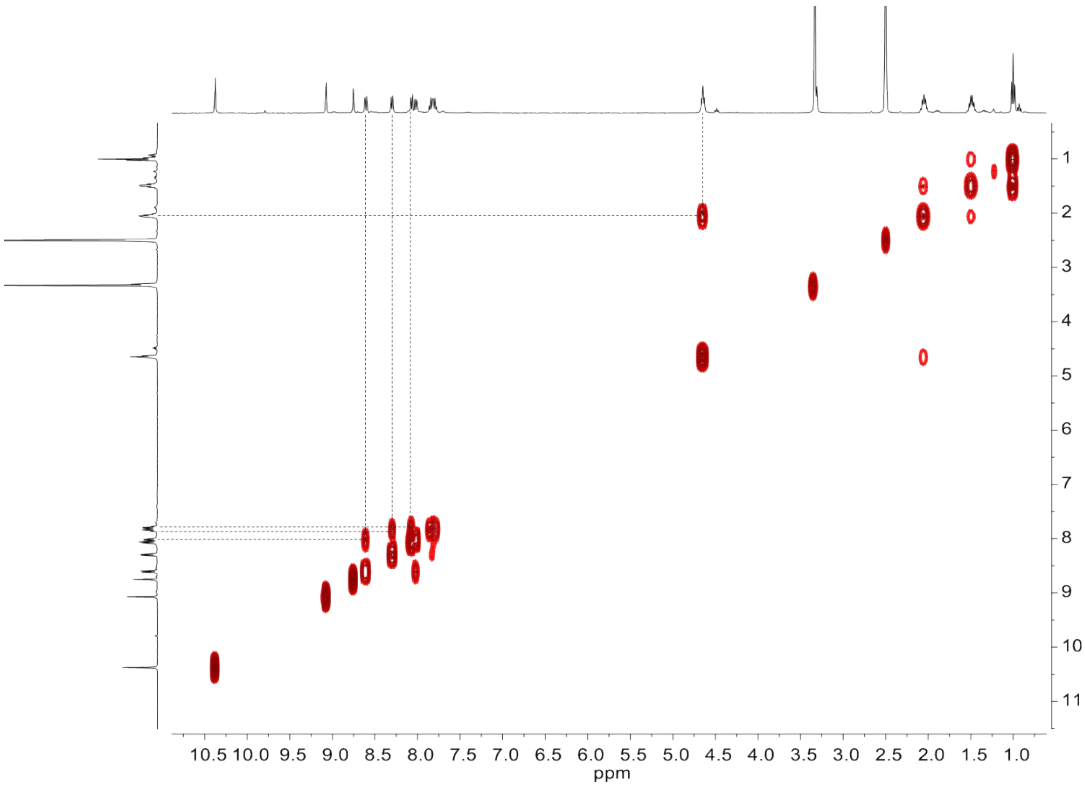

Figure S17. ^{1}H-^{1}H COSY spectrum (400 MHz in DMSO-d_6) of H_2-**1c**$(PF_6)_2$.

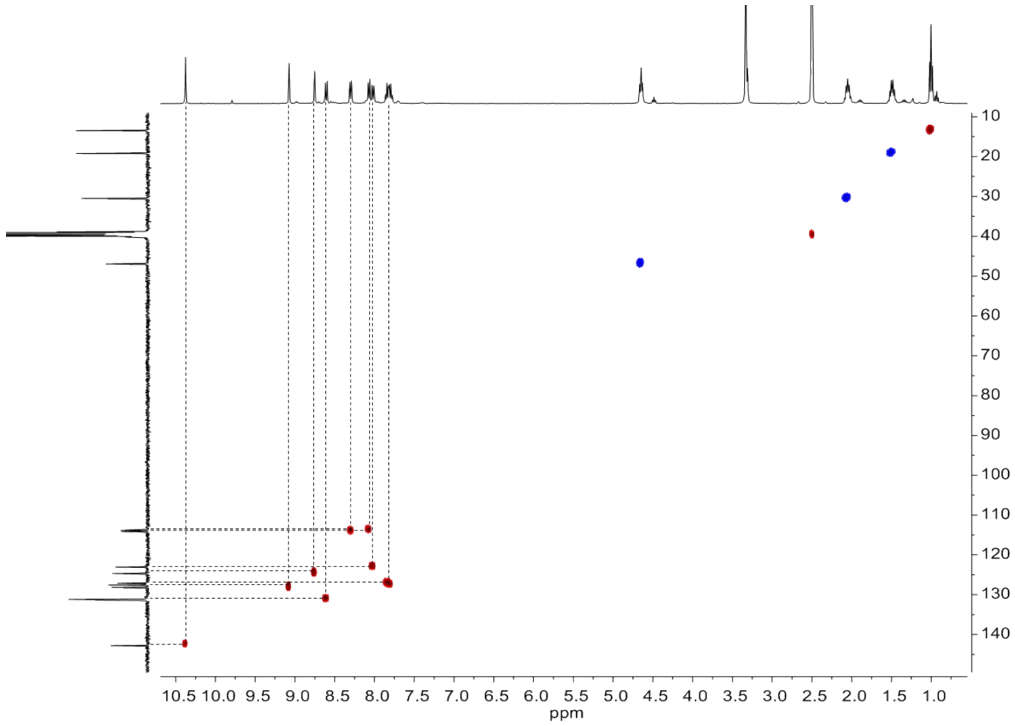

Figure S18. ^{1}H-^{13}C HSQC spectrum (400 MHz in DMSO-d_6) of H_2-**1c**$(PF_6)_2$.

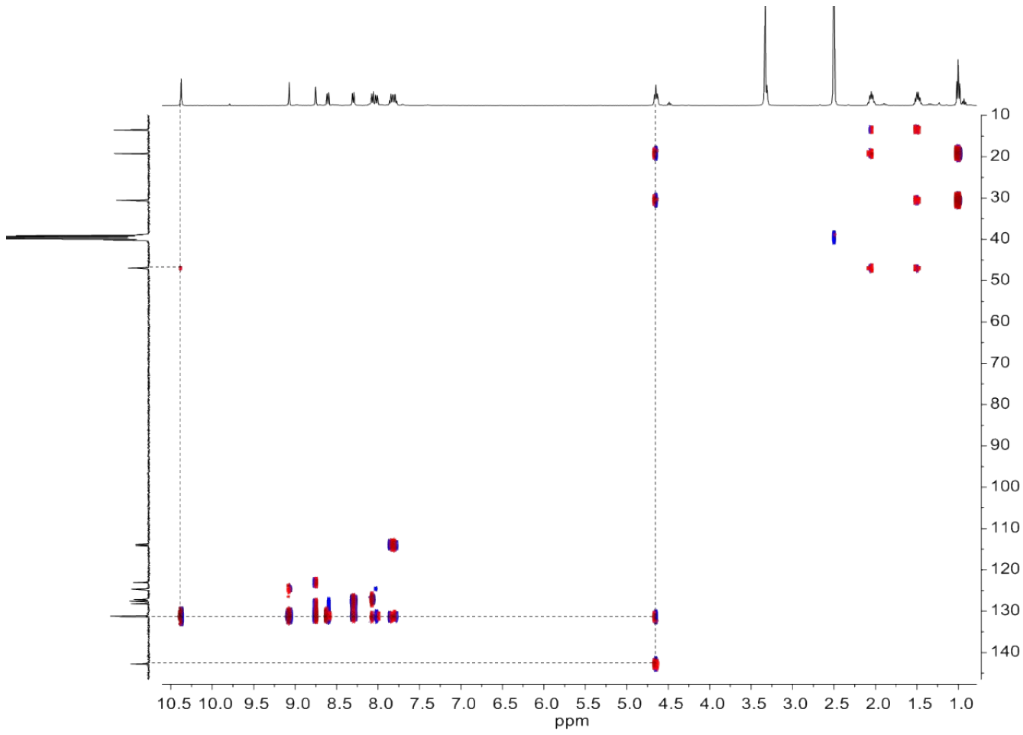

Figure S19. ^{1}H-^{13}C HMBC spectrum (400 MHz in DMSO-d_6) of H_2-**1c**$(PF_6)_2$.

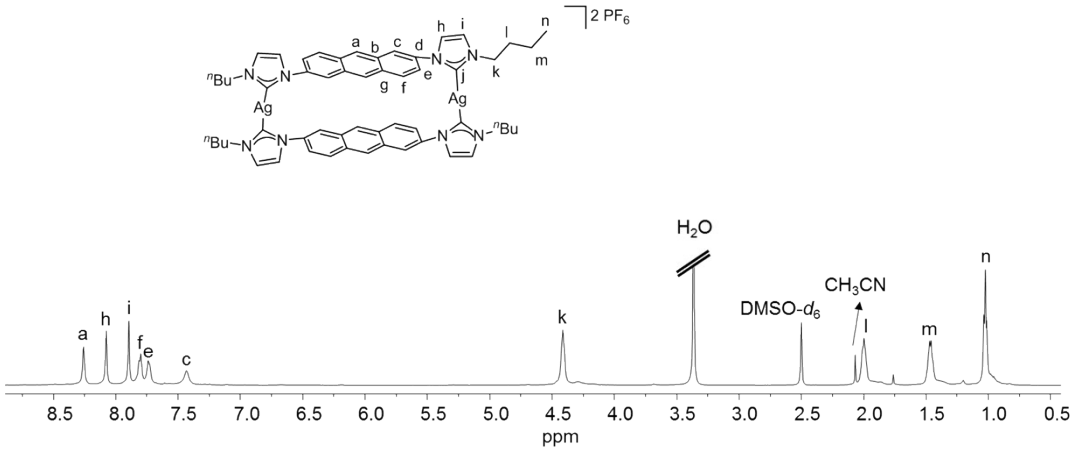

Figure S20. ^{1}H NMR spectrum (600 MHz in DMSO-d_6) of *anti*-[Ag_2(**1a**)$_2$](PF_6)$_2$.

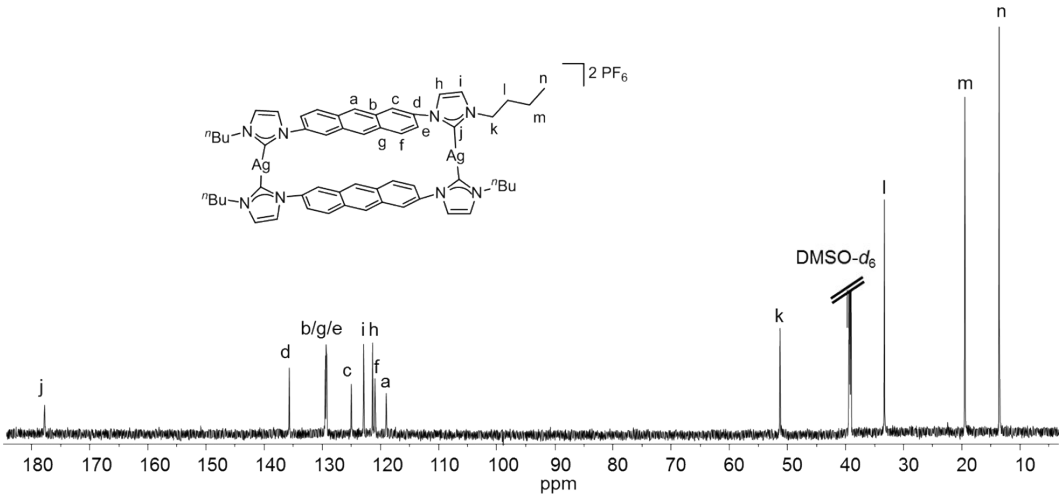

Figure S21. ^{13}C NMR spectrum (150 MHz in DMSO-d_6) of *anti*-[Ag_2(**1a**)$_2$](PF_6)$_2$

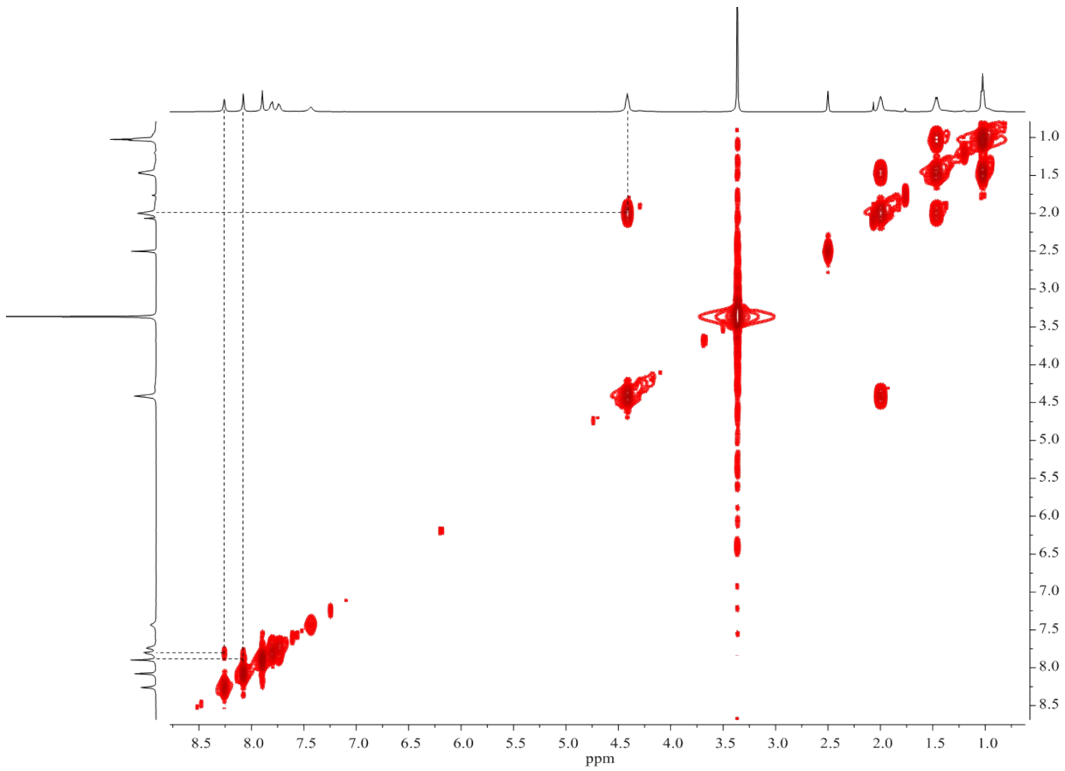

Figure S22. ^{1}H-^{1}H COSY spectrum (600 MHz in DMSO-d_6) of *anti*-[Ag_2(**1a**)$_2$](PF_6)$_2$.

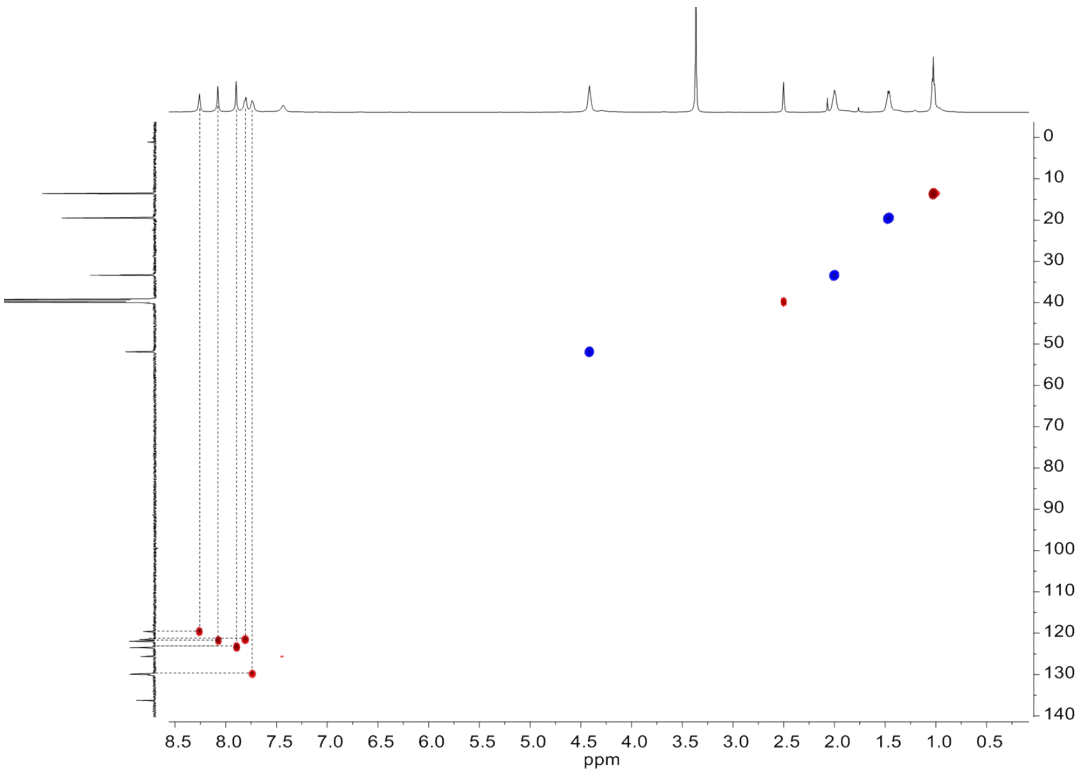

Figure S23. ^{1}H-^{13}C HSQC spectrum (600 MHz in DMSO-d_6) of *anti*-[Ag_2(**1a**)$_2$](PF_6)$_2$.

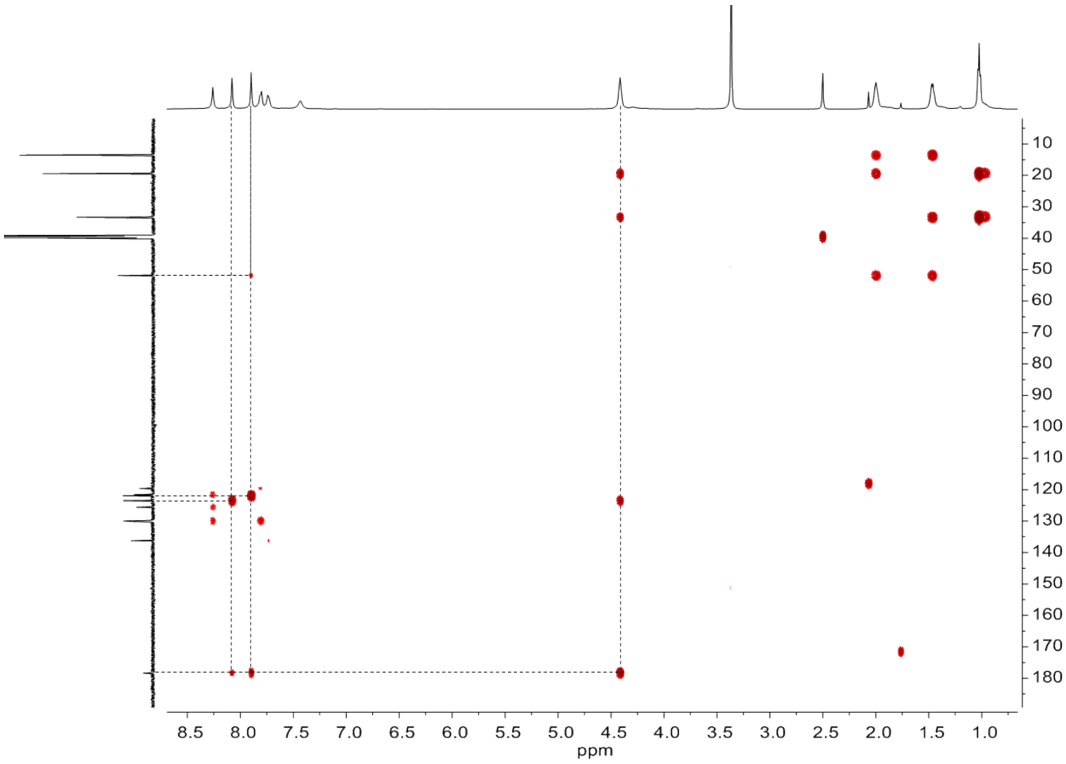

Figure S24. ^{1}H-^{13}C HMBC spectrum (600 MHz in DMSO-d_6) of *anti*-[Ag_2(**1a**)$_2$](PF_6)$_2$.

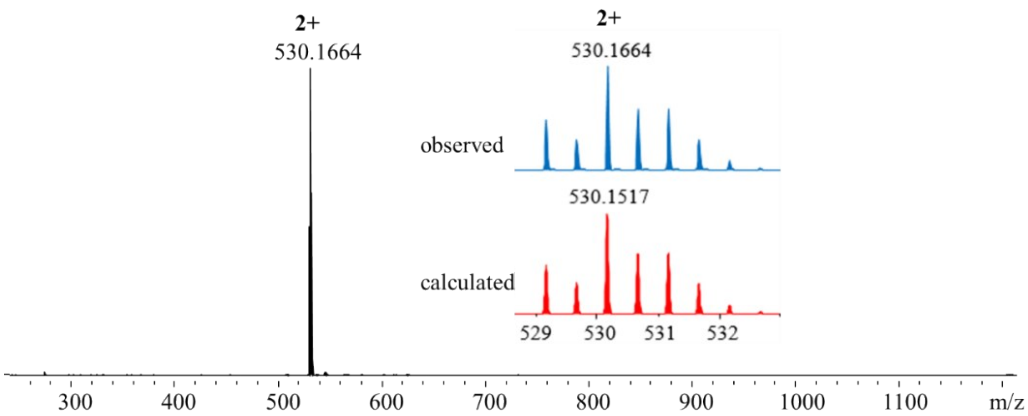

Figure S25. ESI-TOF mass spectrum of *anti*-[Ag_2(**1a**)$_2$](PF_6)$_2$ with isotope distribution for selected peaks.

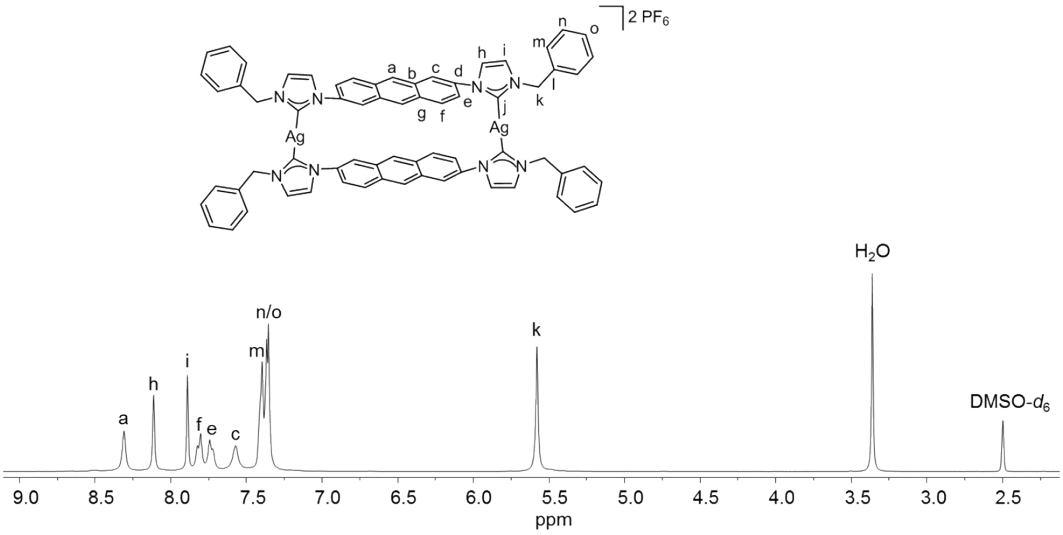

Figure S26. ^{1}H NMR spectrum (400 MHz in DMSO-d_6) of *anti*-[Ag_2(**1b**)$_2$](PF_6)$_2$.

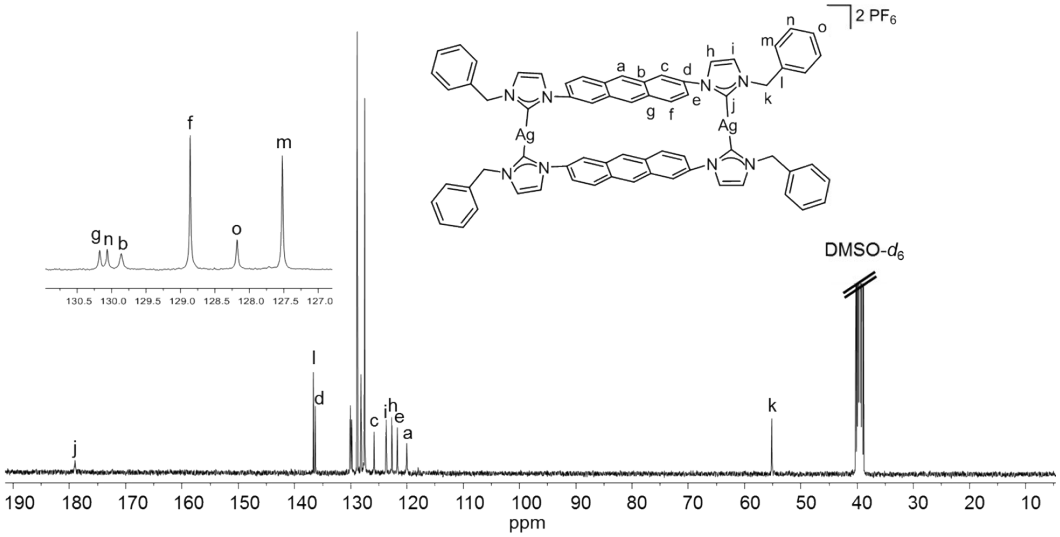

Figure S27. ^{13}C NMR spectrum (100 MHz in DMSO-d_6) of *anti*-[Ag_2(**1b**)$_2$](PF_6)$_2$.

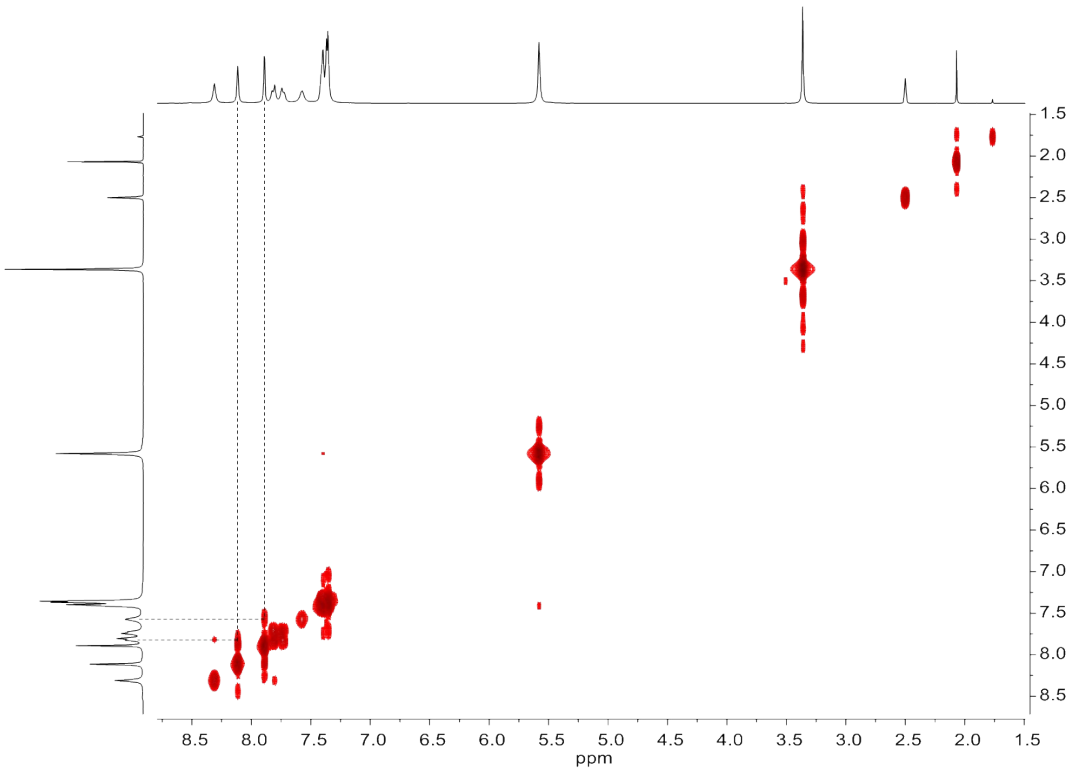

Figure S28. ^{1}H-^{1}H COSY spectrum (400 MHz in DMSO-d_6) of *anti*-[Ag_2(**1b**)$_2$](PF_6)$_2$.

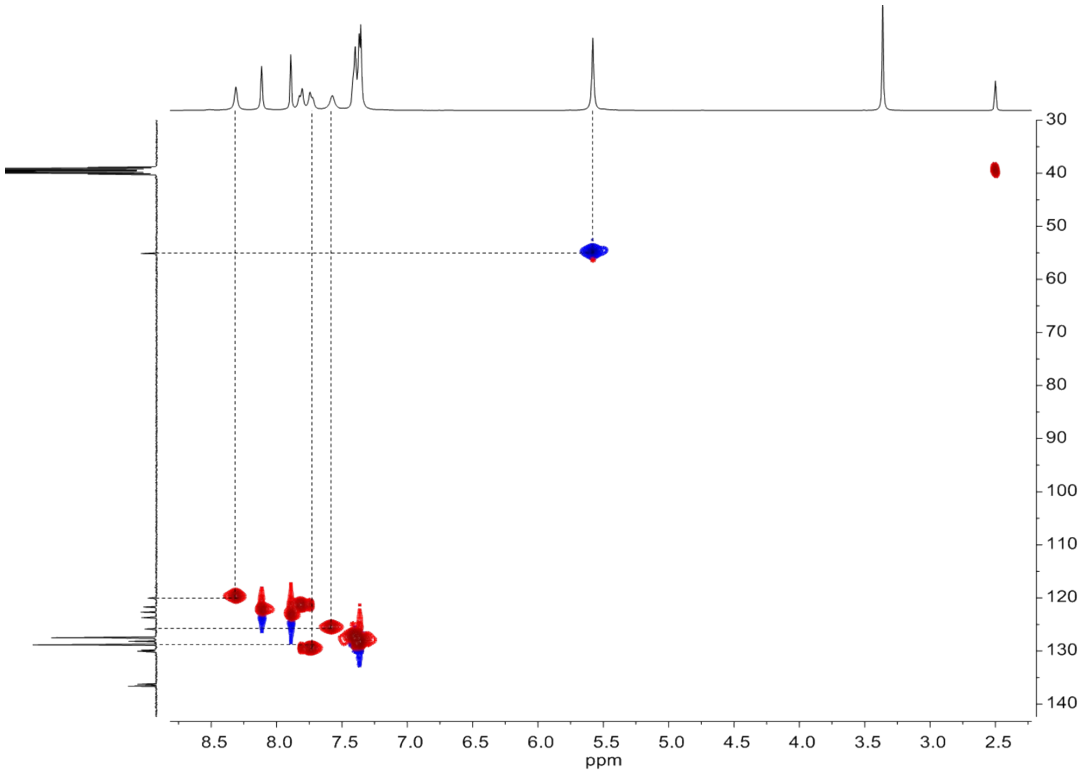

Figure S29. ^{1}H-^{13}C HSQC spectrum (400 MHz in DMSO-d_6) of *anti*-[Ag_2(**1b**)$_2$](PF_6)$_2$.

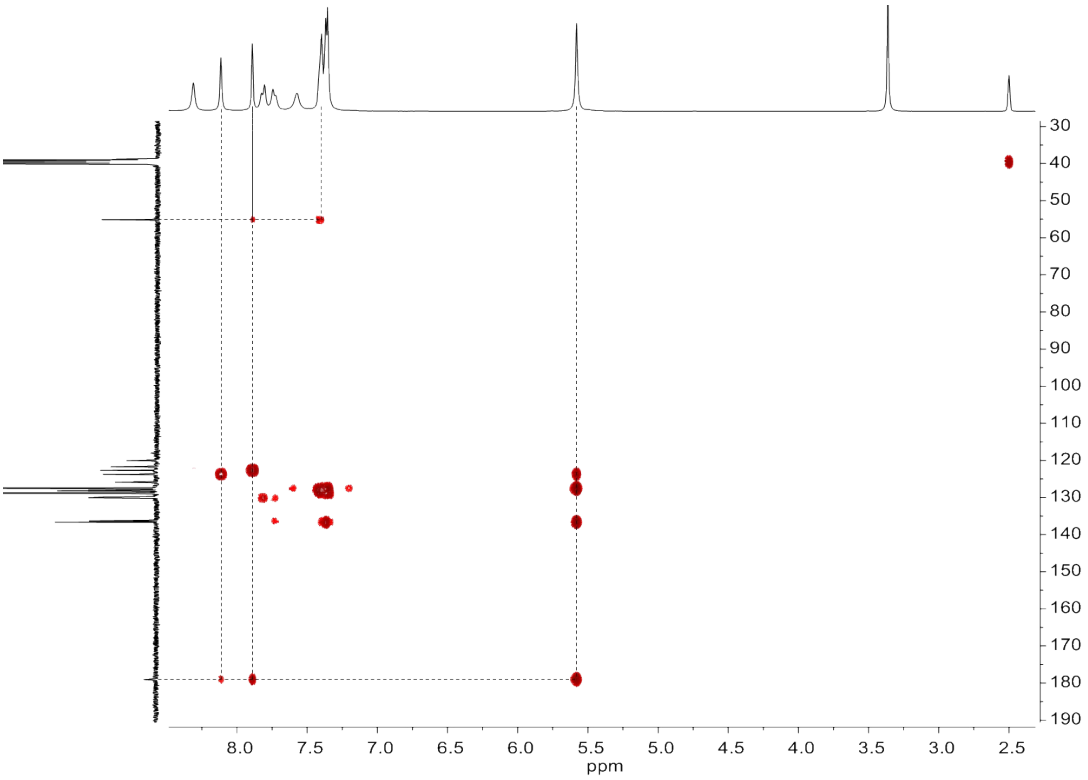

Figure S30. ^{1}H-^{13}C HMBC spectrum (400 MHz in DMSO-d_6) of *anti*-[Ag_2(**1b**)$_2$](PF_6)$_2$.

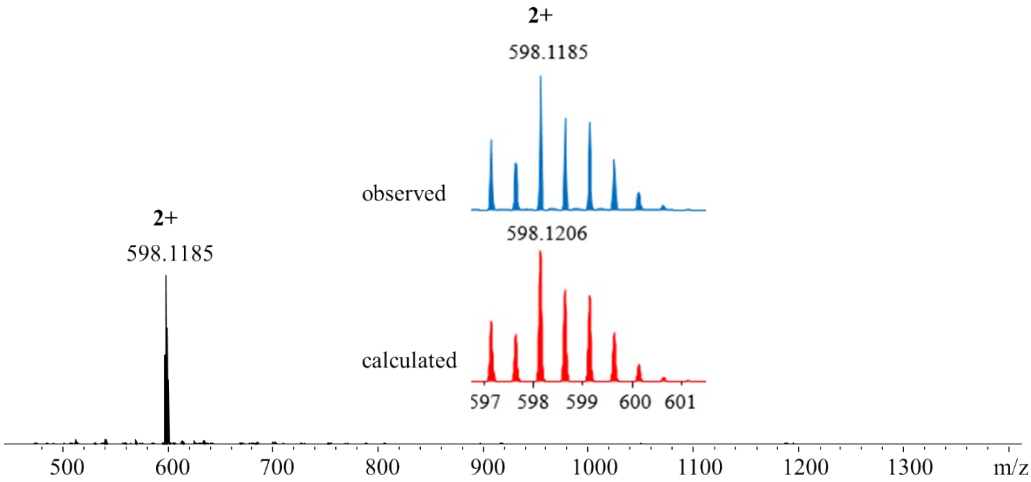

Figure S31. ESI-TOF mass spectrum of *anti*-[Ag_2(**1b**)$_2$](PF_6)$_2$ with isotope distribution for selected peaks.

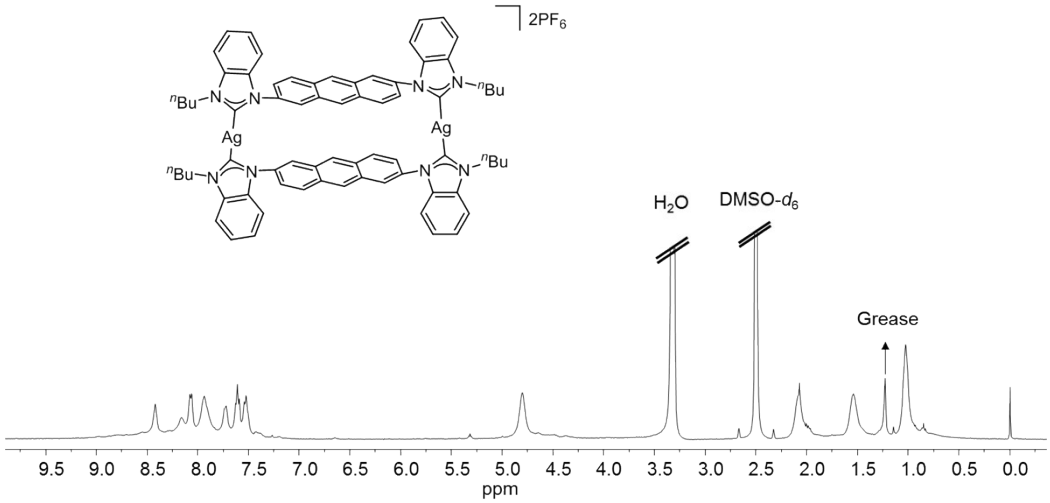

Figure S32. ^{1}H NMR spectrum (400 MHz in DMSO-d_6) of *anti*-[Ag_2(**1c**)$_2$](PF_6)$_2$.

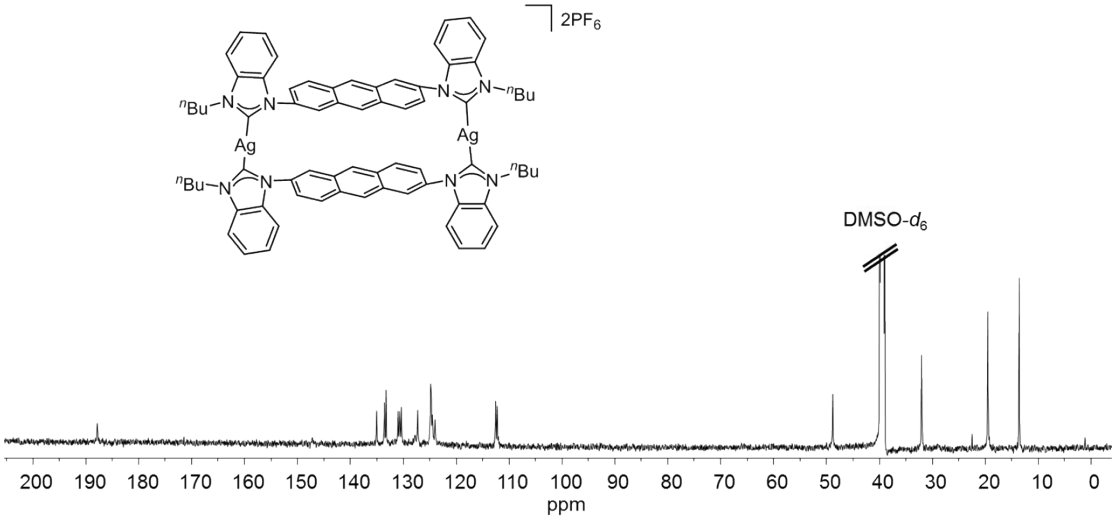

Figure S33. ^{13}C NMR spectrum (100 MHz in DMSO-d_6) of *anti*-[Ag_2(**1c**)$_2$](PF_6)$_2$.

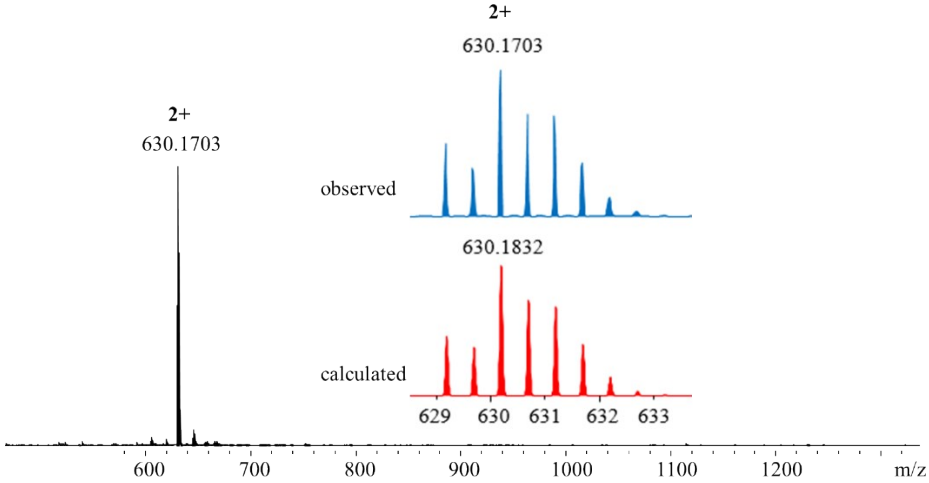

Figure S34. ESI-TOF mass spectrum of *anti*-[Ag_2(**1c**)$_2$](PF_6)$_2$ with isotope distribution for selected peaks.

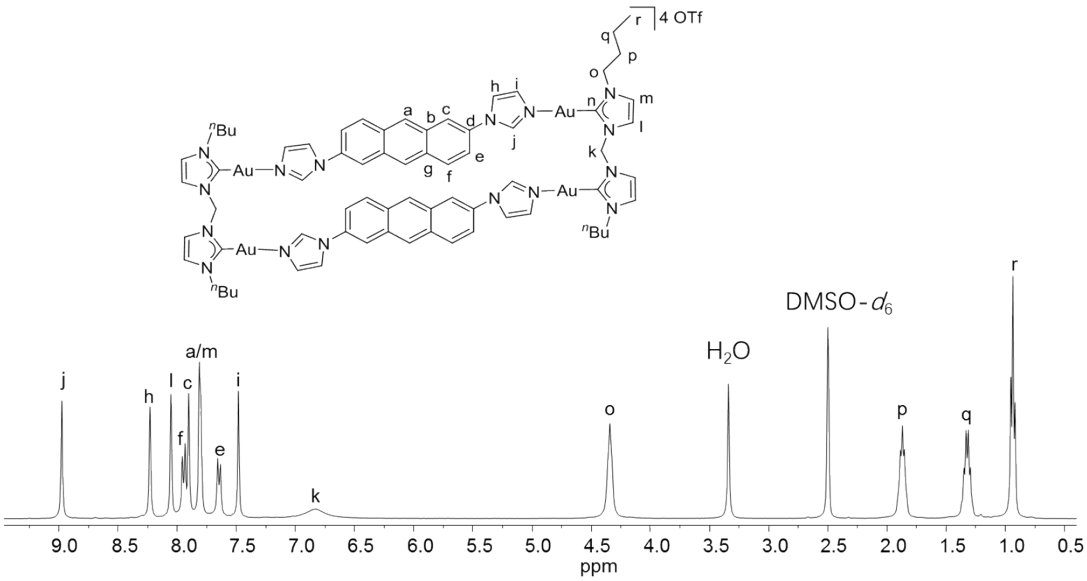

Figure S35. ^{1}H NMR spectrum (400 MHz, DMSO-d_6) of *syn*-[**4a**](OTf)$_4$.

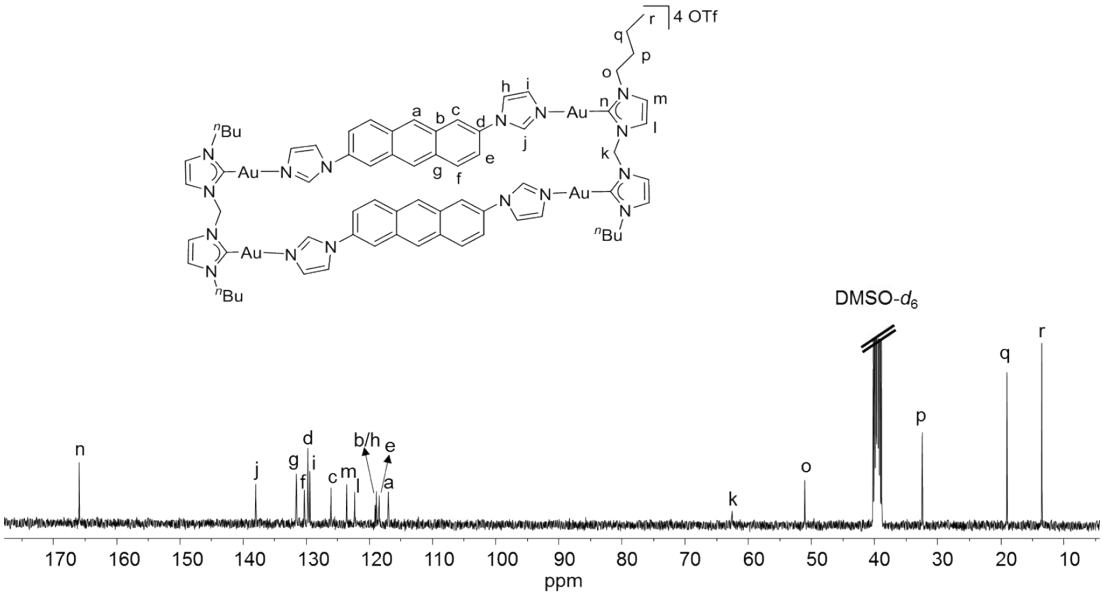

Figure S36. ^{13}C NMR spectrum (100 MHz, DMSO-d_6) of *syn*-[**4a**](OTf)$_4$.

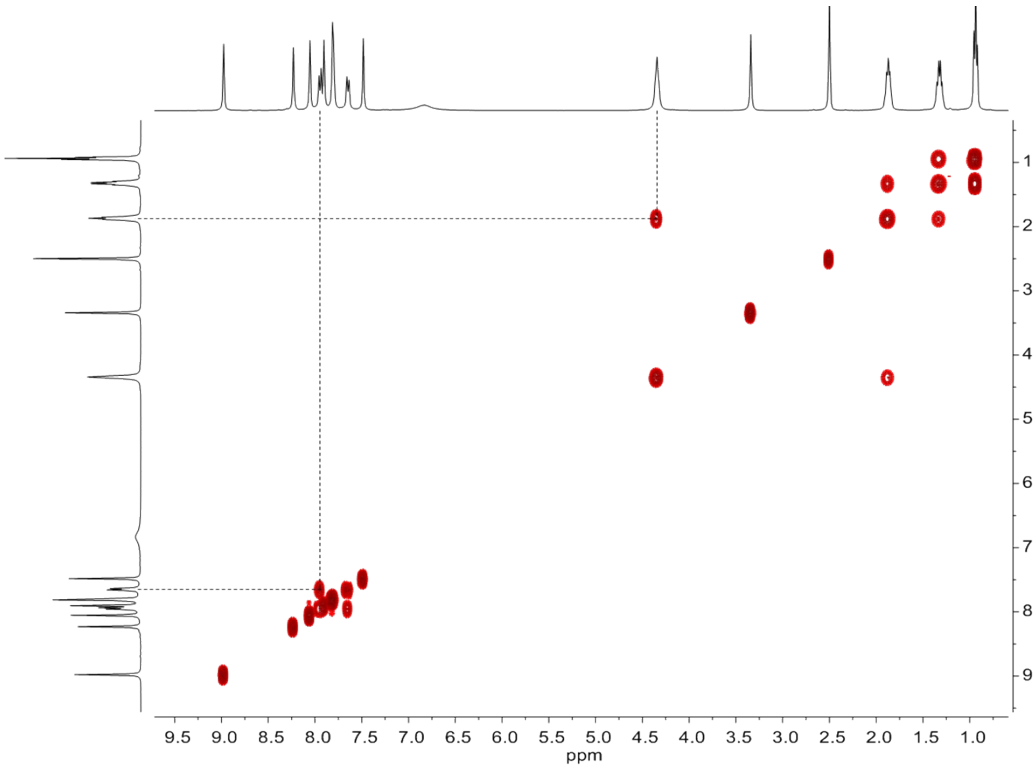

Figure S37. ^{1}H-^{1}H-COSY spectrum (400 MHz, DMSO-d_6) of *syn*-[**4a**](OTf)$_4$.

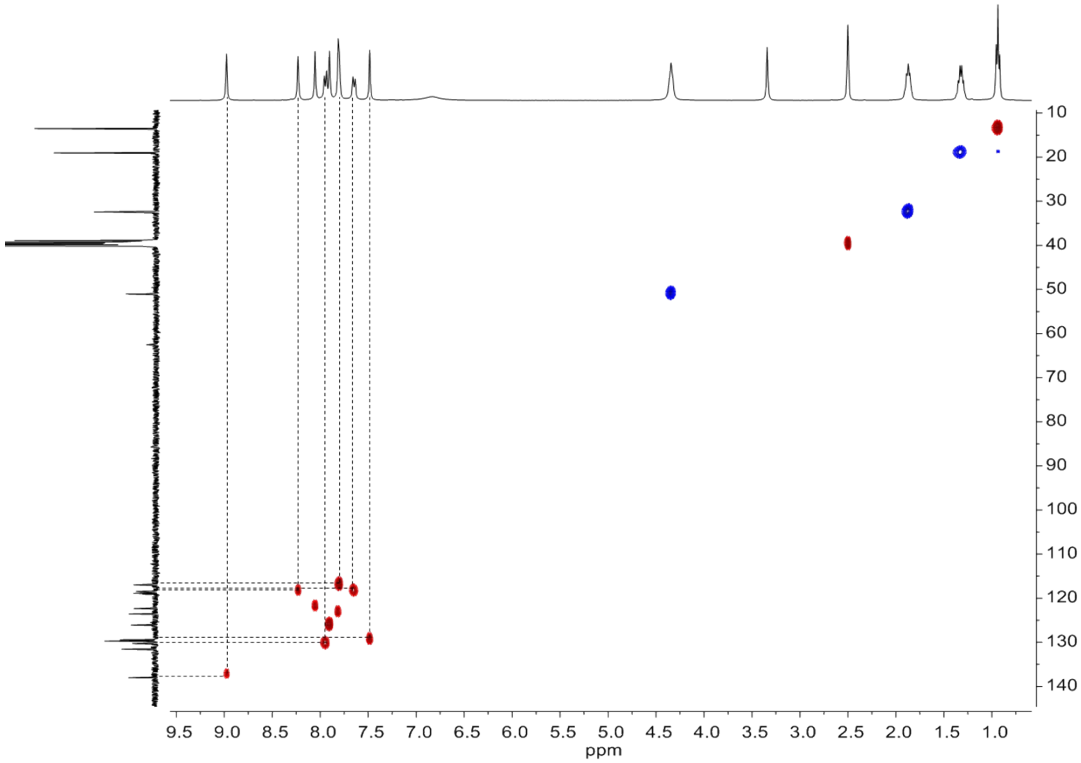

Figure S38. ^{1}H-^{13}C HSQC spectrum (400 MHz, DMSO-d_6) of *syn*-[**4a**](OTf)$_4$.

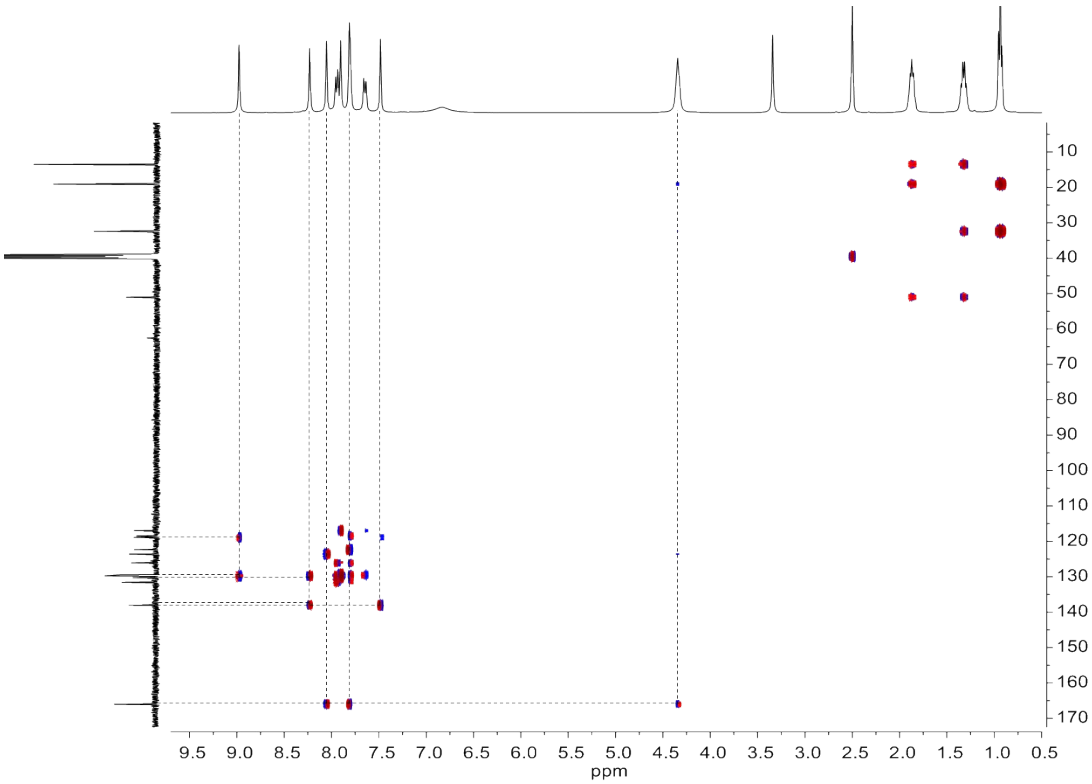

Figure S39. ^{1}H-^{13}C-HMBC spectrum (400 MHz, DMSO-d_6) of *syn*-[**4a**](OTf)$_4$.

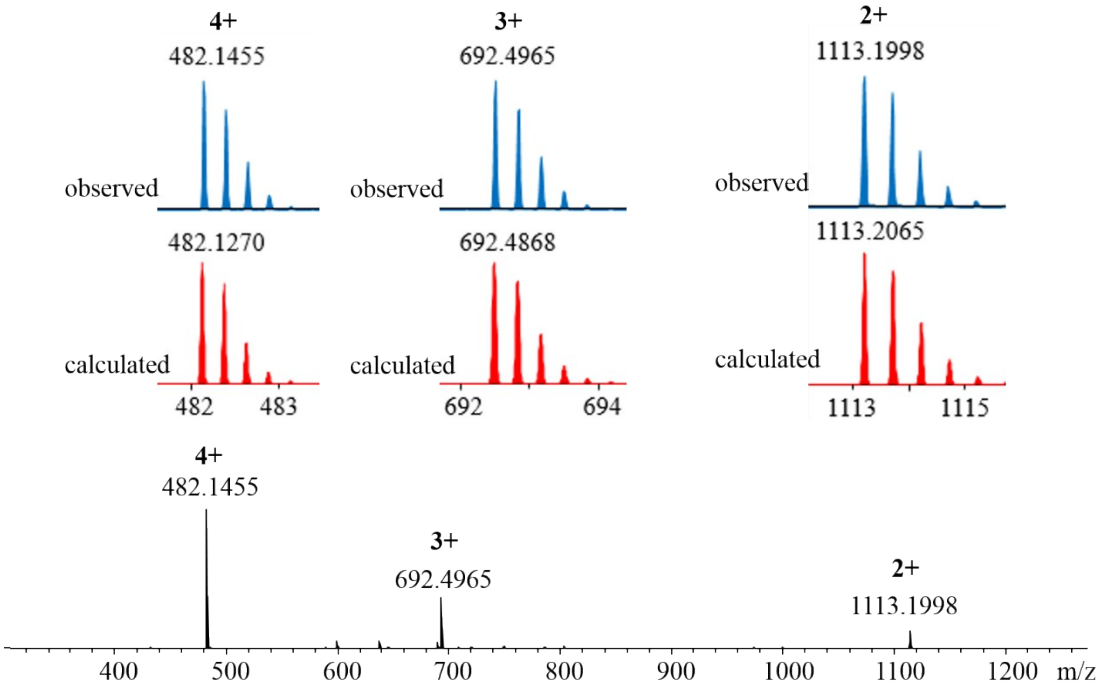

Figure S40. ESI-TOF mass spectrum of *syn*-[**4a**](OTf)$_4$ with isotope distribution for selected peaks.

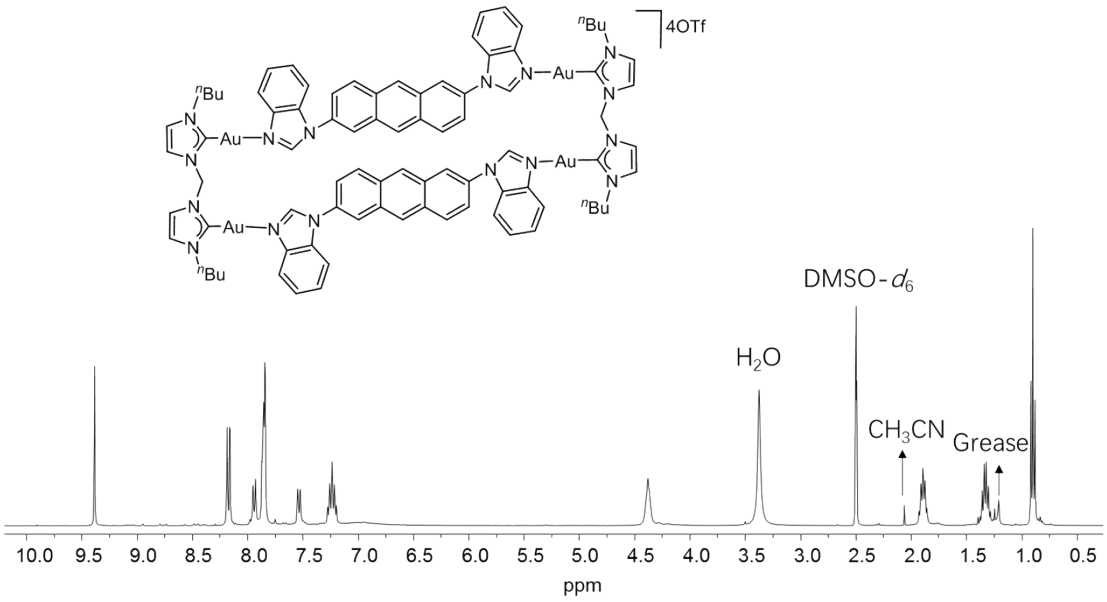

Figure S41. ^{1}H NMR spectrum (400 MHz, DMSO-d_6) of *syn*-[**4b**](OTf)$_4$.

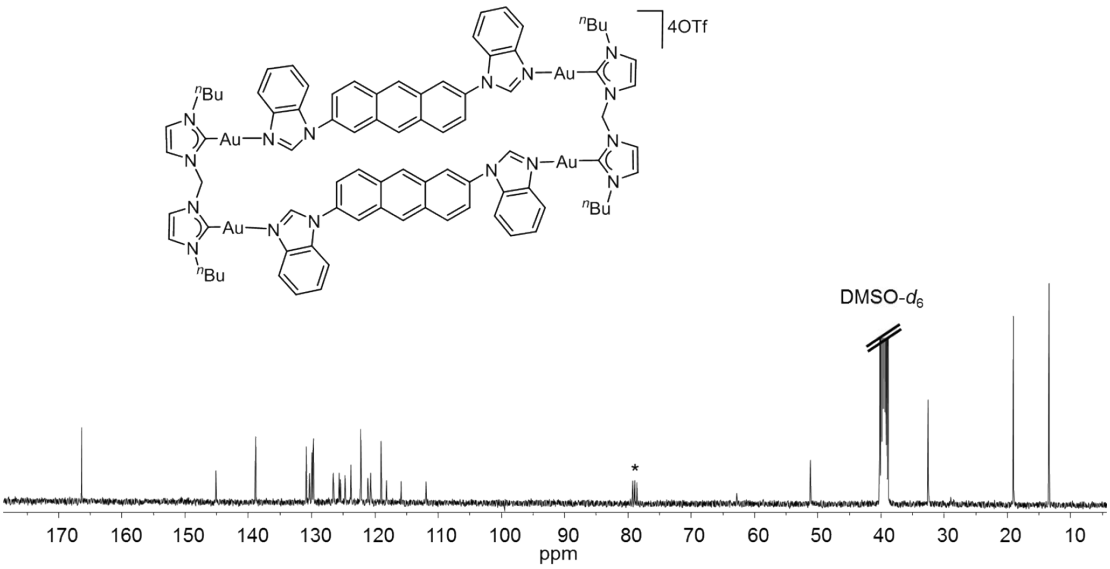

Figure S42. ^{13}C NMR spectrum (100 MHz, DMSO-d_6) of *syn*-[**4b**](OTf)$_4$. * = Chloroform.

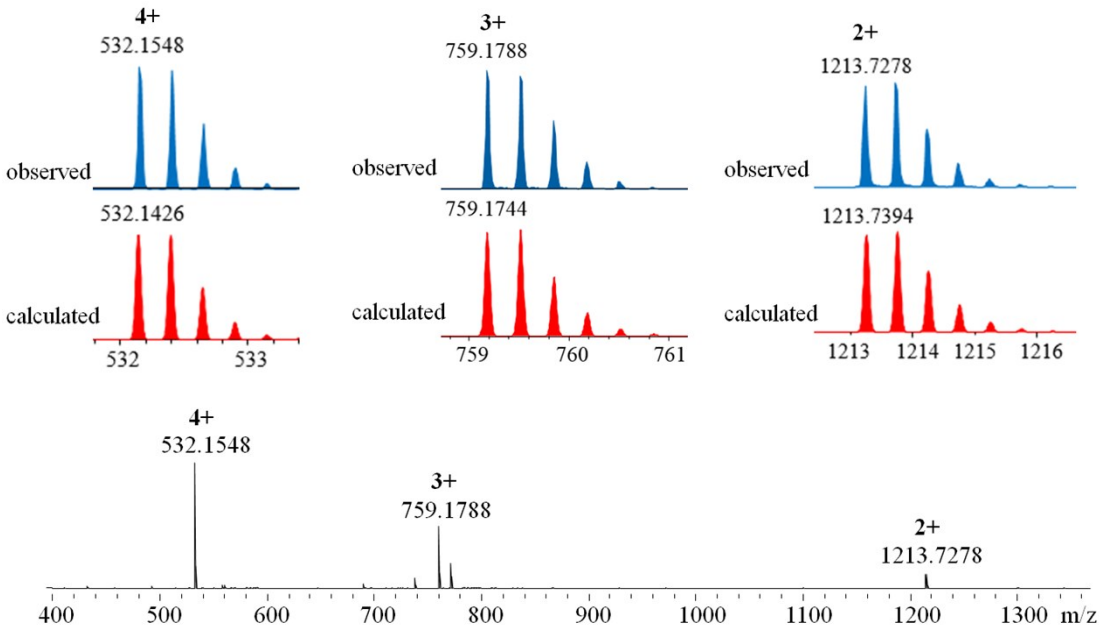

Figure S43. ESI-TOF mass spectrum of *syn*-[**4b**](OTf)$_4$ with isotope distribution for selected peaks.

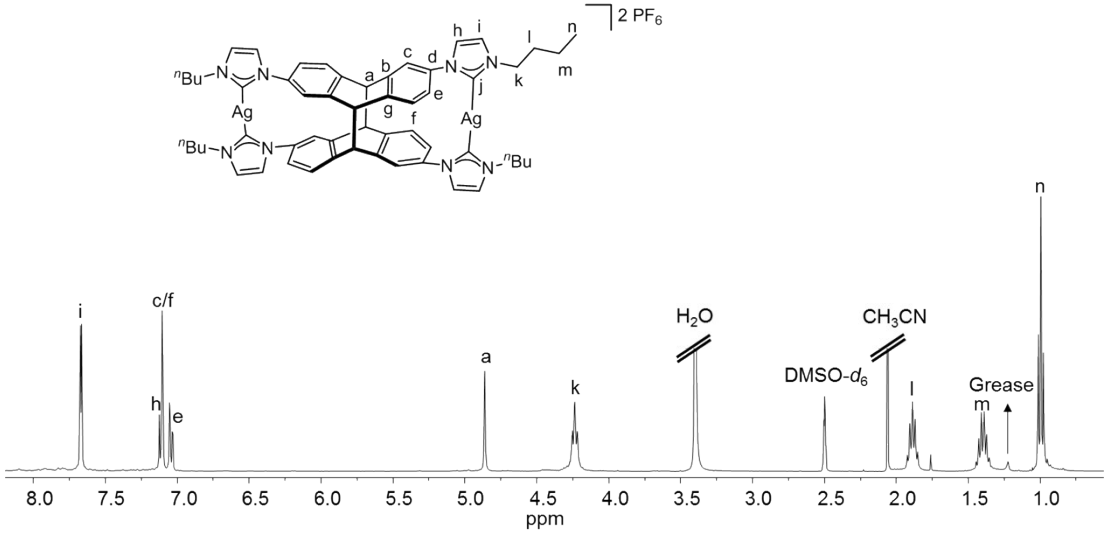

Figure S44. ^{1}H NMR spectrum (400 MHz in DMSO-d_6) of *anti*-[Ag_2(**2a**)](PF_6)$_2$.

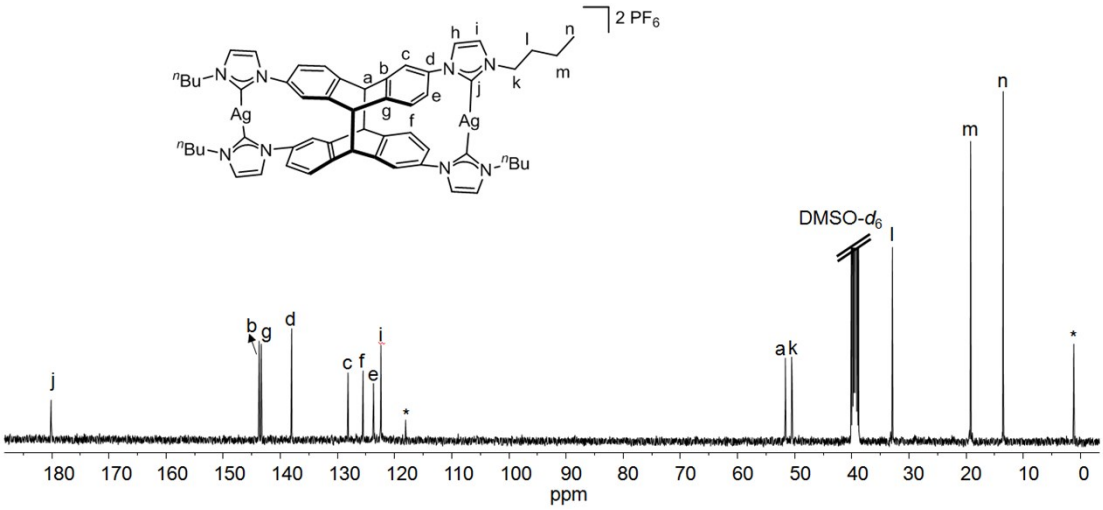

Figure S45. ^{13}C NMR spectrum (100 MHz in DMSO-d_6) of *anti*-[Ag_2(**2a**)](PF_6)$_2$. * = Acetonitrile.

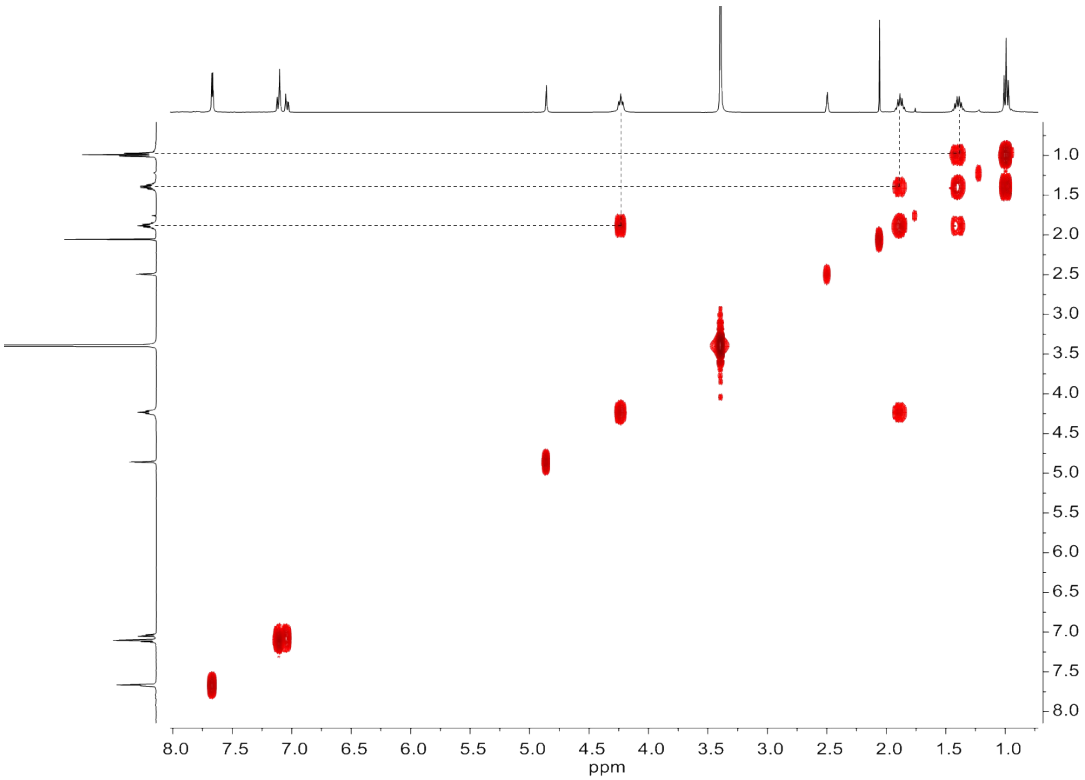

Figure S46. ^{1}H-^{1}H COSY spectrum (400 MHz in DMSO-d_6) of *anti*-[Ag_2(**2a**)](PF_6)$_2$.

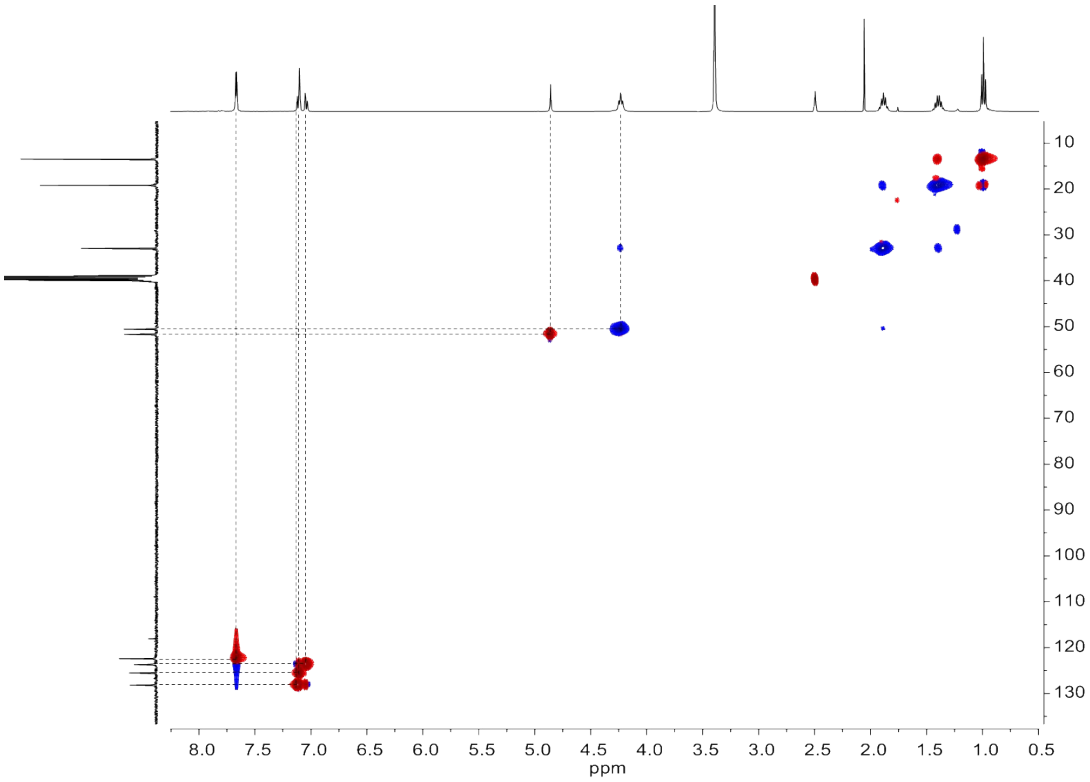

Figure S47. ^{1}H-^{13}C HSQC spectrum (400 MHz in DMSO-d_6) of *anti*-[Ag_2(**2a**)](PF_6)$_2$.

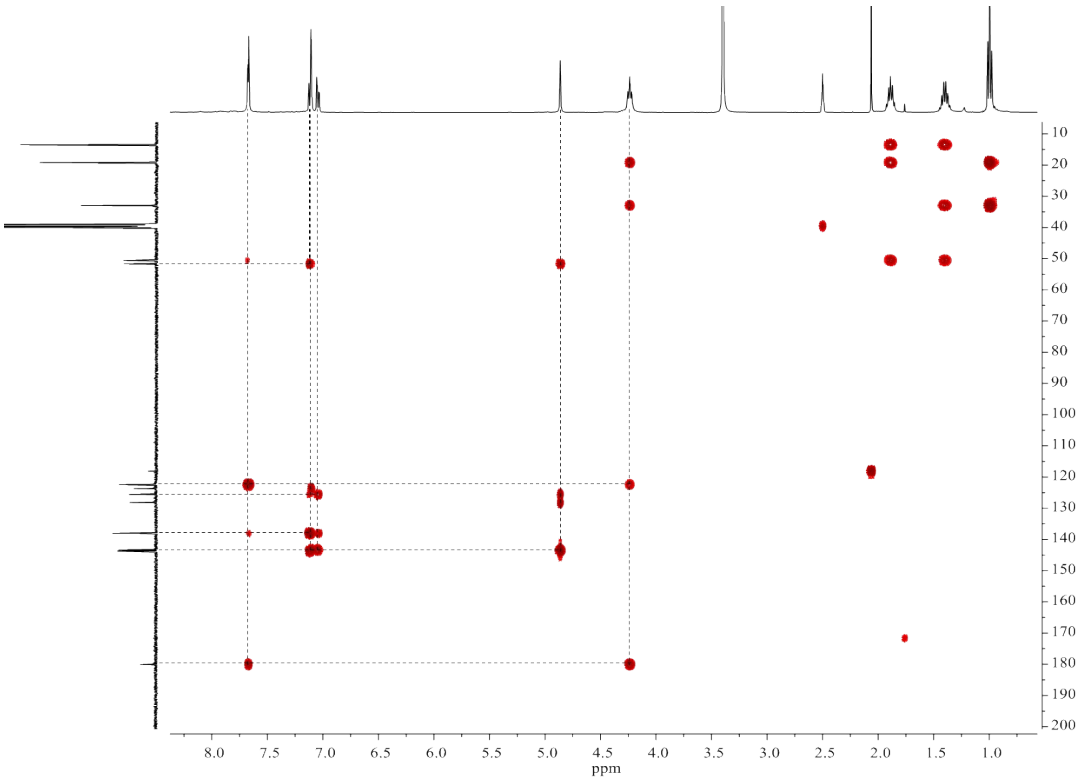

Figure S48. ^{1}H-^{13}C HMBC spectrum (400 MHz in DMSO-d_6) of *anti*-[Ag_2(**2a**)](PF_6)$_2$.

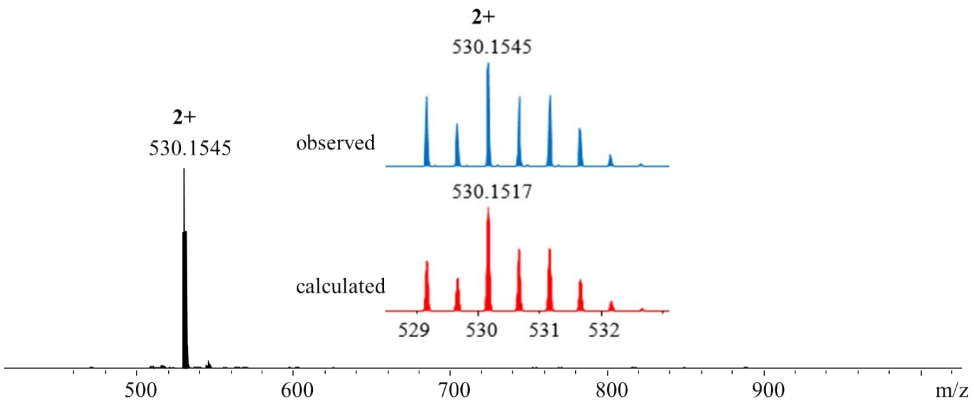

Figure S49. ESI-TOF mass spectrum of *anti*-[Ag_2(**2a**)](PF_6)$_2$ with isotope distribution for selected peaks.

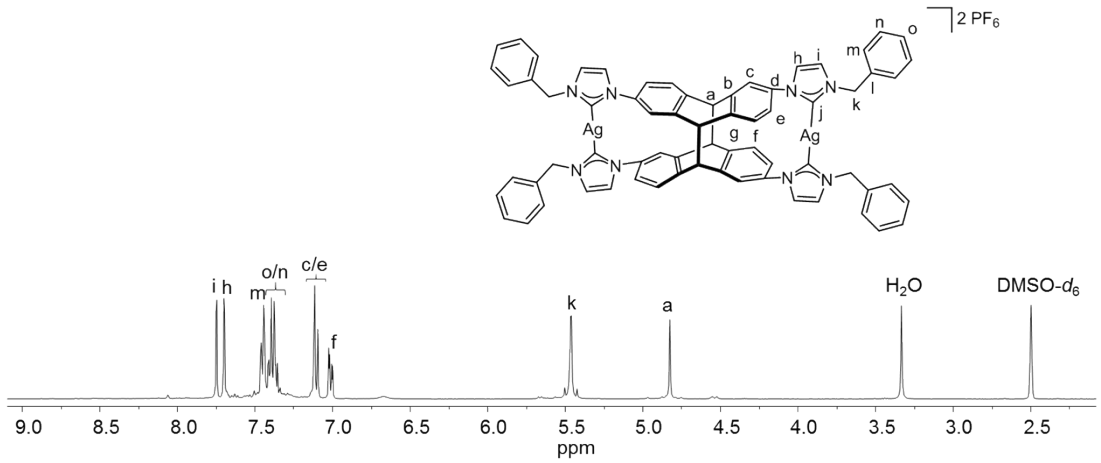

Figure S50. ^{1}H NMR spectrum (400 MHz in DMSO-d_6) of *anti*-[Ag_2(**2b**)](PF_6)$_2$.

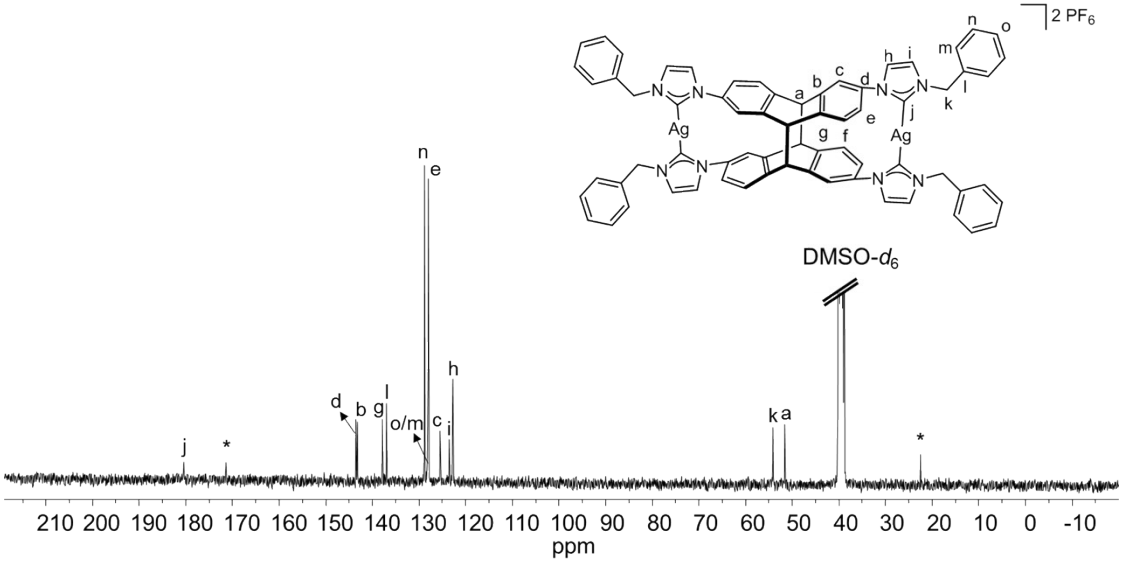

Figure S51. ^{13}C NMR spectrum (100 MHz in DMSO-d_6) of *anti*-[Ag_2(**2b**)](PF_6)$_2$. * = Acetic acid, from acetonitrile.

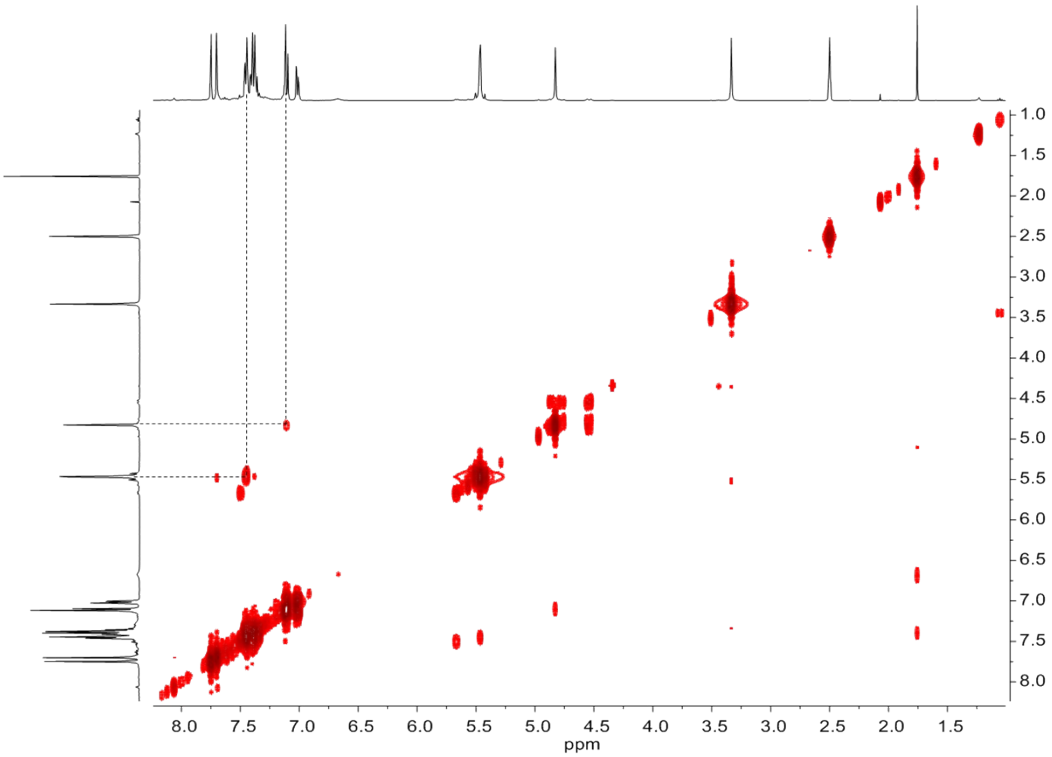

Figure S52. ^{1}H-^{1}H COSY spectrum (400 MHz in DMSO-d_6) of *anti*-[Ag_2(**2b**)](PF_6)$_2$.

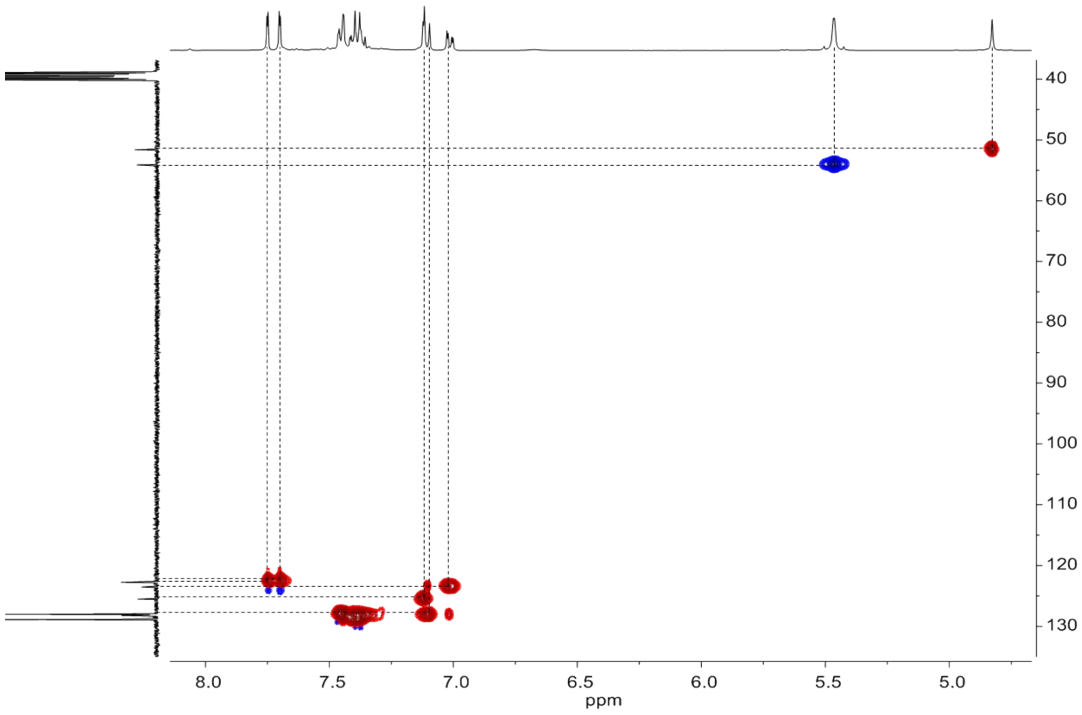

Figure S53. ^{1}H-^{13}C HSQC spectrum (400 MHz in DMSO-d_6) of *anti*-[Ag_2(**2b**)](PF_6)$_2$.

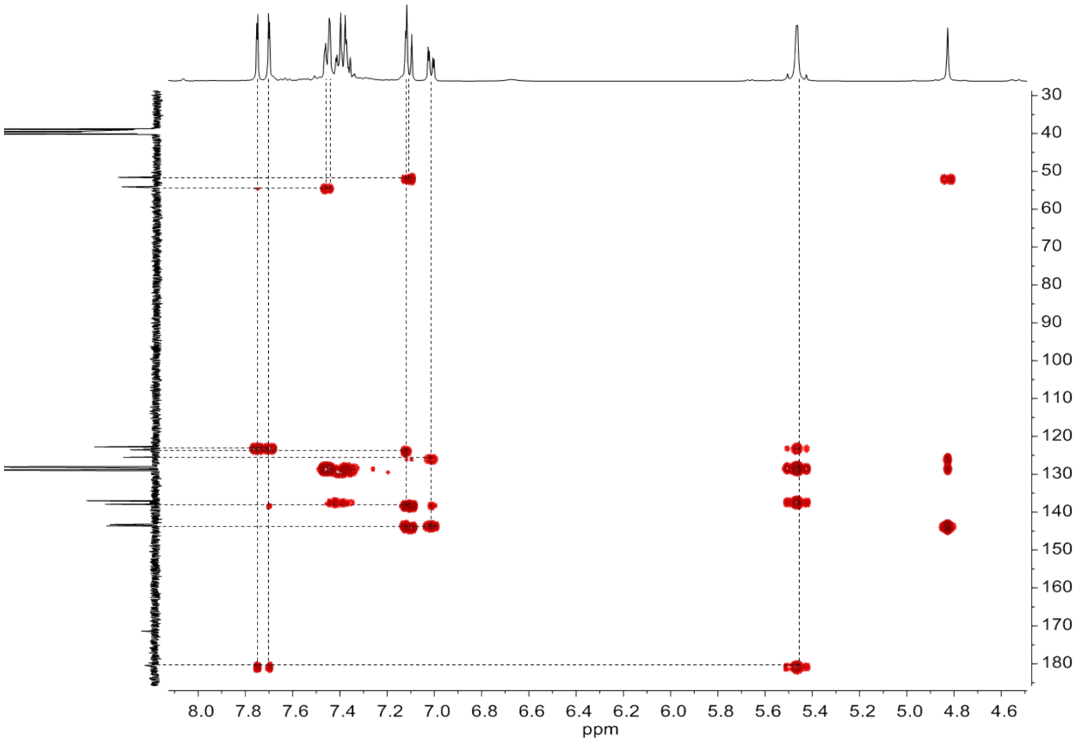

Figure S54. ^{1}H-^{13}C HMBC spectrum (400 MHz in DMSO-d_6) of *anti*-[Ag_2(**2b**)](PF_6)$_2$.

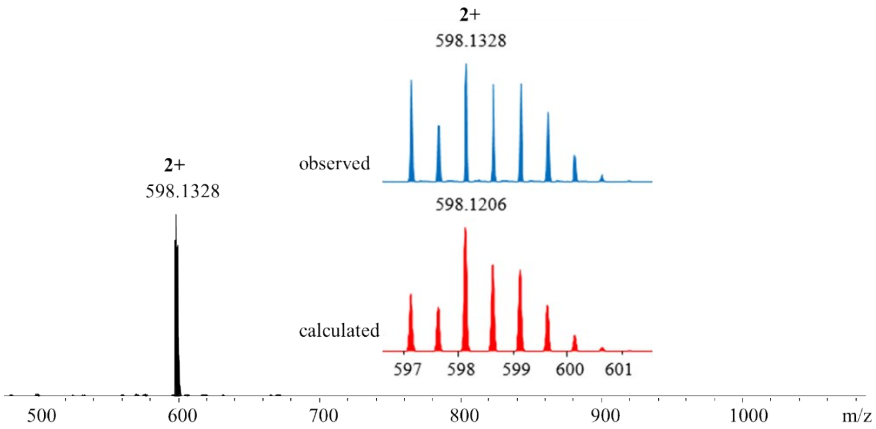

Figure S55. ESI-TOF mass spectrum of *anti*-[Ag_2(**2b**)](PF_6)$_2$ with isotope distribution for selected peaks.

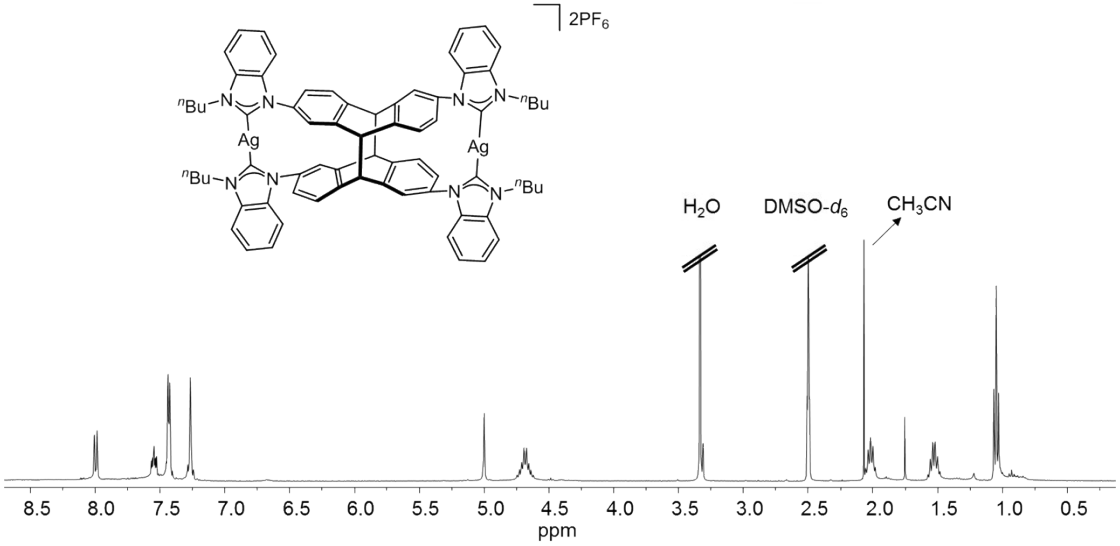

Figure S56. ^{1}H NMR spectrum (400 MHz in DMSO-d_6) of *anti*-[Ag_2(**2c**)](PF_6)$_2$.

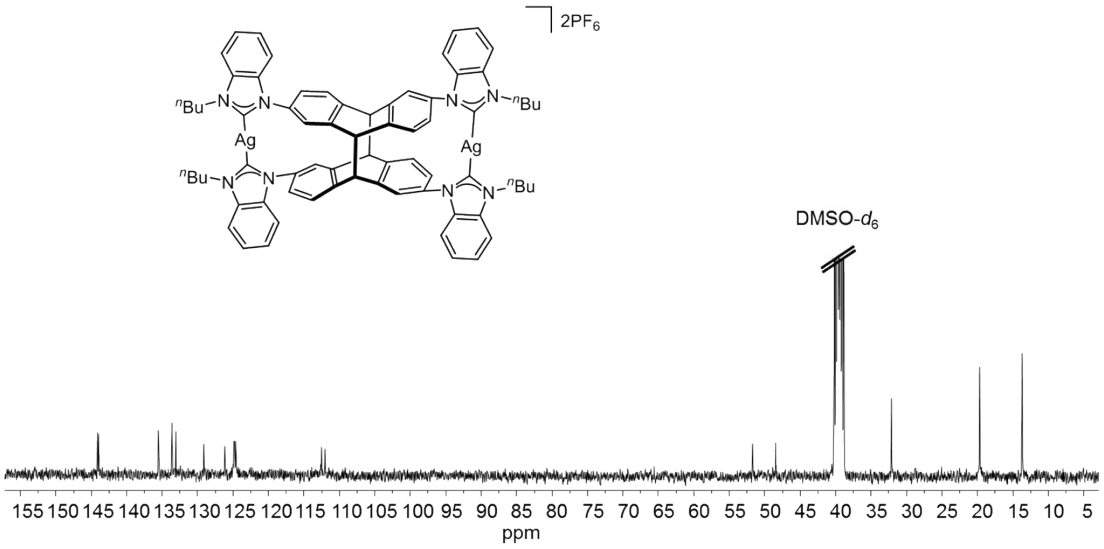

Figure S57. ^{13}C NMR spectrum (100 MHz in DMSO-d_6) of *anti*-[Ag_2(**2c**)](PF_6)$_2$.

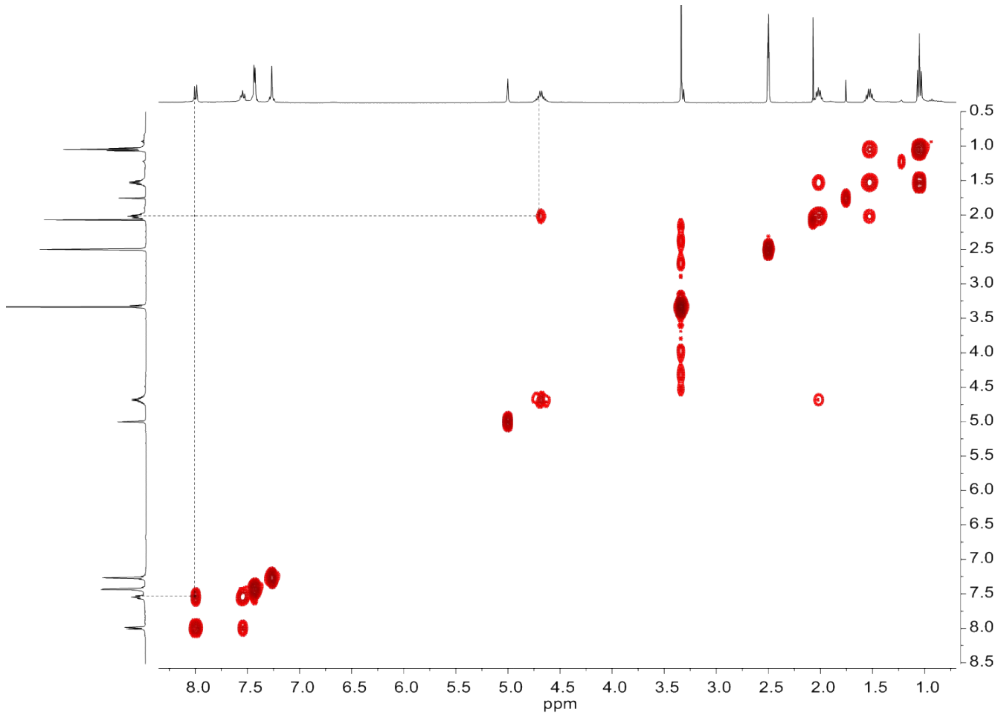

Figure S58. ^{1}H-^{1}H COSY spectrum (400 MHz in DMSO-d_6) of *anti*-[Ag_2(**2c**)](PF_6)$_2$.

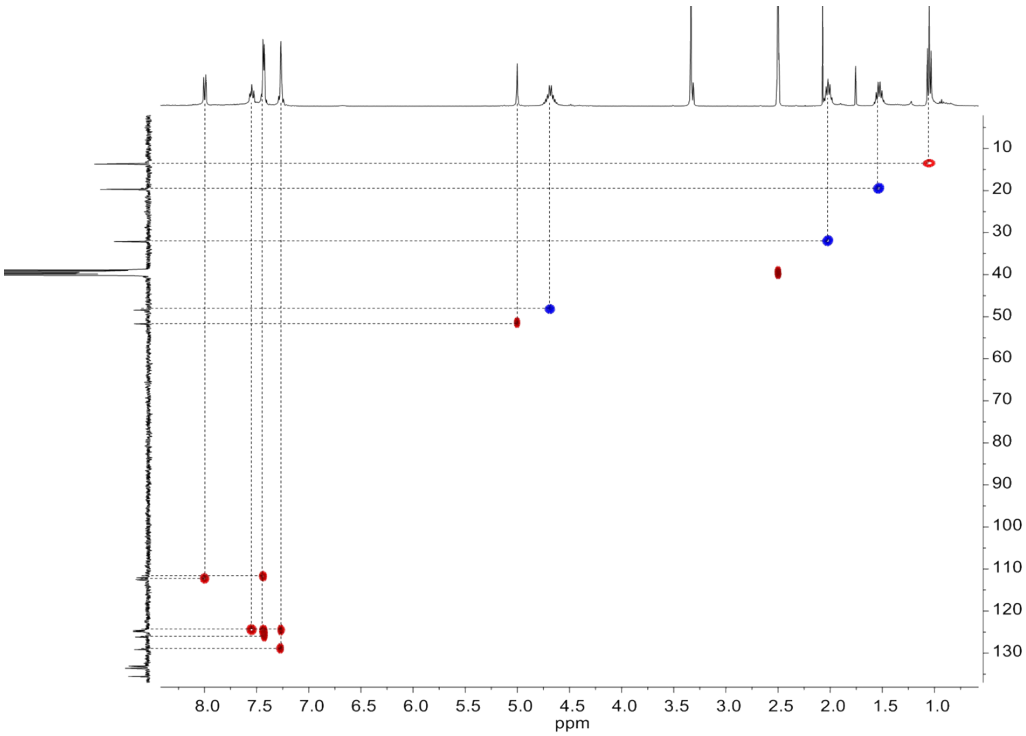

Figure S59. ^{1}H-^{13}C HSQC spectrum (400 MHz in DMSO-d_6) of *anti*-[Ag_2(**2c**)](PF_6)$_2$.

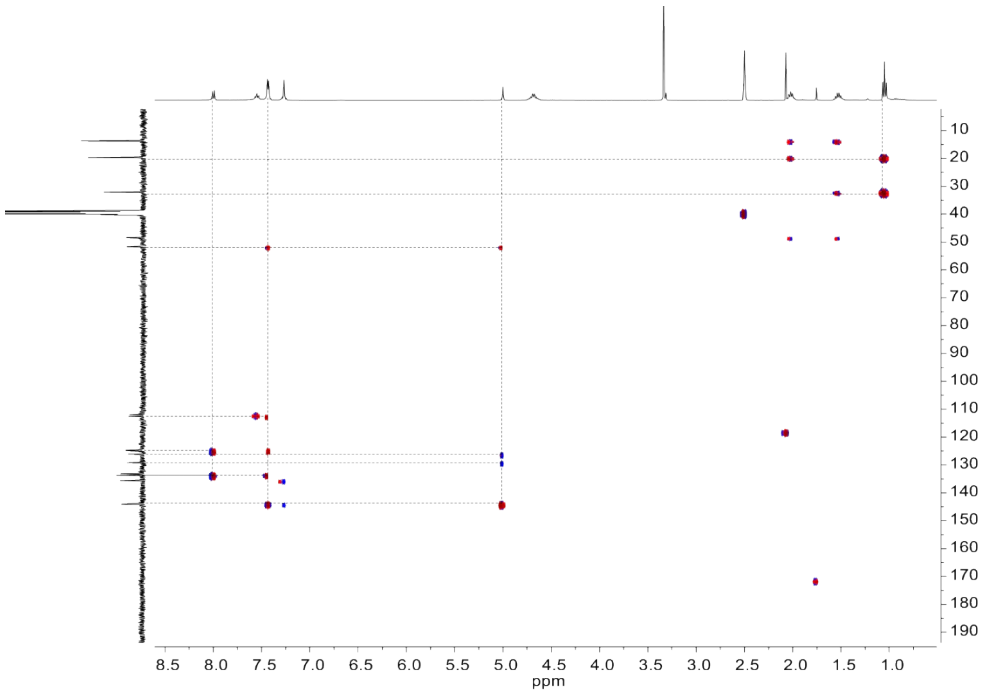

Figure S60. ^{1}H-^{13}C HMBC spectrum (400 MHz in DMSO-d_6) of *anti*-[Ag_2(**2c**)](PF_6)$_2$.

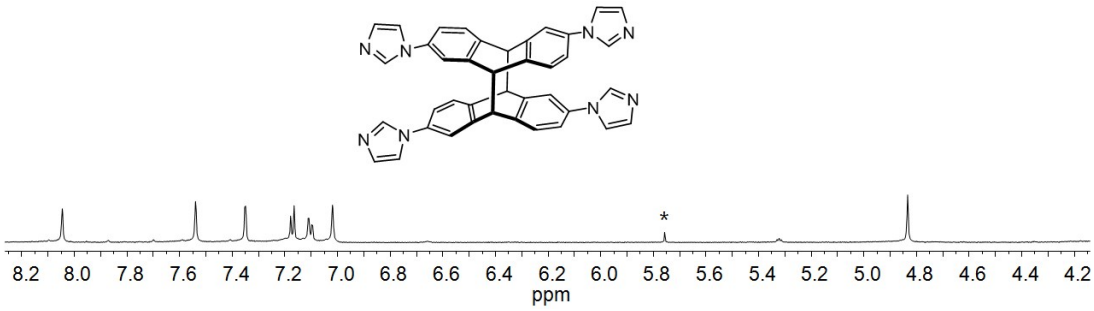

Figure S61. Section of ^{1}H NMR spectrum (400 MHz, DMSO-d_6) of *syn*-**6a**. * = Dichloromethane.

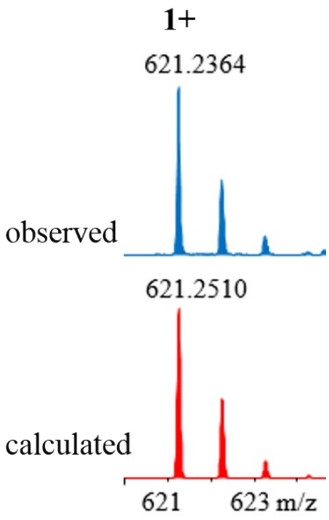

Figure S62. ESI-TOF mass spectrum of *syn*-**6a** with isotope distribution for selected peaks.

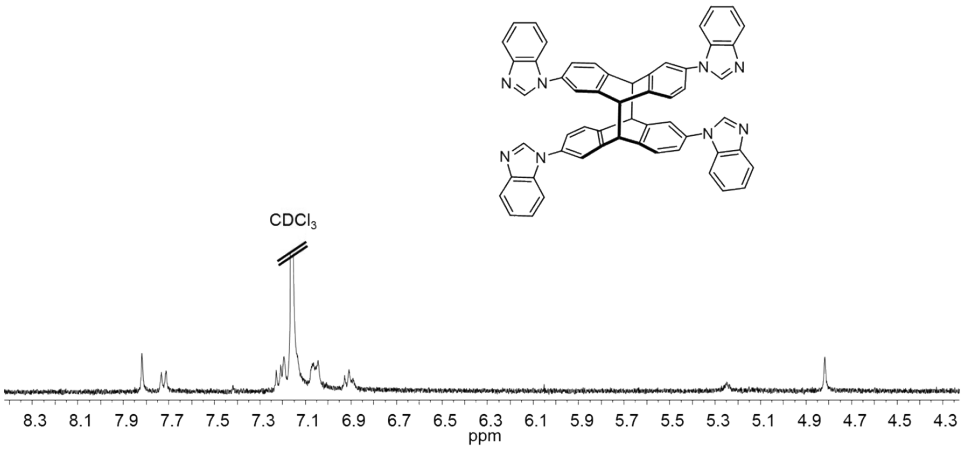

Figure S63. ^{1}H NMR spectrum (400 MHz, $CDCl_3$) of *syn*-**6b**. Note: No better spectrum can be obtained due to the limited solubility of *syn*-**6b**.

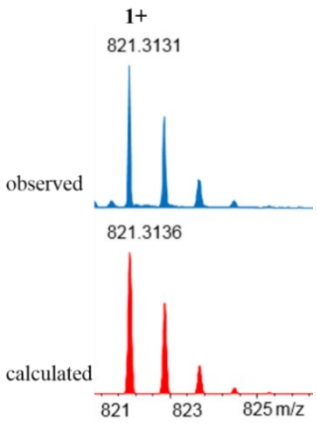

Figure S64. ESI-TOF mass spectrum of *syn*-**6b** with isotope distribution for selected peaks.

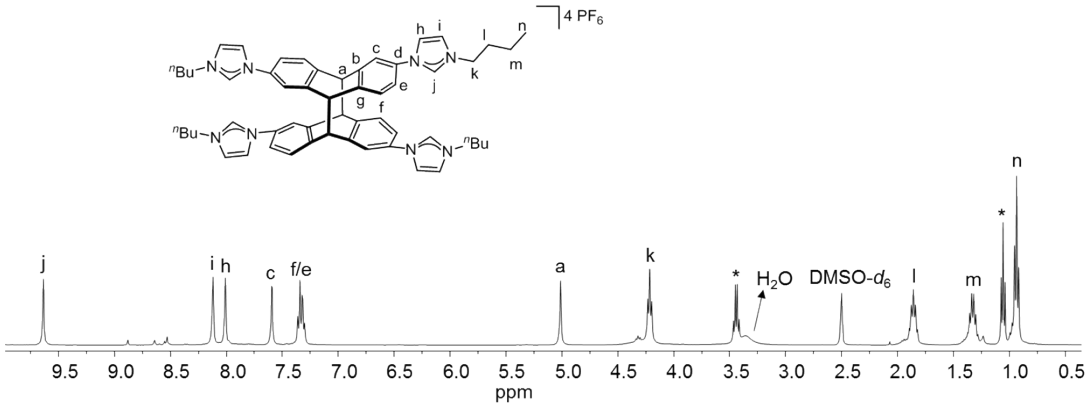

Figure S65. ^{1}H NMR spectrum (400 MHz in DMSO-d_6) of *anti*-H_4-**2a**$(PF_6)_4$. * = Diethyl ether.

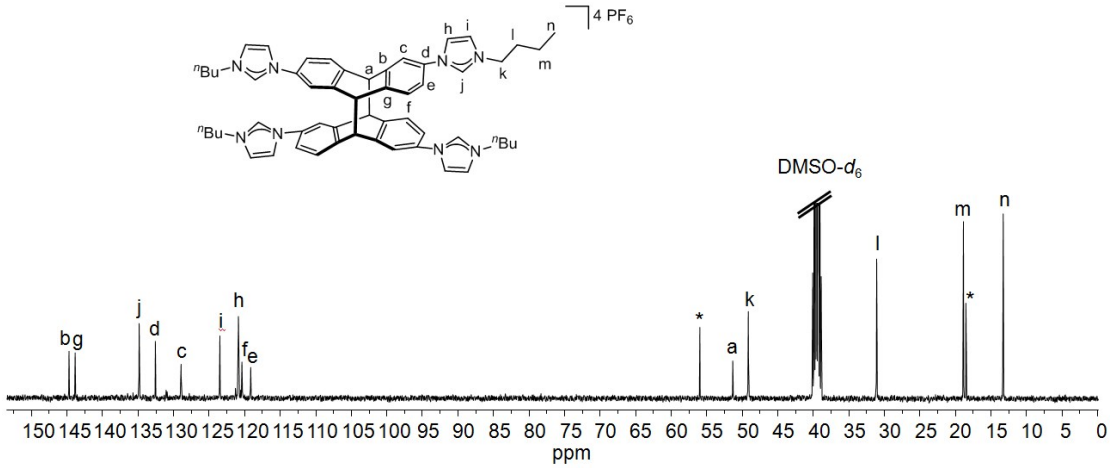

Figure S66. ^{13}C NMR spectrum (100 MHz in DMSO-d_6) of *anti*-H_4-**2a**$(PF_6)_4$. * = Ethanol.

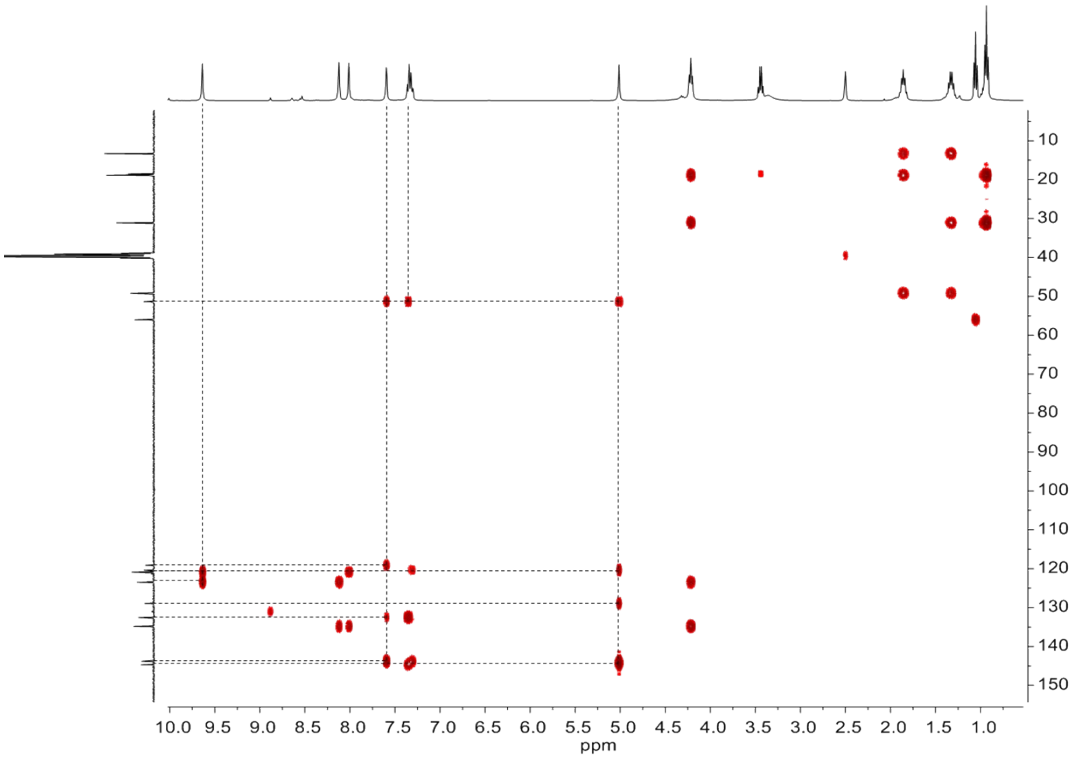

Figure S67. ^{1}H-^{13}C HMBC spectrum (400 MHz in DMSO-d_6) of *anti*-H_4-**2a**$(PF_6)_4$.

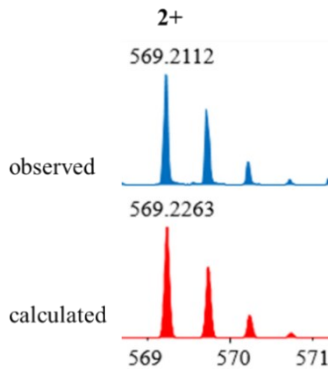

Figure S68. ESI-TOF mass spectrum of *anti*-H_4-**2a**$(PF_6)_4$ with isotope distribution for selected peaks.

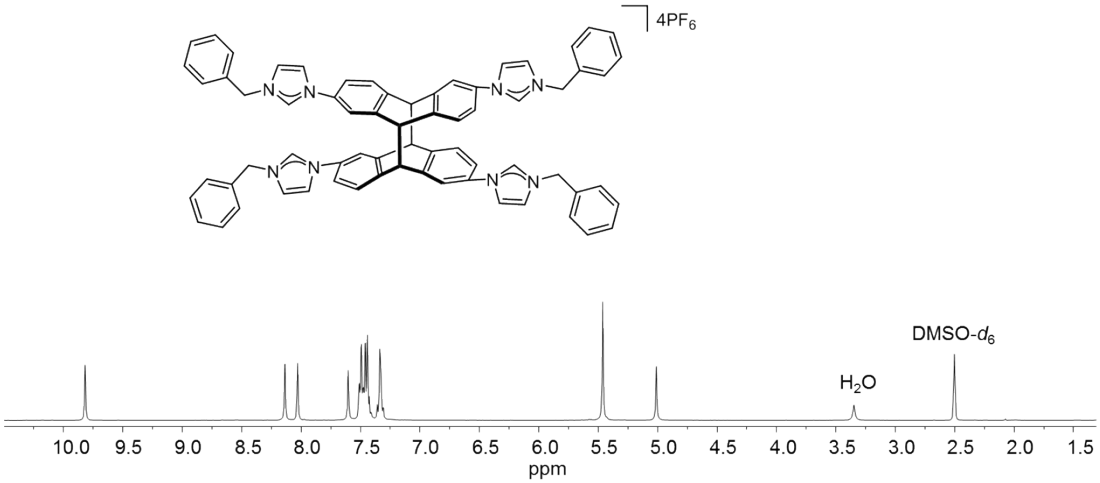

Figure S69. ^{1}H NMR spectrum (400 MHz in DMSO-d_6) of *anti*-H_4-**2b**$(PF_6)_4$.

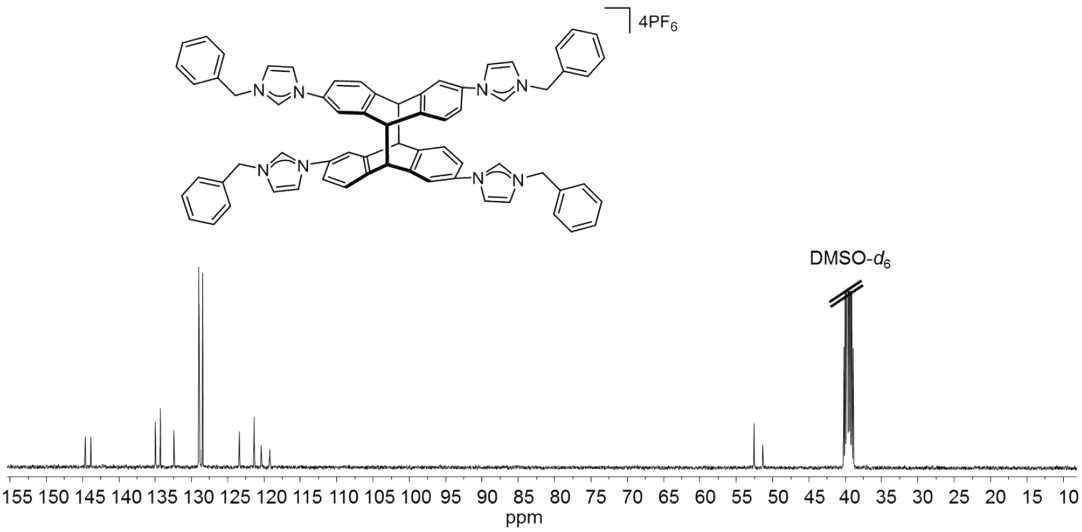

Figure S70. ^{13}C NMR spectrum (100 MHz in DMSO-d_6) of *anti*-H_4-**2b**$(PF_6)_4$.

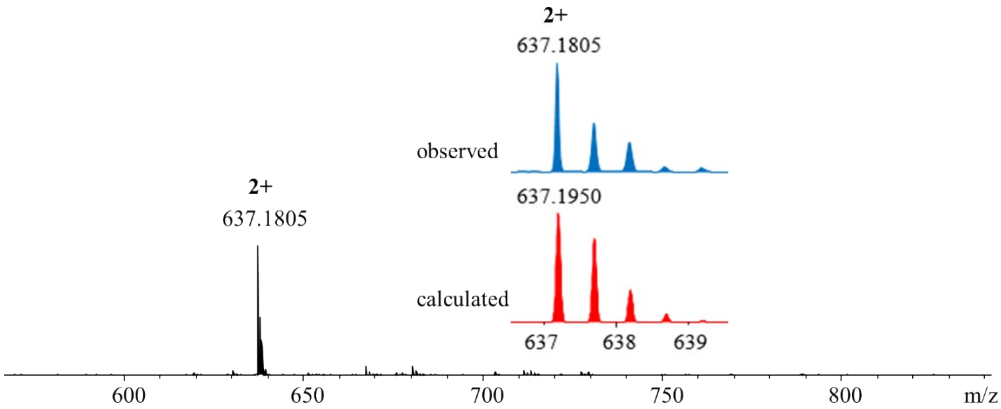

Figure S71. ESI-TOF mass spectrum of *anti*-H_4-**2b**$(PF_6)_4$ with isotope distribution for selected peaks.

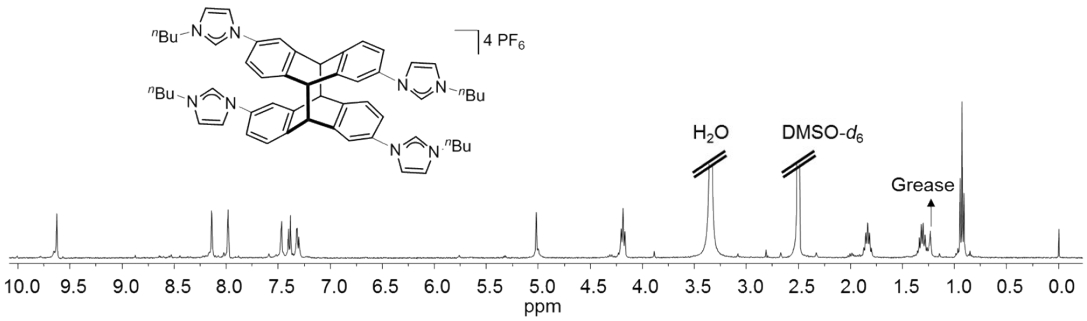

Figure S72. ^{1}H NMR spectrum (400 MHz in DMSO-d_6) of *syn*-H_4-**7a**$(PF_6)_4$.

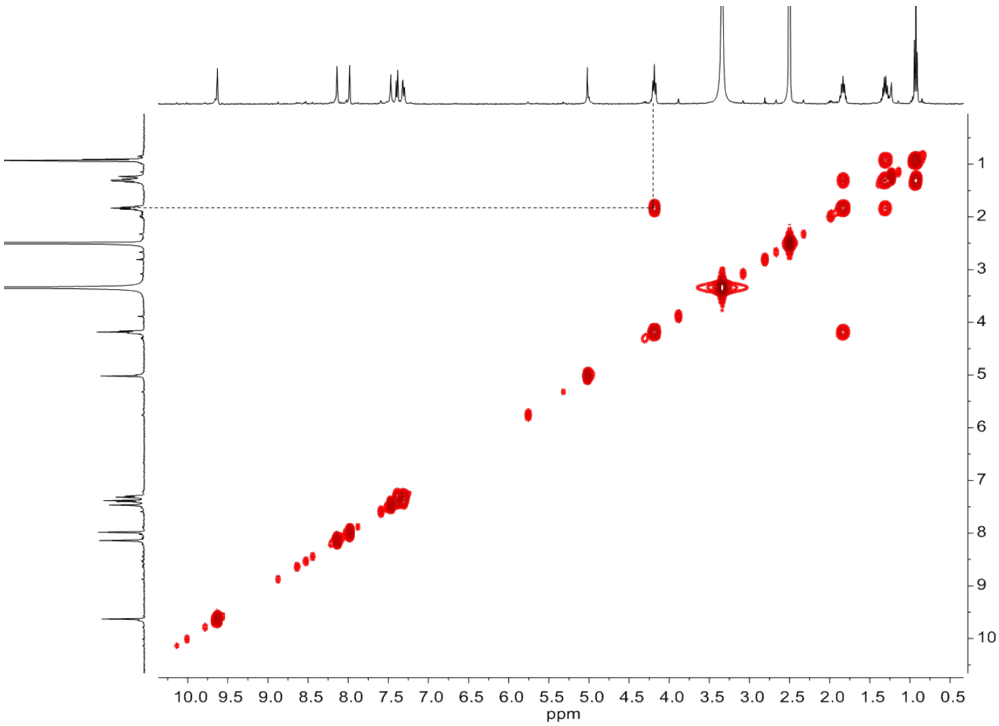

Figure S73. ^{1}H-^{1}H COSY spectrum (400 MHz in DMSO-d_6) of *syn*-H_4-**7a**$(PF_6)_4$.

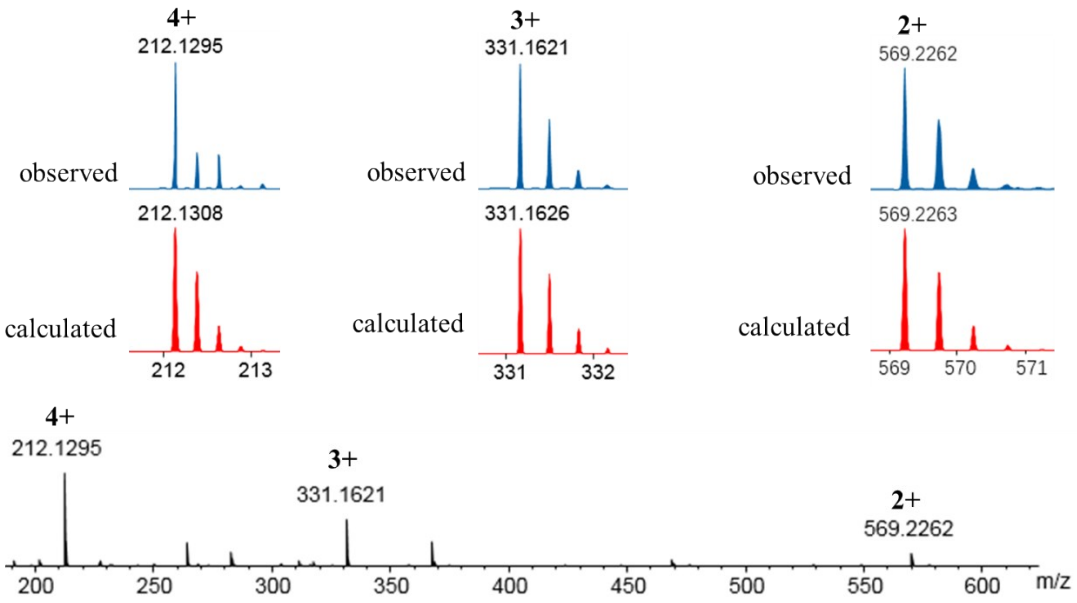

Figure S74. ESI-TOF mass spectrum of *syn*-H_4-**7a**$(PF_6)_4$ with isotope distribution for selected peaks.

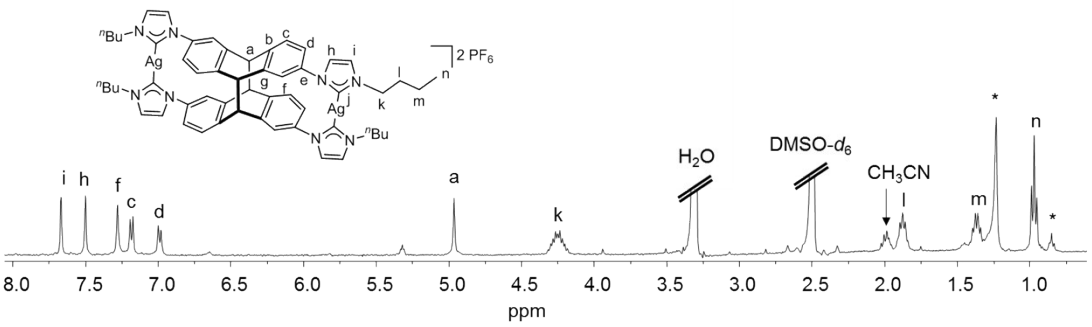

Figure S75. ^{1}H NMR spectrum (600 MHz in DMSO-d_6) of *syn*-[Ag_2**7a**]$(PF_6)_2$. * = H grease.

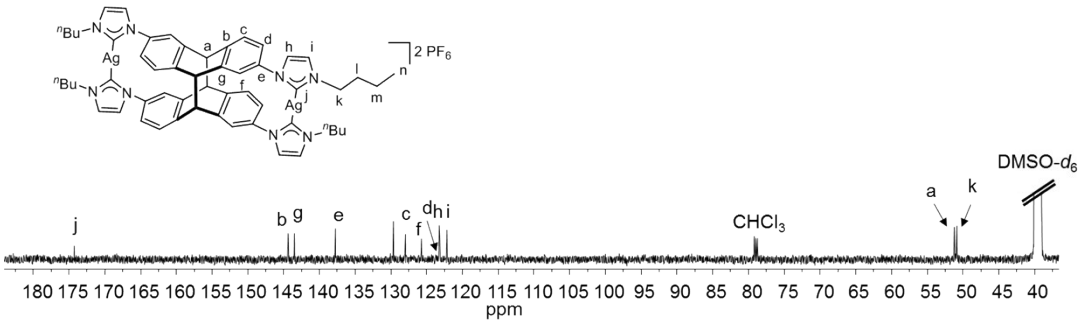

Figure S76. Section of ^{13}C NMR spectrum (150 MHz in DMSO-d_6) of *syn*-[Ag_2**7a**]$(PF_6)_2$.

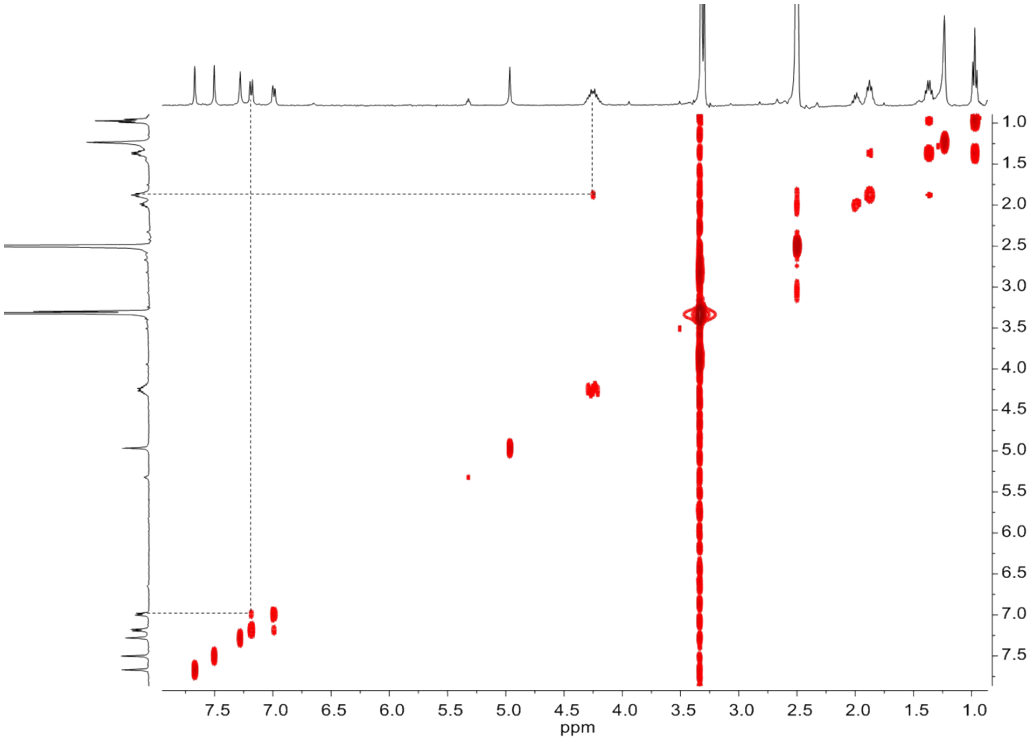

Figure S77. ^{1}H-^{1}H COSY spectrum (600 MHz in DMSO-d_6) of *syn*-[Ag_2**7a**]$(PF_6)_2$.

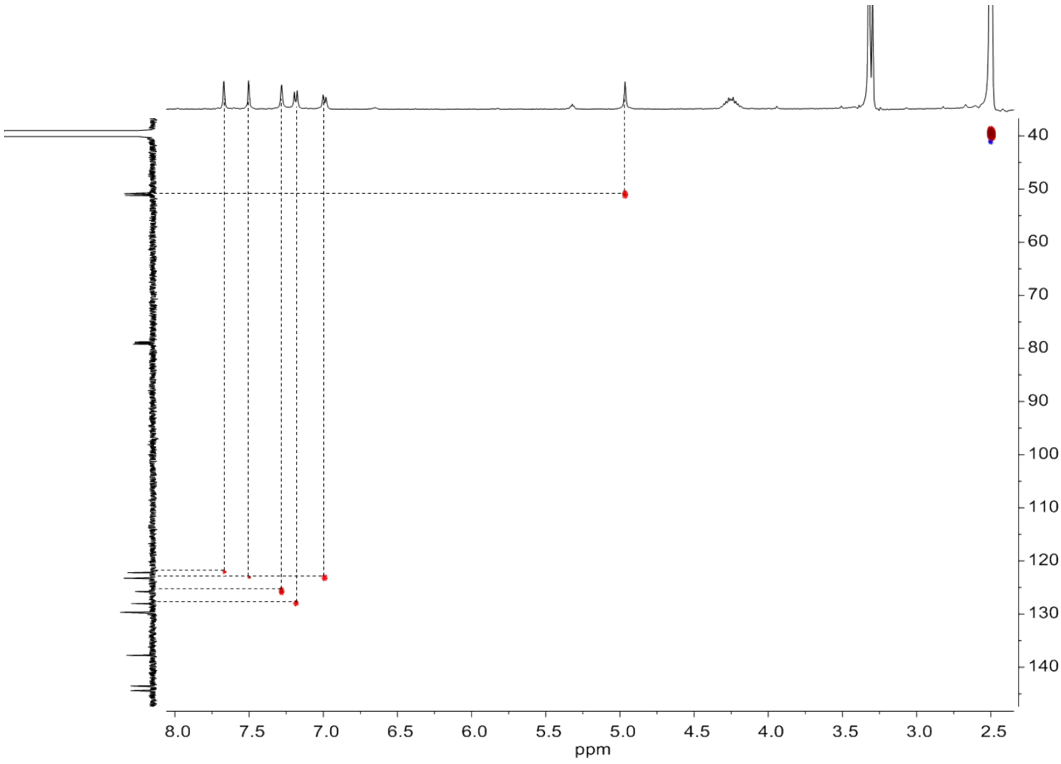

Figure S78. ^{1}H-^{13}C HSQC spectrum (600 MHz in DMSO-d_6) of *syn*-[Ag_2**7a**](PF_6)$_2$.

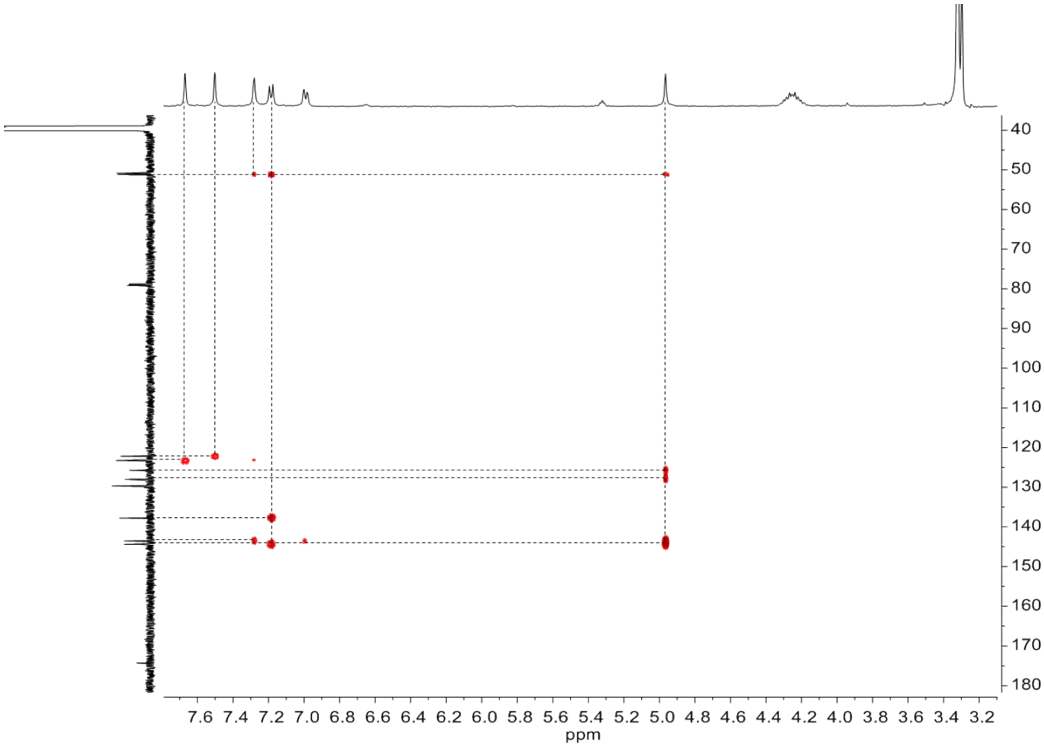

Figure S79. ^{1}H-^{13}C HMBC spectrum (600 MHz in DMSO-d_6) of *syn*-[Ag_2**7a**](PF_6)$_2$.

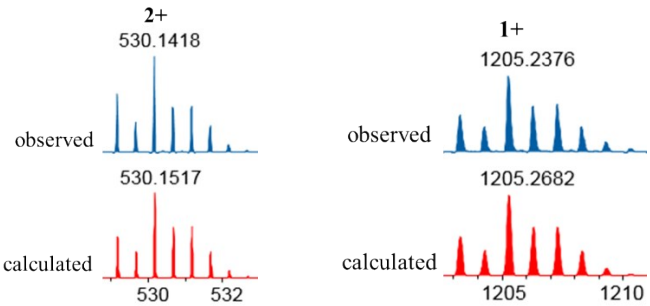

Figure S80. ESI-TOF mass spectrum of *syn*-H_4-**7a**(PF_6)$_4$ with isotope distribution for selected peaks.

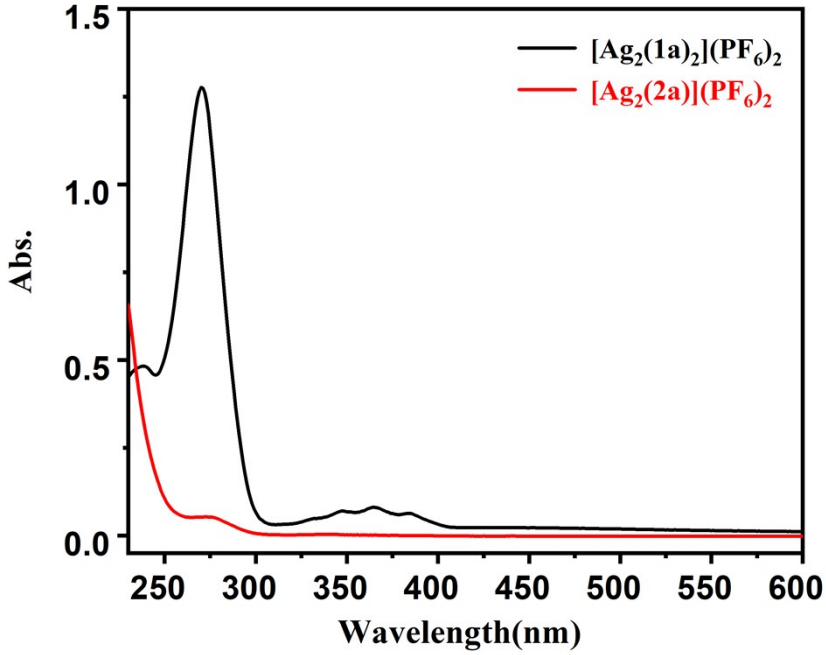

Figure S81. Absorption spectra of *anti*-[Ag_2(**1a**)$_2$](PF_6)$_2$ and *anti*-[Ag_2(**2a**)](PF_6)$_2$ in acetonitrile solutions (T = 298 K, c = 10 μM).

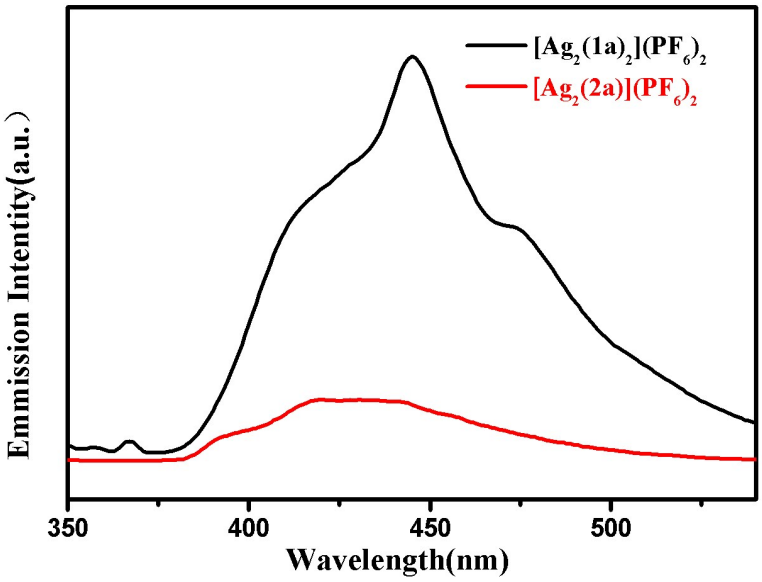

Figure S82. Emission spectra of *anti*-[Ag_2(**1a**)$_2$](PF_6)$_2$ (λ_{ex} = 330 nm) and *anti*-[Ag_2(**2a**)](PF_6)$_2$ (λ_{ex} = 275 nm) in acetonitrile solutions (c = 10 μM, ex/em slit width: 2 nm).

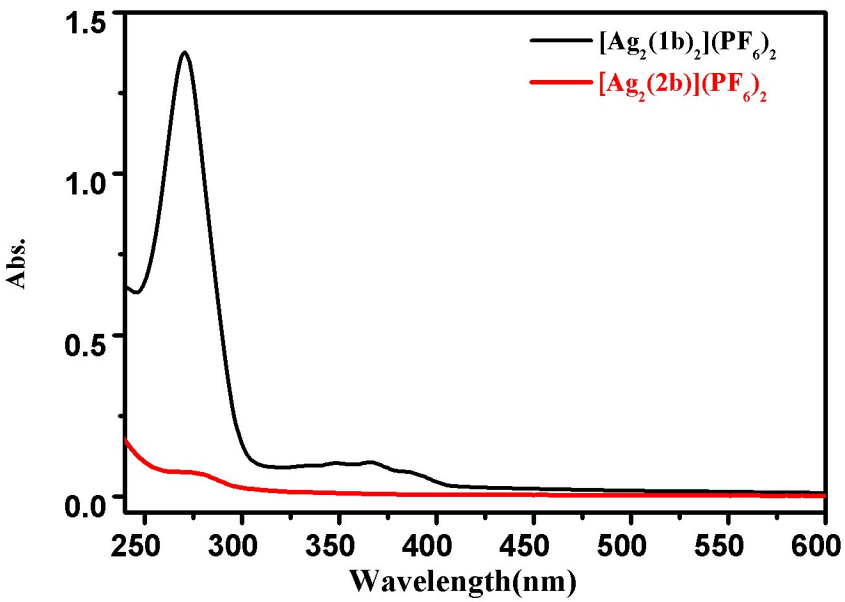

Figure S83. Absorption spectra of *anti*-[Ag_2(**1b**)$_2$](PF_6)$_2$ and *anti*-[Ag_2(**2b**)](PF_6)$_2$ in acetonitrile solutions (T = 298 K, c = 10 μM).

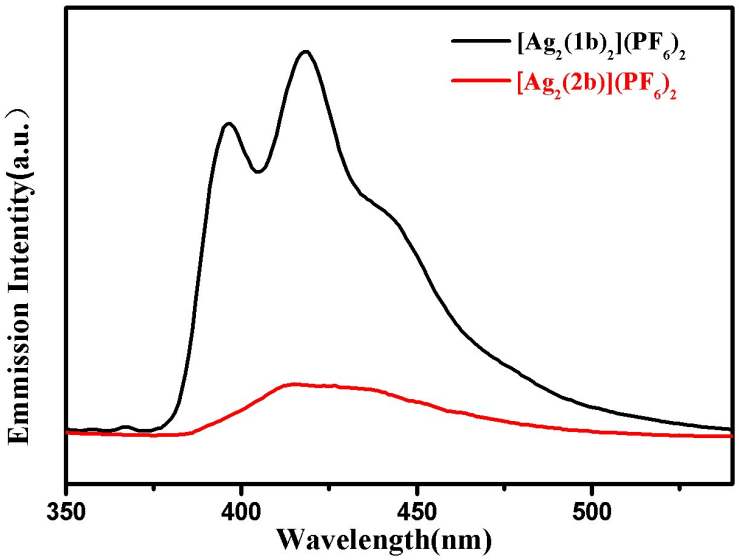

Figure S84. Emission spectra of *anti*-[Ag_2(**1b**)$_2$](PF_6)$_2$ (λ_{ex} = 330 nm) and *anti*-[Ag_2(**2b**)](PF_6)$_2$ (λ_{ex} = 275 nm) in acetonitrile solutions (c = 10 μM, ex/em slit width: 2 nm).

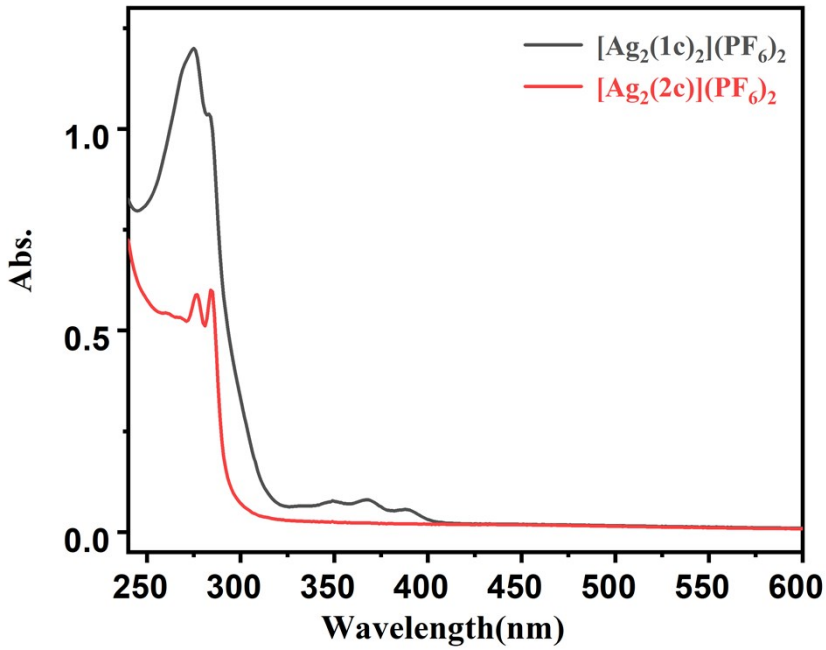

Figure S85. Absorption spectra of *anti*-[Ag_2(**1c**)$_2$](PF_6)$_2$ and *anti*-[Ag_2(**2c**)](PF_6)$_2$ in acetonitrile solutions (T = 298 K, c = 10 μM).

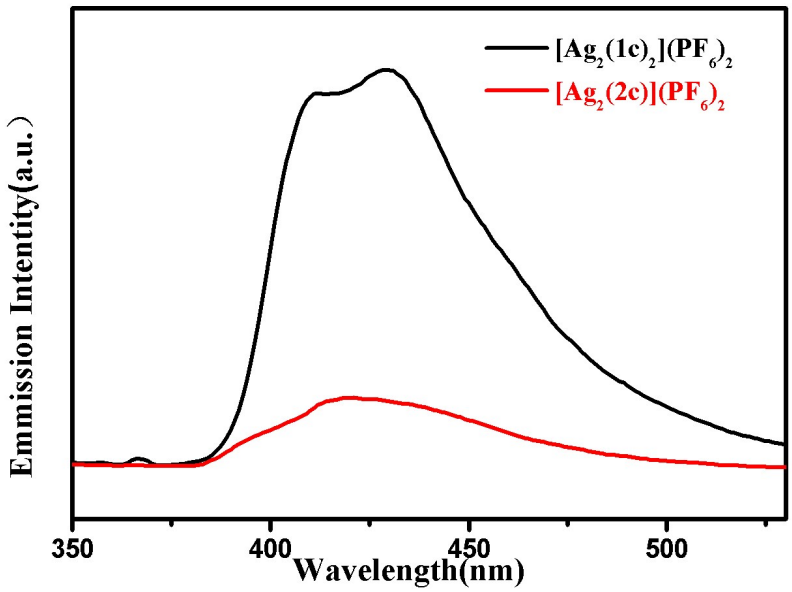

Figure S86. Emission spectra of *anti*-[Ag_2(**1c**)$_2$](PF_6)$_2$ (λ_{ex} = 330 nm) and *anti*-[Ag_2(**2c**)](PF_6)$_2$ (λ_{ex} = 275 nm) in acetonitrile solutions (c = 10 μM, ex/em slit width: 2 nm).

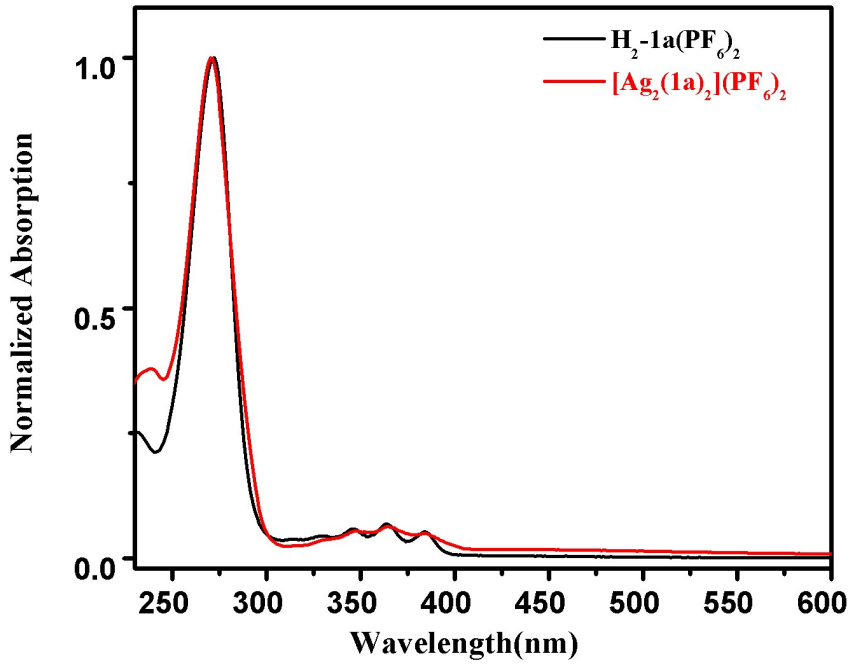

Figure S87. Absorption spectra of imidazolium salt H_4-**1a**$(PF_6)_2$ and *anti*-$[Ag_2(\mathbf{1a})_2](PF_6)_2$ in acetonitrile solutions (T = 298 K, c = 10 μM).

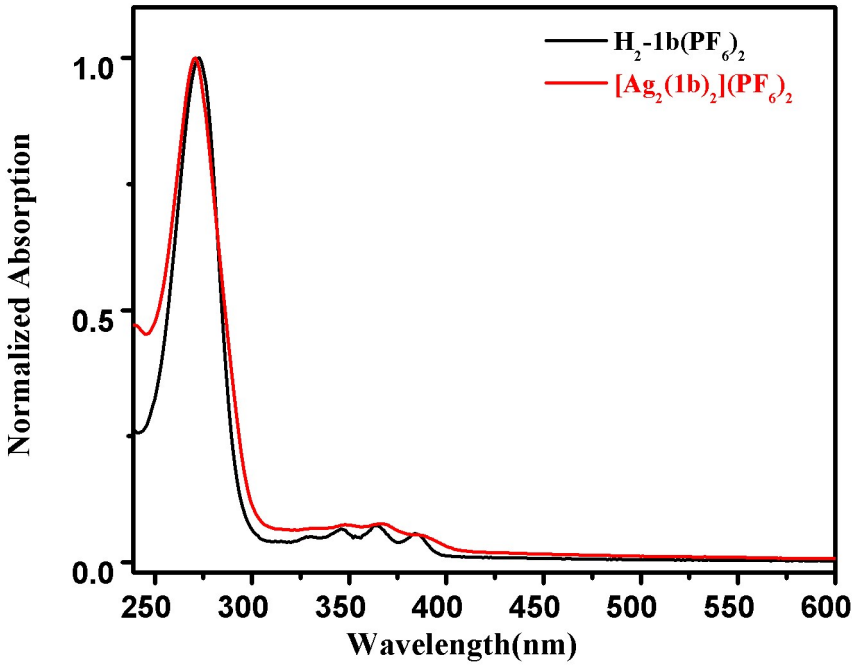

Figure S88. Absorption spectra of imidazolium salt H_4-**1b**$(PF_6)_2$ and *anti*-$[Ag_2(\mathbf{1b})_2](PF_6)_2$ in acetonitrile solutions (T = 298 K, c = 10 μM).

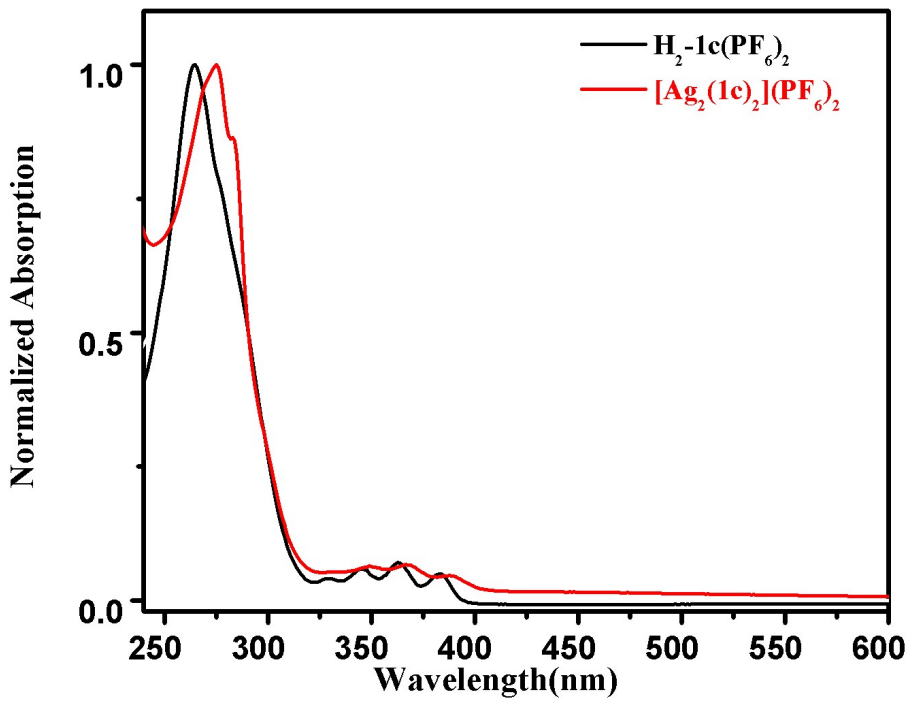

Figure S89. Absorption spectra of imidazolium salt H_4-**1c**$(PF_6)_2$ and *anti*-$[Ag_2(\mathbf{1c})_2](PF_6)_2$ in acetonitrile solutions (T = 298 K, c = 10 μM).

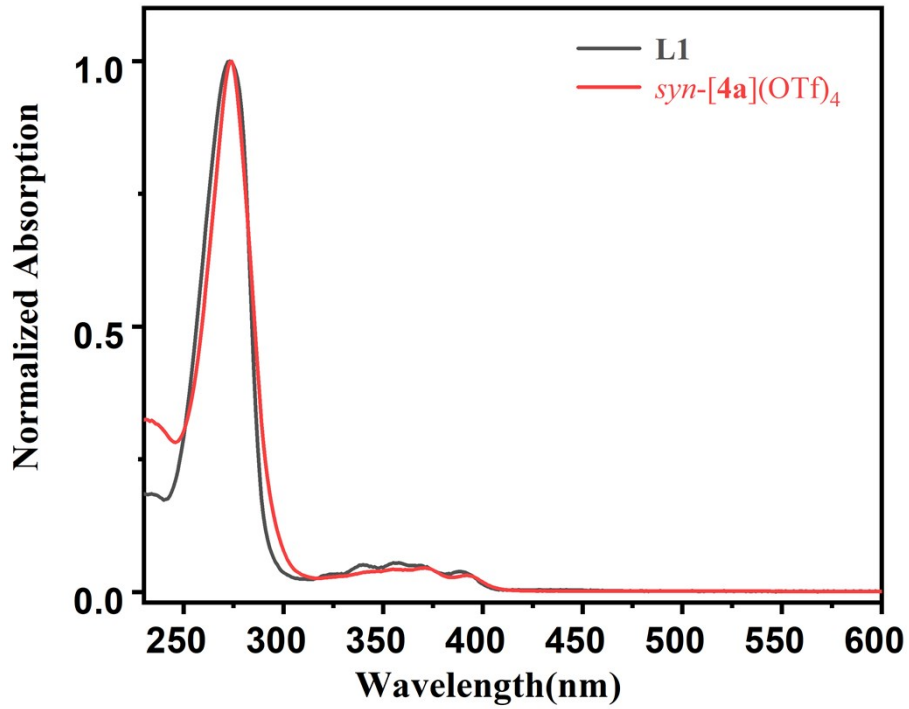

Figure S90. Absorption spectra of ligand **L1** and metallarectangle *syn*-[**4a**](OTf)$_4$ in acetonitrile solutions (T = 298 K, c = 10 μM).

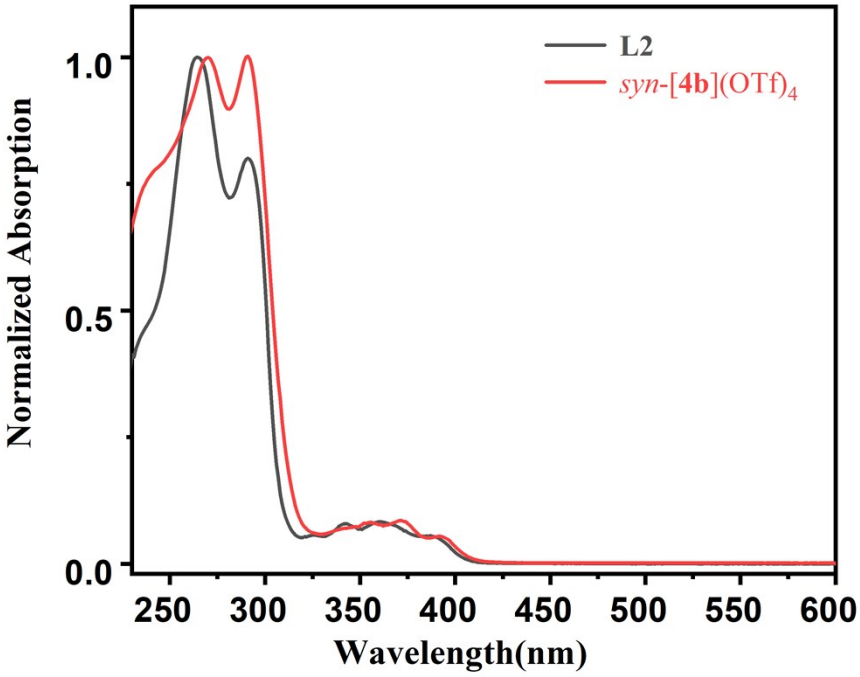

Figure S91. Absorption spectra of ligand **L2** and metallarectangle *syn*-[**4b**](OTf)$_4$ in acetonitrile solutions (T = 298 K, c = 10 μM).

Note: In the UV/vis spectra including monomeric anthracene molecules (**L**, H_2-**1**$(PF_6)_2$) and corresponding complexes (*anti*-[Ag_2(**2**)$_2$]$(PF_6)_2$, *syn*-[**4**](OTf)$_4$) (Figures S87-S91), all the monomeric anthracene compounds and metal-carbene complexes showed a series of vibrationally spaced bands at wavelengths of λ = 325–410 nm, which are typical π–π* absorptions for anthracene systems. After metallation, absorption bands in the range of characteristic anthracene transitions were red-shifted to varying degrees compared with that of monomeric anthracene ligands (Figures S87-S91, black line). For example, for *anti*-metallacycle *anti*-[Ag_2(**1a**)$_2$]$(PF_6)_2$, the adjacent anthracene planes overlapped with each other by about 30% and the vertical distance between them was measured to be approximately 3.57 Å (according to the single crystal structure), which corresponds to the formation of weak π–π interaction between the anthracene planes. The absorption bands of *anti*-[Ag_2(**1a**)$_2$]$(PF_6)_2$ were slightly red-shifted (ca. 0.2 nm for lowest 0→0 transition, 1 nm for 0→1 transition) compared to that of the monomeric anthracene derivative H_2-**1a**$(PF_6)_2$. In

comparison with monomeric anthracene molecules **L1**, the absorption peaks of *syn*-[**4a**](OTf)$_4$ demonstrated bathochromic shift with about 3 and 5 nm (for 0→0 and 0→1 transitions respectively), which induced by the increased π-π interaction between the adjacent anthracene moieties with a face-to-face stacking.

8. X-Ray Crystallography.

Single crystals of **L1** and **L2** were grown by slow diffusion of diethyl ether into saturated dichloromethane solution at ambient temperature. Single crystals of $[Ag_2(\mathbf{1a})_2](BPh_4)_2$, $[H_4\text{-}\mathbf{6b}](OTf)_4$ and $H_4\text{-}\mathbf{7a}(PF_6)_4$ were grown by slow diffusion of diethyl ether into saturated acetonitrile solution at ambient temperature. Single crystal of $H_4\text{-}\mathbf{2a}(PF_6)_4$ was grown by slow diffusion of diethyl ether into saturated acetonitrile and methanol solution at ambient temperature. Single crystal of **6a** was grown by slow diffusion of diethyl ether into saturated dichloromethane and methanol solution at ambient temperature. All data for crystal structure determinations were measured on a Bruker D8 Venture diffractometer, using graphite monochromated MoKα radiation (λ=0.71073 Å). Reduction of data and semiempirical absorption correction were done using SADABS program.[4] The structures were solved by direct methods, which revealed the position of all non-hydrogen atoms. These atoms were refined on F^2 by a full matrix least-squares procedure using anisotropic displacement parameters.[5,6] All hydrogen atoms were assigned to ideal positions and refined using a riding model. For $H_4\text{-}\mathbf{7a}(PF_6)_4$, two hexafluorophosphates and two n-butyl were disordered and they were divided into two parts. For $H_4\text{-}\mathbf{2a}(PF_6)_4$, two disordered hexafluorophosphates were divided into two parts and one disordered n-butyl was divided into three parts. For $Ag_2(\mathbf{1a})_2(BPh_4)_2$, one disordered n-butyl was divided into two parts and some restrictions were used to stabilize the molecular configuration. The SQUEEZE program was used for the analysis to remove the disordered unassignable solvent densities in the void. For $[H_4\text{-}\mathbf{6b}](OTf)_4$, disordered anions were divided into two parts and some restrictions were used to stabilize the molecular configuration. For details, see Table S1-S7.

Table S1. Crystal data of ligand **L1**.

Empirical formula	$C_{20}H_{14}N_4$
Formula weight	310.35
Temperature/K	185.01
Crystal system	monoclinic
Space group	*C*2/*c*
a/Å	15.8604(11)
b/Å	11.0803(8)
c/Å	9.0716(6)
α/°	90
β/°	109.900(2)
γ/°	90
Volume/Å^3	1499.03(18)
Z	4
ρ_{calc}/(g·cm^{-3})	1.375
μ(mm^{-1})	0.085
F(000)	648.0
Crystal size/mm^3	0.25 × 0.20 × 0.18
Radiation	Mo Kα (λ = 0.71073)
2Θ range for data collection/°	5.464 to 52.806
Index ranges	$-19 \leq h \leq 19$, $-13 \leq k \leq 13$, $-10 \leq l \leq 11$

Reflections collected	11365
Independent reflections	1528 [R_{int} = 0.0405]
Data/restraints/parameters	1528/0/109
Goodness-of-fit on F^2	1.073
Final *R* indexes [$I \geq 2\sigma(I)$]	R_1 = 0.0393, wR_2 = 0.1014
Final *R* indexes [all data]	R1 = 0.0502, wR_2 = 0.1105
Largest diff. peak/hole / e $Å^{-3}$	0.21/-0.18
CCDC	1995058

Table S2. Crystal data of ligand **L2**.

Empirical formula	$C_{28}H_{18}N_4$
Formula weight	410.46
Temperature/K	179.98
Crystal system	Triclinic
Space group	*P*-1
a/Å	6.4661(11)
b/Å	8.1703(13)
c/Å	10.3854(17)
α/°	69.264(5)
β/°	78.354(5)
γ/°	79.800(6)
Volume/Å^3	499.20(14)
Z	1
ρ_{calc} (g·cm^{-3})	1.365
μ (mm^{-1})	0.082
F (000)	214.0
Crystal size/mm^3	0.2 × 0.15 × 0.12
Radiation	Mo Kα (λ = 0.71073)
2Θ range for data collection/°	5.636 to 53.394
Index ranges	$-7 \leq h \leq 8$, $-10 \leq k \leq 10$, $-13 \leq l \leq 13$

Reflections collected	5617
Independent reflections	2082 [R_{int} = 0.0204]
Data/restraints/parameters	2082/15/145
Goodness-of-fit on F^2	1.104
Final R indexes [$I \geq 2\sigma(I)$]	R_1 = 0.0588, wR_2 = 0. 1394
Final R indexes [all data]	R_1 = 0.0638, wR_2 = 0.1432
Largest diff. peak/hole / e Å^{-3}	0.69/-0.29
CCDC	1995079

Table S3. Crystal data of complex *anti*-[Ag_2(**1a**)$_2$](BPh_4)$_2$.

Empirical formula	$C_{104}H_{100}Ag_2B_2N_8$
Formula weight	1699.27
Temperature/K	200.02
Crystal system	Orthorhombic
Space group	*Aea*2
a/Å	8.9095(4)
b/Å	41.3302(17)
c/Å	26.6661(11)
α/°	90
β/°	90
γ/°	90
Volume/Å^3	9819.3(7)
Z	4
ρ_{calc} (g·cm^{-3})	1.149
μ (mm^{-1})	0.446
F (000)	3536.0
Crystal size/mm^3	0.32 × 0.3 × 0.28
Radiation	Mo Kα (λ = 0.71073)
2Θ range for data collection/°	4.978 to 54.204
Index ranges	$-11 \leq h \leq 11$, $-52 \leq k \leq 52$, $-34 \leq l \leq 34$

Reflections collected	81378
Independent reflections	10808 [R_{int} = 0.0398]
Data/restraints/parameters	10808/88/562
Goodness-of-fit on F^2	1.051
Final R indexes [$I \geq 2\sigma(I)$]	R_1 = 0.0361, wR_2 = 0.0870
Final R indexes [all data]	R_1 = 0.0453, wR_2 = 0.0931
Largest diff. peak/hole / e Å^{-3}	0.83/-0.75
CCDC	1995080

Table S4. Crystal data of complex *anti*-H_4-**2a**$(PF_6)_4$.

Empirical formula	$C_{56}H_{64}F_{24}N_8P_4$
Formula weight	1429.03
Temperature/K	153.01
Crystal system	Monoclinic
Space group	*P2/n*
a/Å	17.1270(9)
b/Å	8.8196(4)
c/Å	21.3425(12)
α/°	90
β/°	103.355(2)
γ/°	90
Volume/Å^3	3136.7(3)
Z	2
ρ_{calc} (g·cm^{-3})	1.513
μ (mm^{-1})	0.237
F (000)	1464.0
Crystal size/mm^3	0.21 × 0.2 × 0.18
Radiation	Mo Kα (λ = 0.71073)
2Θ range for data collection/°	5.018 to 54.194
Index ranges	$-21 \leq h \leq 21$, $-11 \leq k \leq 11$, $-23 \leq l \leq 27$

Reflections collected	59699
Independent reflections	6930 [R_{int} = 0.0582]
Data/restraints/parameters	6930/248/541
Goodness-of-fit on F^2	1.035
Final R indexes [$I \geq 2\sigma(I)$]	R_1 = 0.0634, wR_2 = 0.1539
Final R indexes [all data]	R_1 = 0.0930, wR_2 = 0.1767
Largest diff. peak/hole / e Å^{-3}	0.61/-0.53
CCDC	1995081

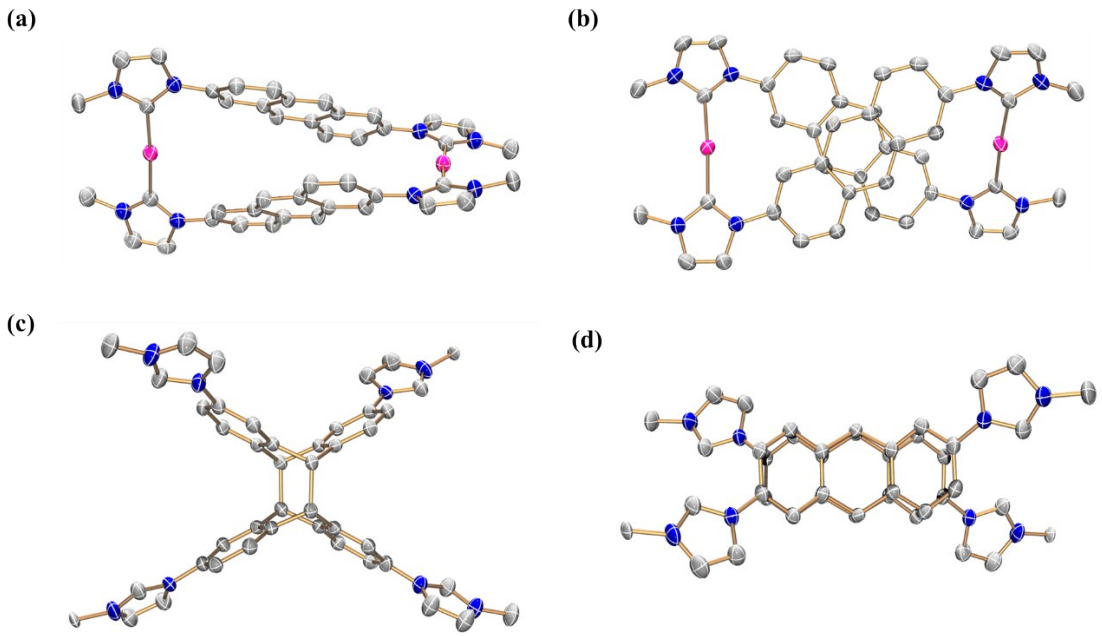

Figure S87. (a,b) Side and top views of the cationic part of the crystal of *anti*-$[Ag_2(\mathbf{1a})_2](BPh_4)_2$ as determined by single-crystal X-ray diffraction; (c,d) Side and top views of the cationic part of the crystal of *anti*-H_4-**2a**$(PF_6)_4$. (N, blue; C, grey; hydrogen atoms have been omitted for clarity, and only the first atom of each N-substituent is depicted.)

Table S5. Crystal data of compound *syn*-**6a**.

Empirical formula	$C_{40}H_{28}N_8$
Formula weight	620.70
Temperature/K	150.0
Crystal system	Monoclinic
Space group	$P2_1/n$
a/Å	9.2542(12)
b/Å	15.7442(18)
c/Å	9.9997(13)
α/°	90
β/°	94.804(4)
γ/°	90
Volume/Å^3	1451.8(3)
Z	2
ρ_{calc} (g·cm^{-3})	1.420
μ (mm^{-1})	0.087
F (000)	648.0
Crystal size/mm^3	0.18 × 0.15 × 0.12
Radiation	Mo Kα (λ = 0.71073)
2Θ range for data collection/°	5.12 to 50.846
Index ranges	$-11 \leq h \leq 10$, $-18 \leq k \leq 18$, $-12 \leq l \leq 12$

Reflections collected	17068
Independent reflections	2664 [R_{int} = 0.0446]
Data/restraints/parameters	2664/0/217
Goodness-of-fit on F^2	1.058
Final R indexes [$I \geq 2\sigma(I)$]	R_1 = 0.0380, wR_2 = 0.0905
Final R indexes [all data]	R_1 = 0.0483, wR_2 = 0.0977
Largest diff. peak/hole / e Å^{-3}	0.18/-0.19
CCDC	1995082

Table S6. Crystal data of compound *syn*-**6b**.

Empirical formula	$C_{61.5}H_{44.5}F_{10.5}N_9O_{11.5}S_{3.5}$
Formula weight	1405.27
Temperature/K	150.01
Crystal system	Monoclinic
Space group	$P2_1/m$
a/Å	8.0294(8)
b/Å	19.1408(16)
c/Å	19.9693(18)
α/°	90
β/°	94.970(3)
γ/°	90
Volume/Å^3	3057.5(5)
Z	2
ρ_{calc} (g·cm^{-3})	1.526
μ (mm^{-1})	0.241
F (000)	1438.0
Crystal size/mm^3	0.25 × 0.2 × 0.18
Radiation	Mo Kα (λ = 0.71073)
2Θ range for data collection/°	4.614 to 50.778
Index ranges	$-9 \leq h \leq 9$, $-23 \leq k \leq 23$, $-22 \leq l \leq 24$

Reflections collected	36901
Independent reflections	5783 [R_{int} = 0.0563]
Data/restraints/parameters	5783/14/525
Goodness-of-fit on F^2	1.050
Final R indexes [$I \geq 2\sigma(I)$]	R_1 = 0.0686, wR_2 = 0.1876
Final R indexes [all data]	R_1 = 0.0988, wR_2 = 0.2131
Largest diff. peak/hole / e Å^{-3}	0.72/-0.58
CCDC	1995083

Note: The single crystal of the OTf^- salt of compound *syn*-**6b** was obtained by adding one drop of HOTf into the CH_3CN and CH_3OH solution of *syn*-**6b**, then allowing slow diffusion of n-hexane into the mixture at ambient temperature for several days.

Table S7. Crystal data of complex *syn*-H_4-**7a**$(PF_6)_4$.

Empirical formula	$C_{56}H_{64}F_{24}N_8P_4$
Formula weight	1429.03
Temperature/K	180.01
Crystal system	Triclinic
Space group	*P*-1
a/Å	8.8950(8)
b/Å	12.0690(10)
c/Å	15.1617(15)
α/°	103.060(3)
β/°	94.575(3)
γ/°	103.138(3)
Volume/Å^3	1529.2(2)
Z	1
ρ_{calc} (g·cm^{-3})	1.552
μ (mm^{-1})	0.243
F (000)	732.0
Crystal size/mm^3	0.24 × 0.23 × 0.22
Radiation	Mo Kα (λ = 0.71073)
2Θ range for data collection/°	5.162 to 50.068
Index ranges	$-10 \leq h \leq 10$, $-14 \leq k \leq 13$, $-17 \leq l \leq 18$

Reflections collected	17745
Independent reflections	5369 [R_{int} = 0.0408]
Data/restraints/parameters	5369/316/626
Goodness-of-fit on F^2	1.046
Final R indexes [$I \geq 2\sigma(I)$]	R_1 = 0.0814, wR_2 = 0.2030
Final R indexes [all data]	R_1 = 0.1146, wR_2 = 0.2294
Largest diff. peak/hole / e Å^{-3}	0.91/-0.56
CCDC	2026357

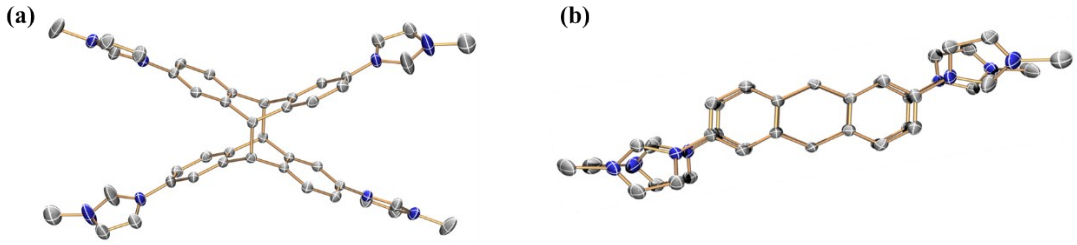

Figure S88. (a,b) Side and top views of the cationic part of the crystal of *syn*-H_4-**7a**$(PF_6)_4$. (N, blue; C, grey; hydrogen atoms have been omitted for clarity, and only the first atom of each N-substituent is depicted.)

9. References

1. N. Sinha, L. Stegemann, T. T. Y. Tan, N. L. Doltsinis, C. A. Strassert, F. E. Hahn, *Angew. Chem. Int. Ed*., 2017, **56**, 2785–2789.

2. M. Baron, E. Battistel, C. Tubaro, A. Biffis, L. Armelao, M. Rancan, C. Graiff, *Organometallics*, 2018, **37**, 4213–4223.

3. M. J. Frisch, G. W. Trucks, H. B. Schlegel, G. E. Scuseria, M. A. Robb, J. R. Cheeseman, G. Scalmani, V. Barone, B. Mennucci, G. A. Petersson, H. Nakatsuji, M. Caricato, X. Li, H. P. Hratchian, A. F. Izmaylov, J. Bloino, G. Zheng, J. L. Sonnenberg, M. Hada, M. Ehara, K. Toyota, R. Fukuda, J. Hasegawa, M. Ishida, T. Nakajima, Y. Honda, O. Kitao, H. Nakai, T. Vreven, J. A. Montgomery Jr., J. E. Peralta, F. Ogliaro, M. J. Bearpark, J. Heyd, E. N. Brothers, K. N. Kudin, V. N. Staroverov, R. Kobayashi, J. Normand, K. Raghavachari, A. P. Rendell, J. C. Burant, S. S. Iyengar, J. Tomasi, M. Cossi, N. Rega, N. J. Millam, M. Klene, J. E. Knox, J. B. Cross, V. Bakken, C. Adamo, J. Jaramillo, R. Gomperts, R. E. Stratmann, O. Yazyev, A. J. Austin, R. Cammi, C. Pomelli, J. W. Ochterski, R. L. Martin, K. Morokuma, V. G. Zakrzewski, G. A. Voth, P. Salvador, J. J. Dannenberg, S. Dapprich, A. D. Daniels, Ö. Farkas, J. B. Foresman, J. V. Ortiz, J. Cioslowski, D. J. Fox. (2009).

4. O. V. Dolomanov, L. J. Bourhis, R. J. Gildea, J. A. K. Howard, H. Puschmann, *J. Appl. Cryst*., 2009, **42**, 339–341.

5. L. J. Bourhis, O. V. Dolomanov, R. J. Gildea, J. A. K. Howard, H. Puschmann, *Acta Cryst*. 2015, **A71**, 59–75.

6. G. M. Sheldrick, *Acta Cryst*. 2015, **C71**, 3–8.